Towards Optimal Design of Reinforced Concrete Structures for Corrosive Environments in Saudi Arabia

BY

Yusuf, Moruf Olalekan

A Thesis Presented to the

DEANSHIP OF GRADUATE STUDIES

KING FAHD UNIVERSITY OF PETROLEUM & MINERALS

DHAHRAN, SAUDI ARABIA

In Partial Fulfillment of the
Requirements for the Degree of

MASTER OF SCIENCE

In

Civil Engineering

May, 2009

KING FAHD UNIVERSITY OF PETROLEUM AND MINERALS
DHAHRAN, 31261, SAUDI ARABIA

DEANSHIP OF GRADUATE STUDIES

This thesis, written by **MORUF OLALEKAN YUSUF** under the direction of his Thesis Advisor and approved by his Thesis Committee, has been presented to and accepted by the Dean of Graduate Studies, in partial fulfilment of the requirement for the degree of **MASTER OF SCIENCE IN CIVIL ENGINEERING**.

Thesis Committee,

Dr. Saeid A. Alghamdi (Advisor)

Dr. Shamsad Ahmad (Co-advisor)

Dr. Mohammed Maslehuddin (Member)

Dr. Husain J. Al-Gahtani (Member)

Dr. Mazen Khaled (Member)

Dr. Hussain J. Al-Gahtani
Department Chairman

Dr. Salam A. Zummo
Dean of Graduate Studies

30/5/09
Date

In the name of Allah, Most Gracious, Most Merciful.

Dedicated to my Parents, Wife and Family

TABLE OF CONTENTS

LIST OF TABLES

LIST OF FIGURES

ACKNOWLEDGEMENTS

All praises and thanks are due to Allah the Eternal for the successful completion of this work. May His peace and infinite mercy be upon the noble soul of the Prophet Muhammad (PBUH), his households, companions and the entire Muslim community till the day of recompense.

I acknowledge with deep gratitude the encouragement, inspiration, guidance and valuable time given to me by my Committee Chairman Dr Saeid A. Alghamdi. Special and unalloyed appreciation is due to my Committee Co-Chairman Dr Shamsad Ahmad for his patient attention and guidance.

The professional and intellectual guidance of Dr Mohammed Maslehuddin and Dr Mazen Khaled of the Research Institute and Chemistry Department respectively as Committee members towards the completion of this work is greatly appreciated. Similarly, the sincere moral support and guidance of Dr Husain .J Al-Gahtani will remain unforgettable.

This piece will be incomplete without mentioning the assistance of Engr. Muhammad Isa, Engr. Imran Ali, Engr. Mukarram, and Engr. Umar, all in the departmental laboratories for their timely attention in making the experimental work successful. Similarly, Engineers Shameem and Barry of Corrosion Laboratory in the University Research Institute are appreciated for their ready assistance during the data validation and analysis.

Special thanks to the Nigerian community here in the University. Their moral and spiritual guidance and most importantly the spirit of brotherhood displayed by them will remain indelible. I am greatly indebted to the following families for their support, assistance and moral advice as and when necessary: Alli's, Olatunde's, Lamidi's, Tijani's, Adejumo's, Adesokan's, Adeniran's and late Taofeek Amzat's. Furthermore, my colleagues in the university such as Bashir, Nemi's, Akeem (Yemenis), Ibrahim (Ugandan), Malik and Khalil (Indians) are appreciated for their spirit of comradeship and concern in my academic progress.

Finally, thanks are due to my mother and father, my wife and all my family members most importantly my siblings for their love, patience and spiritual and moral support throughout my academic work in Saudi Arabia.

ملخص الرسالة

التصميم الأمثل لمنشات الخرسانة المسلحة في بيئة الخليج العربي لمقاومة تأكل الحديد المعرض للكلور مهمة أساسية من اجل تخفيض الكلفة الدورية وللتأكد من أن المنشأ لن ينهار قبل عمر الخدمة التصميمي، من اجل ضمان السلامة والديمومة للمنشات، الخرسانة العالية الجودة وقطر التسليح الكافي وسماكة الغطاء الخرساني لتعويض فقدان الخرسانة والحديد نتيجة للتدهور في البيئة المعرضة للتآكل. العمل البحثي المقدم في هذه الرسالة اعتمد على مواد الإنشاء الطبيعية العامة المتوفرة و المستخدمة في المملكة العربية السعودية. ولتحقيق الهدف الأساسي لتصميم منشات الخرسانة ذات الديمومة، تم الحصول على مقاومة ضغط الخرسانة وعامل المرونة باستخدام بيانات التجارب التي تم الحصول عليها بالتجارب على عينات الخرسانة العادية باستخدام الركام من الطائف(في المنطقة الغربية) والدمام (في المنطقة الشرقية) مع نسب ماء /اسمنت متغيره (٠,٤ ؛ ٠,٤٥ ؛ ٠,٥) ونسبة الكنكري الناعم إلى الركام الكلي (٠,٣٥ ؛ ٠,٤ ؛ ٠,٤٥) ونسبة محتوى المواد الإسمنتية (٣٥٠؛ ٣٧٥؛ ٤٠٠ كيلوغرام لكلّ متر مكعّب) مع إضافة نسبة ثمانية بالمائة في السليكا فيوم في جميع خلطات الخرسانة.

تم تطوير النموذج الرياضي لقياس معدل اختراق التآكل لحديد التسليح باستخدام معطيات التجارب التي تم الحصول عليها باختبار عينات خرسانة صممت بنفس نسب الخلط لحساب المقاومة والمرونة وباستخدام ثلاث قيم لسماكة تغطية خرسانة (٢٥ ؛ ٣٧,٥ ؛ ٥٠ ملليمتر) ، وتم وضع العينات الإختبارية في ظروف تصدء تشبيهيه وذلك بوضعها في محلول الكلور باستخدام ثلاثة مستويات من تركيز ملح كلوريد الصوديوم (٣% ؛ ٧% ؛ ١٢%) .

تم تطوير طريقة للتصميم الأمثل لكمرات الخرسانة المسلحة وللأعمدة في البيئة القاسية، فالنموذج الرياضي المقترح يتكون أولا من إختيار المقاومة المثلى والمرونة ومعدل الاختراق التآكلي باستخدام نماذج إحصاء رياضية طُورت من التحليل العددي لنتائج الدراسات المعملية التي صُممت لأغراض البحث، ومن ثم حساب المتغيرات الأخرى للديمومة مثل فقدان الخرسانة ومعامل انتشار الكلور ووقت بداية وانتشار التآكل في الحديد باستخدام نماذج رياضية توفرت للبحث من إعمال بحوث سابقة تم التحقق من مناسبتها التكاملية مع أعمال هذا البحث ، وأخيرا تكون الخطوة التالية للتصميم الأمثل هي التصميم الإنشائي للعناصر الإنشائية وفقا لتحقيق شروط الكلفة الكلية الصغرى مع تحقيق شروط الخدمة والديمومة الهيكلية.

ولتوضيح الفائدة المتحققة من استخدام طريقة التصميم الإنشائي المبرمجة والمقترحة في هذا البحث، تم إيراد عينة من أمثلة تصميم إنشائي لكمرات (جوائز) وأعمدة خرسانة مسلحة صُممت باستخدام برنامج الحاسب الآلي المعروف "مايكروسفت إكسيل" (*Microsoft Excel Solver*).

درجة الماجستير في العلوم

جامعة الملك فهد للبترول والمعادن

THESIS ABSTRACT

Name: **Moruf Olalekan Yusuf**

Title: **Towards Optimal Design of RC Structures for Corrosive Environments in Saudi Arabia**

Department: **Civil Engineering**

Date: **May, 2009**

The optimal design of reinforced concrete (RC) structure in the Arabian Gulf environment to withstand chloride-induced reinforcement corrosion is an indispensable task so as to reduce the life cycle costs and to ensure that structures do not fail before their designed service-life. For safety and durability in structures, high quality concrete, adequate cover thickness are required that can accommodate the loss of concrete and steel due to deterioration in a given corrosive environment. With the ultimate objective of designing durable RC structures, the research presented in this thesis is based on the common construction materials available locally and used in corrosive environments in Saudi Arabia.

Regarding compressive strength and elastic moduli, models were generated from experimental data obtained by testing the plain cement concrete specimens cast by using aggregate from Taif (Western region) and Dammam (Eastern region) with varied water-to-cementitious materials ratios (w/cm) (0.4, 0.45 and 0.5), fine to total aggregate ratios (0.35, 0.4 and 0.45) and cementitious materials contents (350, 375 and 400 kg/m^3) with addition of eight percent silica fume in all the concrete mixtures. Models for reinforcement corrosion penetration rates were developed from the experimental data obtained by testing RC specimens cast with same mixture proportions as that for strength and elasticity but with varied cover thickness (25 mm, 37.5 mm and 50 mm) and subjected to varied chloride exposures by using three NaCl concentrations of 3%, 7% and 12%.

An approach for optimal design of RC beams and column for aggressive environments was developed. The proposed design approach consists of first optimizing strength, elasticity, and corrosion penetration rate by using models developed in the present study and then calculating other durability parameters, such as loss of concrete, chloride diffusion coefficient, time to initiation and propagation of reinforcement corrosion by using the models reported in the literature. The next steps of optimal design consist of structural design of the members corresponding to a minimum total cost satisfying the serviceability and durability constraints. To illustrate the utility of the proposed approach, typical examples of optimal design of beam and column were considered, and optimal designs were carried out by using the programs written on *Microsoft Excel* package supported Solver.

CHAPTER 1

INTRODUCTION

1.1 DURABILITY OF REINFORCED CONCRETE (RC) IN CORROSIVE ENVIRONMENTS

The corrosion of metal, especially reinforcing steel, in concrete has received increasing attention in recent years because of its widespread occurrence in certain types of structures and the high cost of repair and maintenance of the structures. The corrosion of steel reinforcement was first observed in marine structures and chemical manufacturing plants [1]. The corrosion of reinforcing steel in concrete is recognized as a significant problem for concrete infrastructure subjected to chloride environments [2]. This problem drains resources in both the public and private sectors. The menace of reinforcement corrosion has been widely reported to be the main cause of deterioration of many reinforced concrete (RC) structures leading to premature failures before their design life is attained. For instance, in the United States, about 173,000 bridges on the interstate system are structurally deficient or functionally obsolete, in part due to deterioration caused by corrosion of reinforcing steel [3]. Implementation of solutions is needed, both in the design of structures resistant to corrosion and the rehabilitation of structures that are already suffering the effects of corrosion.

Reinforced concrete (RC) structures deteriorate with time if subjected to an aggressive environment. As civil infrastructure is aging, owners have to spend an increasing percentage of their budgets on rehabilitatio[1] existing RC structures. To improve

durability, reduce maintenance costs and extend service-life, special design requirements for RC structures built in aggressive environments are usually specified. These requirements include the use of high- performance concrete (with low water/cement ratio), increased concrete cover (e.g. AS 3600 [4]), and the use of admixtures (i.e. corrosion inhibitors) [5].

Research conducted in the Arabian Gulf environment has revealed that the service-life of buildings in this region may be expected to be between 10 to 15 years, and sometimes only 5 years, owing to the prevailing aggressive weather conditions [6]. In some cases, reinforcement corrosion has been found to be so severe that the damage occurred even before the completion of construction [7].

Chloride (either admixed or diffused) has been observed to be mainly responsible for reinforcement corrosion in concrete. Recently, numerous reports of reinforcement corrosion occurrence in bridge decks and parking structures exposed to chloride ions have actually proved this point, and at the same time made the problem particularly prominent. Extensive research on factors contributing to reinforcement corrosion has increased our understanding of the mechanisms of corrosion, especially concerning the role of chloride ions [8].

Chloride ions are common in nature and very small amount are normal in concrete-making materials. These ions may be intentionally added to the concrete, most often as a constituent of accelerating admixtures. Dissolved chloride ions may also penetrate hardened concrete in structures exposed to marine environments or to deicing salt. Besides, the environment influences the corrosion rate, as it contains oxygen and moisture which

are essential substances in electrochemical corrosion. Macrocell corrosion is imminent in RC with a significant gradient in chloride ions, especially when subjected to wetting and drying.

Heterogeneity of the concrete matrix and reinforcing steel, reduction in pH, cracks in the concrete, less dense concrete microstructures or high permeability, stray current, design features and construction practices are among other factors that affect the corrosion rate or extent of corrosion of the reinforcing bar in the concrete. Therefore, mixture proportions of concrete, thickness of concrete cover over the reinforcing steel, crack control measures, and implementation of measures designed specifically for corrosion protection, are some of the factors that can help to control the onset and rate of corrosion [9].

The effects of reinforcement corrosion range from loss of cross-section of rebar to cracks formation due to stresses exerted within the concrete which cannot be supported by the limited plastic deformation of the concrete. This eventually results in economic waste due to high costs of maintenance, durability incompetence, structural and service failure [10] that may ultimately cause loss of lives due to sudden structural collapse [11].

Several models have been proposed for prediction of carbonation depth, chloride concentration at a given depth and time, corrosion initiation time, corrosion rate, concrete cover cracking and residual load-bearing capacity of corroded members [12-14]. Many studies have been reported on optimal design of concrete mixtures [15-17]. Considerable research has been reported on optimal design of RC members [18–23] while only a few research studies regarding durability-based service-life design of RC members are reported in the literature [24,25].

However, the optimal design of RC members, combining the cost optimization of materials (i.e. optimization of concrete mixture, and optimal proportioning of concrete and steel in the member) and durability of structures, has not got the desired attention in corrosive environments including the coastal areas of Saudi Arabia.

This study is aimed at first obtaining models for compressive strength of concrete and reinforcement corrosion rate by using the experimentally generated data for concrete cast by using aggregates from the Eastern and Western regions of Saudi Arabia. This was followed by developing a methodology for using the strength and durability models to carry out cost-effective structural design of RC members.

1.2 NEED FOR THIS RESEARCH

Considerable research has been carried out on the optimal design of RC members in corrosive environments. However, two important design issues have not been studied in a unified format. These two design issues are: (i) optimization of concrete design to satisfy the requirement for strength, workability and durability at a minimum cost; and (ii) incorporation of the target service-life as one of the design criteria for durable structures. These two issues are implicitly inter-related in a rather complex manner. A meaningful and unified design methodology should account for the multi-criteria inter-relationships. Therefore, the present study aims at providing the required unified methodology towards achieving the optimal design of RC structures.

This research was conducted to develop models for concrete strength, elasticity, and reinforcement corrosion penetration rate, in terms of key parameters affecting performance of concrete such as water cement ratio, cementitious materials content, and fine-to-total

aggregate ratio. Cover over reinforcing steel, and chloride concentrations, were additionally considered in the case of reinforcement corrosion penetration rate modelling. The development of models is a pre-requisite for designing durable and cost-effective design of the RC members.

1.3 OBJECTIVES

The primary objective of this work was to develop models for strength, elastic modulus, and reinforcement corrosion penetration rate, by using the experimental data obtained through testing concrete specimens prepared with aggregates from two different sources in Saudi Arabia (namely: Western Province-Taif and Eastern Province). Strength and corrosion deterioration models are developed in this study after an extensive survey of issues most relevant to durability-based design of RC structures. These models can be used to help design RC members. Specific objectives of this research are as follows:

- To provide guidelines for optimizing the concrete cost through the variation of cross-sectional dimension and area of steel in RC beams and columns.
- To utilize the target service-life as one of the design constraints included in the durability design of the RC members.

CHAPTER 2

LITERATURE REVIEW

2.1 OPTIMIZATION OF CONCRETE MIXES

The optimization of concrete mix design through full factorial techniques was carried out by Soudki *et al.* [26]. They investigated concrete compressive strength by varying concrete constituent materials and parameters, such as water-cementitious material ratio, coarse aggregate to total aggregate ratio, total aggregate/cement ratio and temperature. The experimental data were analyzed by using polynomial regression. Mathematical polynomials were developed for concrete strength as a function of temperature and mix proportion. Similarly, Waseem [27] adopted the same approach to develop economic mix proportions for given strength and workability requirements. Shakhmenko and Birsh [15] developed a computer program for the optimization of concrete mix by selecting the most suitable aggregate and through analytical and numerical methods. They also took into account granulation parameter of aggregate mix with a view to reducing the material cost, improving the quality of aggregate packing and reducing the cement consumption.

Goltermann *et al.* [16] have suggested a packing model for the aggregate selection and combination to obtain aggregate mixes having the lowest void contents with maximum packing degree (the ratio between bulk density and the aggregate grain density). Thus, the packing degree according to them is a characteristic of the specific aggregate type or mix and it indicates the void volume and the amount of cement paste necessary in the concrete.

Maruyana *et al.* [28] have used a genetic algorithm to optimize concrete mix by categorising the problems as multi-criteria optimization. The concept of Pareto optimality of evaluation of plural was applied to derive the optimum solution. In this contribution, two proportioning problems were solved by the genetic algorithm: a request of delayed setting time and high flowability (consistency) in hot weather on one hand and of accelerated setting and high flowability in cold weather on the other.

2.2 OPTIMUM DESIGN OF RC STRUCTURES

An optimum design is a design which minimizes or maximizes a certain objective function, and still meets its design requirements [29]. The advancement of computer enables design optimization process to be conducted systematically and consistently. Optimization techniques that are based on optimality criteria approach, mathematical programming and genetic algorithms [30] are widely employed now. It is possible to apply analytical methods of design to search for an optimal concrete-mix composition at lowest cost [17].

Concrete mix can be optimized first developing the models for strength, workability, permeability /durability, and unit cost of concrete in terms of the key variables including water/cement ratio, cement content, fine aggregate/total aggregate ratio, and percentage of mineral admixtures. These models can then be utilized for obtaining the optimal composition of a concrete mix corresponding to a minimum unit cost satisfying the strength, workability, and durability requirements.

2.2.1 General Formulation of the Optimal Design Problems

For a structural frame model comprising beams and columns with reinforcement areas A_{s1}, and A_{s2} in tension, and compression, respectively, and for prescribed structural supports/joints conditions, Garstecki *et al.* [18] have suggested the following generalized objective function F(s) for optimal design:

$$F(s) = c_c b \sum_{i=1}^{NE} h_i l_i + c_s \sum_{i=1}^{NC} (A_{s1} + A_{s2})_i l_i$$

$$+ c_s \left(\sum_{i=1}^{NB} 0.7(A_{s1} + A_{s2}) l_i + 0.2(A_{s1}^1 + A_{s2}^1 + A_{s1}^r + A_{s2}^r) l_i \right)$$

$$+ c_f \sum_{i=1}^{NC} 2(b + h_i) l_i + c_f \sum_{i=1}^{NB} (b + 2h_i) l_i \quad , \qquad \ldots(2.1)$$

where:

F(s) = objective function representing the cost of a frame

b = width of the cross-section

h = overall depth of the cross section

d = effective depth

c_c, c_s and c_f = unit cost of concrete, steel and formwork, respectively

NB = number of beams

NC = number of columns

NE = number of structural elements (NE = NB + NC)

The above objective function is subject to the following constraints:

(i) *Limit state load bearing capacity constraint*: this is called the ultimate limit state constraint of beams and columns

$$\Phi\ (M, N) \leq 0$$

with M and N denoting the bending moment and axial force, respectively, (where N > 0 for compression). For computation of M and N, the equilibrium state (shown in Figure 2.1a) may be assumed in using the following equilibrium equations:

$$M = b \int_{-\frac{h}{2}}^{+\frac{h}{2}} \sigma_c [\varepsilon(y)]\, y\, dy + N_{s2}(0.5h - a_{s2}) + N_{s1}(0.5h - a_{s1}) \quad \ldots(2.2)$$

$$N = b \int_{-\frac{h}{2}}^{+\frac{h}{2}} \sigma_c [\varepsilon(y)]\, dy + N_{s2} - N_{s1} \quad \ldots(2.3)$$

While the bending moment M and axial force N are obtained from linear finite element analysis, the bending moment in column is increased to allow for random eccentricities, which are assumed as deterministic values. A typical example of the limit interaction curve $\Phi\ (M, N) = 0$ computed from above equations for M and N for a rectangular cross-section un-symmetrical reinforcement is shown in Fig. 2.1b.

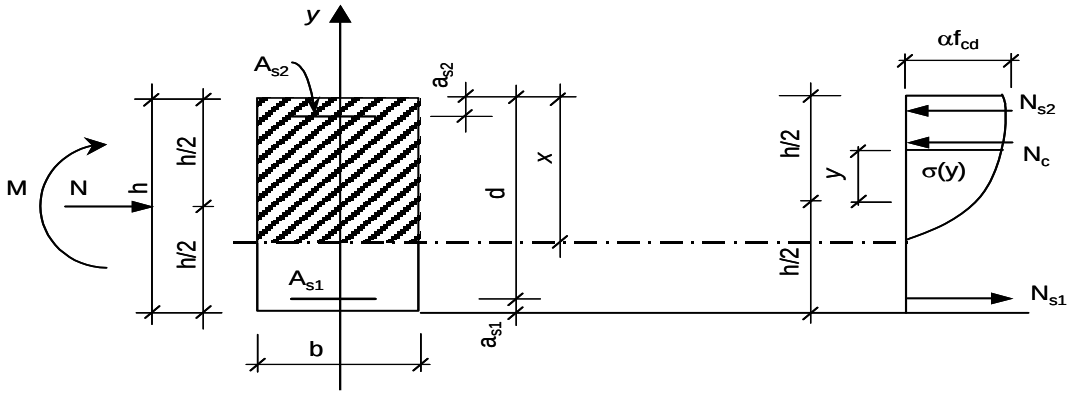

a: Ultimate state of stress.

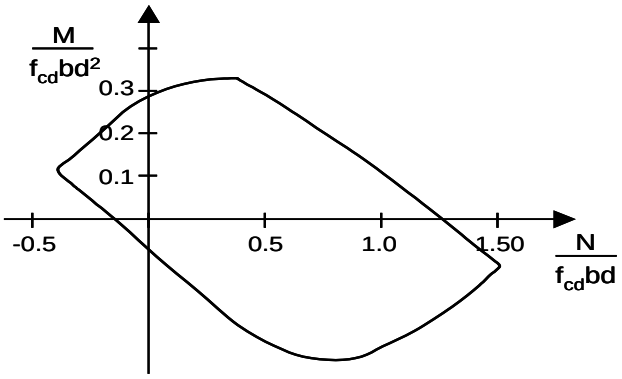

b: Limit interaction curve for a rectangular cross-section with $A_{s1} < A_{s2}$.

Figure 2.1: Ultimate limit state and interaction diagram for rectangular section [19].

(ii) *Column stability (buckling) constraint*

$$(N_{sd})_i \leq \beta\,(N_{crit})_i \quad \text{for } i = 1, 2, \ldots, NC \qquad \ldots(2.4)$$

where: β is the user-supplied coefficient (usually less than unity).

(iii) *Beam displacement constraint*

$$a_i \leq (a_{adm})_i \quad \text{for } i = 1, 2, \ldots, NB \qquad \ldots(2.5)$$

(iv) *Crack-width constraint*: for beams and columns it is required that

$$(w_k)_{ij} \leq w_{adm} \quad \text{for } i = 1,2,\ldots,NB;\ j = 1, 2, 3$$

$$(w_k)_{ij} \leq w_{adm} \text{ for } i = 1,2,\ldots,NC;\ j = 1, 2, 3 \qquad \ldots(2.6)$$

where: j = 1 – left support, j = 2 – span, j = 3 – right support.

(v) *Shear force constraint*: for beams and columns it is required that

$$(V_{sd})_{ij} \leq V_{Rd2} \quad \text{for } i = 1,2,\ldots, NE;\ j = 1, 2, 3 \qquad \ldots(2.7)$$

where: V_{sd} denotes the design shear force, whereas V_{Rd2} denotes the maximum design shear force that can be carried without crushing the concrete.

(vi) *Steel reinforcement constraint*: for beams and columns it is required that the steel content should satisfy the following percentages:

$$\frac{(A_{s1})_i}{bd_i} \geq \rho_{min} \qquad \text{for } i = 1, 2,\ldots, N E, \qquad \ldots(2.8\text{-}1)$$

$$\frac{(A_{s2})_i}{bd_i} \geq \rho_{min} \qquad \text{for } i = 1, 2,\ldots, N E, \qquad \ldots(2.8\text{-}2)$$

$$\frac{(A_{s1})_i + (A_{s2})_i}{bd_i} \geq \rho_{max} \qquad \text{for } i = 1, 2,\ldots, N E. \qquad \ldots(2.8\text{-}3)$$

where: ρ is the ratio of steel area to concrete area.

(vii) *Structural joint stiffness constraint*:

$$\left[\frac{\left(k\frac{EI}{l}\right)_{\max}}{\left(k\frac{EI}{l}\right)_{\min}}\right] \le 7 \qquad \text{for} \quad i = 1, 2,\ldots, N\,J \qquad \ldots (2.9)$$

where: k = 4 for clamped-clamped members, and k = 3 for clamped-hinged members.

(viii) *Structural member dimensions constraint*: for beams and columns it is often required that the following key design constraints are satisfied:

$$b^{lower} \le b \le b^{upper} \qquad \ldots (2.10\text{-}1)$$

$$h^{lower} \le h \le h^{upper} \qquad \ldots (2.10\text{-}2)$$

$$1.0 \le \frac{h_i}{b} \le 3.5 \qquad \text{for} \quad i = 1, 2,\ldots, N\,DV, \qquad \ldots (2.10\text{-}3)$$

$$\frac{l_{oi}}{h_i} \le 30 \qquad \text{for} \quad i = 1, 2,\ldots, N\,C \qquad \ldots (2.10\text{-}4)$$

where

NE = number of independent element

NJ = number of joints

NDV= number of dimensional design variables

The solution of the optimization problem, formulated as shown above, requires that design variables vector $\boldsymbol{s}$, is decomposed into two vector parts: cross-sectional dimensions sub-vector, $s_1 = [b_i, h_i]$; and reinforcement sub-vector, $s_2 = [(As_1)_i, (As_2)_i]$.

Step (a): For fixed cross section dimensions of *b, h*, and for fixed values of *M, N*, and the minimal reinforcement can be computed. Step (b): At each iteration step, the sub-vector $\boldsymbol{s_1}$ is found by using the feasible direction method of nonlinear programming coupled with the Finite Element Method (FEM), whereas the sub-vector $\boldsymbol{s_2}$ is computed by using the procedure for minimization of $(As_1)_i + (As_2)_i$ separately for each cross-section [18].

The above problem is a continuum-type optimization, where the optimal design is found by using nonlinear programming. In engineering practice, however, discrete sets of reinforcements and dimensions *b, h* are invariably used, and the discrete solution can be approximated by the following two-step optimization: determination of continuum-type solution $(h, As_1, As_2)_i$ for a cross-section fixed width *b;* and use of h_i as next elements in a discrete set and find the optimal reinforcement.

The solution obtained will satisfy all constraints, but it is only "near to optimal". Therefore, for practical design situations, the cross-sectional dimensions of beams and columns are unified within only few manageable groups. For this purpose, it is usually not difficult to improve step (b) given above by a systematic search of the discrete values of h_i in the vicinity of the continuum-type solution provided by step (a) as given above.

2.2.2 Optimal Design of RC Beams and Columns

In a traditional design methodology, a solution is proposed, utilized and verified by a mathematical analysis in order to verify that the problem requirements are satisfied. If they are not satisfied, a new solution is proposed. This trial-and-error process as shown in Figure 2.2a enables engineers to gain design experience, but this is usually achieved at a very high cost in terms of time and efforts. Alternatively, the optimal design process, as shown in Figure 2.2b, consists of changing the design according to a certain optimality condition [19] to ensure a unified multi-criterion optimal structural design. This design approach would integrate all required tools of mechanics, analysis, and design within a selected automated research tool for design optimization process based on experimentally determined phenomenological models of the strength and workability of the constituent materials [20].

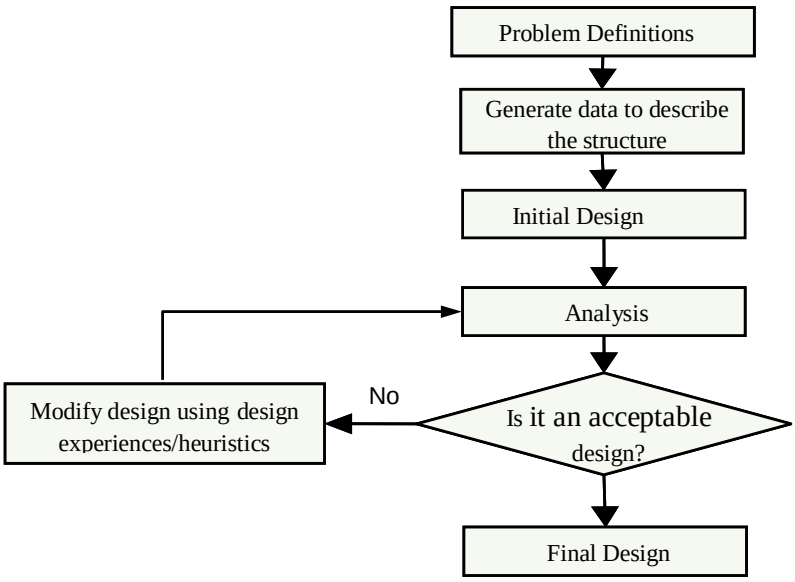

Figure 2.2a: Traditional methodology of a structural design [19].

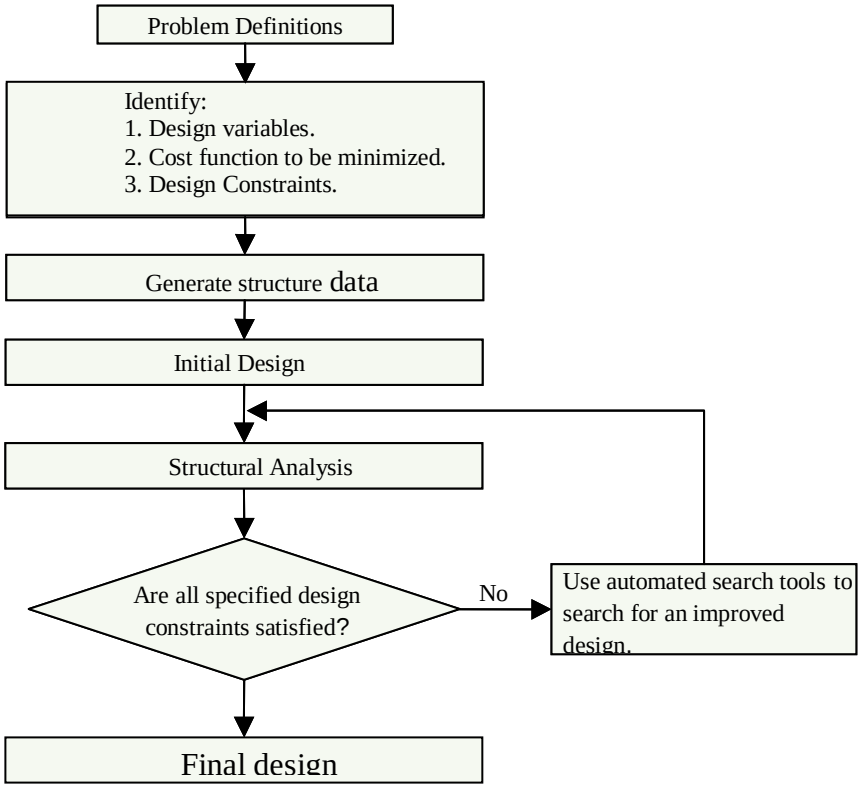

Figure 2.2b: Automated methodology for an optimal [19] .

2.2.3 Approaches Adopted for Optimal Design of RC Members

Several approaches were previously adopted for the optimal design of RC members. Coello *et al.* [19] have presented a method, based upon a search technique using Genetic Algorithms. The suggested an optimal design model subject to various constraints pertaining to equilibrium, bending moment compatibility, width-height ratio, acting moment, minimum width, and non-negativity. To solve the optimization problem, they used the Simple Genetic Algorithm (SGA), and they experimented with several representations. Several applications show how their system provides more realistic designs than other methods based on mathematical programming techniques.

Dole *et al.* [22] applied the polynomial optimization technique for optimum design of RC beams. They used this technique to determine the minimum cost of RC members by

considering several design variables including member breadth, depth, and area of reinforcing steel. Three cases of optimum design of RC beams subjected to pure bending were considered: (i) singly reinforced rectangular beam; (ii) doubly reinforced rectangular beam; and (iii) flanged beam (T-section). To simplify the work in the design office, where it is difficult for the designer to become familiar with the mathematical computation required, they represented the resulting optimum design expressions in the form of "nomograms".

Reddy *et al.* [31] proposed a formal method for the cost optimization of RC structures. A cost function was derived to estimate the optimum size of members at the conceptual design stage. An expert system, called EXFORM, was developed for the cost-optimum design of RC members. EXFORM made use of cost function along with heuristic knowledge of the designer. The scope of the work was extended to the design of columns, beams and slabs.

Azmy and Eid [21] presented an optimization procedural method for the design of rectangular beams. The optimization procedure was formulated as finding the minimum cost of design with constraints imposed based on ACI code provisions. The cost of concrete, flexural reinforcement and formwork was included in the formulation of the objective function. The behavioral constraints, that is ACI requirements for flexure strength, serviceability requirements, (such as, deflection, and practical constraints on cross-section dimensions of beams) were included in the formulation.

A closed-form solution of the optimization problem expressed the optimal values of the flexure reinforcement and section dimensions in terms of material costs, strength and

ductility parameters. A complete flow-charts and computer programs of the algorithm were presented, and several numerical examples were given to show the validity of the proposed optimization method. In another paper, Azmy and Eid [32] also presented an optimization procedural method for the shear design of rectangular beam.

Balaguru [33] presented an algorithm for the cost-optimum design of singly reinforced rectangular beams. Four different types of problems with specified restrictions on dimensions of the beam and the amount of reinforcement were considered. The solution satisfies the structural bending equations as applied to the ultimate load design. The cost of concrete, steel and formwork were considered in arriving at the total cost. Based on the numerical results obtained, it was recommended that a near-optimum solution can be obtained by using the maximum amount of steel allowed in the code of practice followed for the design and the minimum practicable breadth-by-depth ratio. Using this recommendation, the optimum dimensions of the beam and the amount of reinforcement can be obtained by solving a third-order polynomial equation.

Balaguru [34] presented an algorithm to calculate the optimum dimensions and the amount of reinforcements for a doubly reinforced rectangular beam. The method was based on ultimate strength design by using rectangular stress block for concrete. Dead weight of the beam was incorporated as a variable. A simple equation to determine whether a doubly RC beam was more economical than the singly reinforced cross section was presented with a flow chart represents the sequence of operations. A numerical example was worked out to clarify the design steps involved.

A model for the optimal design of rectangular RC sections was presented by Barros *et al.* [35] considering the stress-strain diagrams described in EC2-2001 and MC90. Expressions were developed for economic bending moment, optimal area of steel, and for optimal steel ratio between upper and lower steel. All the expressions was in non-dimensional form. The presented model was applied to four different classes of concrete described in MC90. It was concluded that in non-dimensional form the equations are nearly coincident for both singly and doubly reinforced section. It was also concluded that the ultimate strain for concrete in the compression zone, $\boldsymbol{\varepsilon_{cm}}$, lies between the strain for peak stress $\boldsymbol{\varepsilon_{c1}}$ and the ultimate strain ε_{cu}. This result was relevant once the maximum moment was obtained for this value, and not the value $\boldsymbol{\varepsilon_{cu}}$, as defined in EC2-2001. Cost optimization was implemented in the code and compared with other optimum models based on the ultimate design of ACI.

Min and Kikuchi [36] adopted the homogenization design method for optimal reinforcement design of structures under the buckling load. Their buckling analysis was restricted to the linear buckling behavior of a structure. The global stability requirement was defined as a stiffness constraint, and determined by solving the Eigen-value problem. The optimality conditions to update the design variables, based on the sequential convex approximation method and the dual method, were illustrated with examples to validate the feasibility of this method in the design of structures.

Zielinsky *et al.* [23] presented a procedure for optimal design of RC short-tied columns. The proposed procedure includes two sets of iterations. The first set of iterations found the resistance capacity of a column of given dimensions, and the second set of iterations

performed the optimization process. The optimization process was formulated as finding the minimum cost design with the constraints imposed by the Canadian Specifications CSA CAN3-A23.3-M84 [23]. The internal penalty function algorithm for nonlinear programming was used in the optimization procedure.

2.3 CHLORIDE-INDUCED REINFORCEMENT CORROSION

Chloride contamination of concrete is a frequent cause of corrosion of reinforcing steel [37]. Modern design codes of reinforced and prestressed concrete structures restrict the amount of chloride that may be introduced from raw materials containing significant amount of chlorides. According to the European Standard EN 206, the maximum allowed chloride contents are 0.2-0.4% chloride ions by mass of binder for reinforced and 0.1-0.2% for prestressed concrete. These restrictions are thought to eliminate corrosion due to chloride in the fresh mix. In some structures built in the past, chlorides were added into the concrete mix, unknowingly or deliberately, through contaminated mixing water, aggregates or admixtures. The other main source of chloride is the penetration from the environment [38,39]. Chloride contents from accelerating admixtures, in amounts ranging from 0.5% to well over 2% by mass of cement caused extensive corrosion-induced damage after carbonation and even in alkaline conditions [40,41].

2.3.1 Corrosion Initiation

Corrosion begins when the chloride content at the surface of the reinforcement reaches a threshold value (or critical chloride content). A certain time is required from the breakdown of the passive film and the formation of the first pit. From practical point of

view, the initiation time can be considered as the time when the reinforcement, in concrete that contains substantial moisture and oxygen, is characterized by an average sustained corrosion rate higher than 2 mA/m^2 (0.2 $\mu A/cm^2$) [42].

The chloride threshold for the initiation of pitting corrosion for a given structure depends on numerous factors. These include the concrete pH (the concentration of hydroxyl ion in the pore solution), the potential of the steel, and the presence of voids at the steel/concrete interface. The pH depends on the type of cement and admixtures. The electrochemical potential of steel is the second factor that affects the threshold value. In fact, as the potential of steel decreases, the chloride threshold may increase by more than one order of magnitude. The chloride threshold has been found to depend on the presence of macroscopic voids in the concrete near the concrete-rebar interface [43].

Voids that can be found normally in real structures due to incomplete compaction may weaken the layer of cement hydration products deposited at the steel/concrete interface, and thus may favour a local acidification that is required for sustained propagation of pits. For instance, it was shown that, by decreasing the volume of entrapped air in the steel-concrete interfacial zone from 1.5% to 0.2% (by volume), the chloride threshold increased from 0.2% to 2% by mass of cement [44].

The presence of voids or microcracks can also explain the lower values of chloride thresholds that are normally found in real structures compared with those found in (usually well compacted) laboratory specimens with similar materials [45]. Several other factors, such as temperature, the composition of cement or surface roughness of the steel reinforcement, or polarization with anodic or cathodic current, may affect the chloride threshold. It is suggested that pitting may take place above a critical ratio of chloride and

hydroxyl ion [46]. Chloride penetration from the environment produces a profile in the concrete characterized by high chloride content near the external surface and by decreasing content at greater depths.

The chloride content in the concrete, and thus the chloride threshold, can be expressed in several ways referring either to chloride concentration in the pore solution (i.e., free chloride) or to the total chloride contents in the concrete, i.e. including the chloride bound to the constituent of the cement paste. It is generally believed that only the chloride ions that dissolve in pore solution can promote pitting corrosion while the bound chlorides do not. However, Glass and Buenfield [43] stated that large parts of bound chloride are released as soon as the pH drops to values below 12, which may happen locally in voids at the steel/concrete interface. The bound chloride dissolves and may subsequently be involved in the initiation of corrosion.

Equilibrium conditions tend to establish between the free chloride ions and bound chlorides, depending on the composition of cement and its binding capacity. Therefore, it is possible that the concentration of free chloride ions in the pore solution of different concrete varies, even if the total chloride content is the same. Binding in ordinary Portland cement concrete depends on the content of tricalcium aluminate (C_3A) phase. For example, the risk of corrosion in sulfate resistant cement is higher than in normal Portland cement, which is characterized by a low content of the tricalcium aluminate in relation to an equal content of total chloride [47].

Similarly, slag and fly-ash blended cement have lower free-chloride concentrations than the original Portland cement, although their pH is lower [47]. Adsorption of chloride ions in the calcium silicate hydrate (C-S-H) may be even more important than chemical

binding, and this could explain the higher binding capacity which tends to form a finer microstructure of the hydration products in blended cements [48].

In practice, since the total chloride content can be measured more easily than the free chloride concentration, the chloride threshold is expressed as critical total chloride content. The critical value is usually given as a percentage of chlorides with respect to the mass of cement, since the amount of chlorides that can be tolerated increases as the cementitious material content in the concrete increases.

2.3.2 Propagation of Corrosion

Chlorides lead to a local breakdown of a protective oxide layer on the reinforcement in alkaline concrete, so that a subsequent localized corrosion attack takes place. The areas that are no longer protected by the passive film act as anode (active zones) with respect to the surrounding still passive areas where the cathodic reaction of oxygen reduction takes place. If very high levels of chlorides reach the surface of the reinforcement, the attack may involve larger areas, so that the morphology of pitting will be less evident [13].

Once the corrosion has initiated, a very aggressive environment will be produced inside the pits. In fact, current flowing from anodic areas to surrounding cathodic areas both increases the chloride content (chlorides, being negatively charged ions, migrate to the anodic region) and lowers the alkalinity (increased acidity is produced by hydrolysis of corrosion products inside the pits). On the other hand, the current strengthens the protective film on the passive surface since it tends to eliminate the chloride, while the cathodic reaction produces alkalinity.

Much higher level of chloride are required to initiate corrosion in structures immersed in seawater or in zones where the concrete is water-saturated, so that the oxygen supply is hindered and thus, the potential of the reinforcement is rather low [38]. Consequently, both the anodic behavior of active zones and the cathodic behavior of passive zones are stabilized. Corrosion is then accelerated (autocatalytic mechanism of pitting) and it can reach a very high rate of penetration (as high as 1 mm/year) that can quickly lead to a remarkable reduction in the cross-section of the rebars [39].

The chloride ingress model used in the present study is based on Fick's second law of diffusion, and the quality of concrete is quantified in terms of three factors (namely: apparent diffusion coefficient at one year, $\boldsymbol{D_{app}}$; surface chloride concentration, $\boldsymbol{C_s}$; and critical chloride level, C_{th}. The service-life was estimated from the standard deviations of the basic factors: the cover depth, $\boldsymbol{D_{app}}$, $\boldsymbol{C_s}$, and $\boldsymbol{C_{th}}$. Khatri and Sirivivantnanon [49] presented the results of a study on characteristic service-life for concrete exposed to marine environments. They noted that the service-life is more sensitive to the cover depth, ***cv*** than to the diffusion coefficient, $\boldsymbol{D_{app}}$, and that it is also more sensitive to the surface chloride concentration, $\boldsymbol{C_s}$ than to the critical chloride level, $\boldsymbol{C_{th}}$.

2.4 CORROSION DETECTION METHODS

Since chlorides are known to be at the crux of reinforcing steel corrosion in concrete, several invasive and non-destructive methods have been developed to assess the level of corrosion taking place or the potential for corrosion. Because corrosion is an electrochemical process, some of the most commonly used non-destructive field methods for measuring corrosion activity are: resistivity of concrete, corrosion potentials, and linear

polarization of the steel reinforcement [50]. The invasive (destructive) corrosion assessment methods include: chloride content analysis from powdered samples, chloride permeability tests, and gravimetric loss of steel specimens.

2.4.1 Concrete Resistivity

A non-destructive testing procedure that is becoming increasingly popular, due to its low cost and ease of implementation, is measuring the concrete resistivity by the Wenner-four probe method, as shown in Figure 2.3.

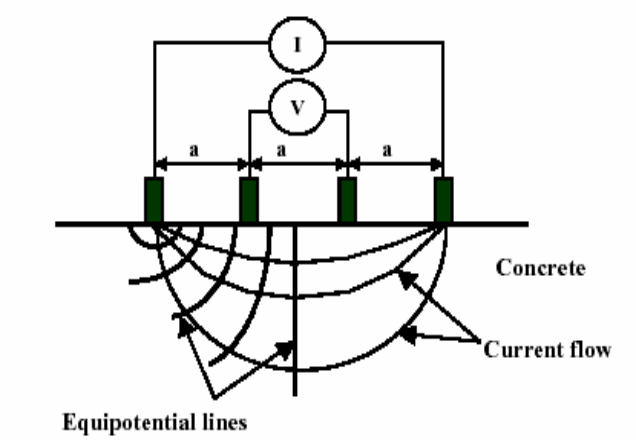

Figure 2.3: Four-probe Wenner Resistivity Set-up [51].

Originally developed by Wenner in 1916 to measure the resistivity of soils, this method uses four equally spaced probes. Although resistivity cannot be used to determine the rate of corrosion, it can be used to assess other concrete properties, such as permeability to chlorides and the ability to sustain corrosion. To minimize the polarization effects on the reinforcing steel, “a small alternating current is applied between the outer electrodes while the potential is measured between the inner electrodes” [52]. Thus, electrical resistance of

concrete is measured, which affects the ionic current flow from the cathode to the anode, and the rate at which corrosion can occur [53]. Resistivity (ρ) is then calculated as follows:

$$\rho = 2\pi aR \quad \ldots(2.11)$$

where: ρ = Resistivity in units of ohm-cm or ohm-in

a = spacing between the four probes in cm or in

R = actual measured resistance in ohms

High concrete resistivity decreases the current flow, and it impedes the corrosion process. Since concrete resistivity is affected by chlorides (mostly from deicing salts) and other ions, concrete resistivity by Wenner's method has been used to assess other concrete properties, such as permeability [54].

2.4.2 Corrosion Potential

Corrosion potential is different from resistivity in that it indicates the potential of corrosion taking place on the reinforcing steel embedded in concrete. The basic process for the corrosion of steel in concrete is the development of micro and macro cells. That means the coexistence of passive (non-corroding) and active (corroding) areas on the same bar or separate bars. A short-circuited galvanic element, with the corroding area as anode and the passive area as cathode, is formed. The direct measurement is the potential difference created between the metal in the corrosion and the steel in concrete [55]. Therefore, places on the reinforced structure with higher concentrations of iron in solution – in this case the concrete pore solution – will exhibit higher (more negative) potential differences. The

measurements are obtained by using a high-impedance voltmeter. A typical measurement set-up (described in ASTM C 876) is shown in Figure 2.4 [56].

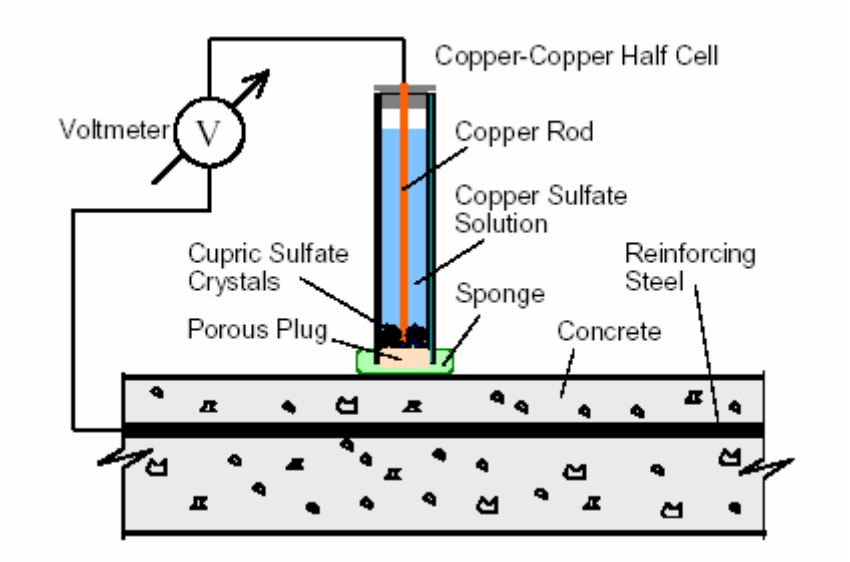

Figure 2.4: Corrosion potential measurement set-up [56].

Several types of corrosions reference electrodes are commercially available: copper/copper sulphate (CSE), silver/silver chloride (Ag/AgCl), mercury/mercury oxide (Hg/HgO) and saturated calomel electrode (SCE) [55]. It is important to note what type of half-cell is used to perform the test, since the interpretation of results from half-cells other than CSE will have to be offset according to their respective chemical composition. The ASTM C 876 interpretation criteria for tests performed using a CSE reference electrodes on structures reinforced with bare steel is presented in the Table 2.1.

Table 2.1: Potential interpretation guidelines (ASTM C 876) [55].

Potential level, mV CSE	Interpretation
Greater (more positive) than -200	90% probability of no active corrosion
Between -200 and -350	Uncertain
Less than -350	90% probability of active corrosion

2.4.3 Linear Polarization Resistance Method

A more sophisticated inspection method is the three-electrode linear polarization resistance method (LPRM). This is a convenient method for measuring corrosion current density. It yields reinforcing steel corrosion current densities that correlate reasonably well with the gravimetric metal loss. The technique is based upon the fact that a DC current applied to alter the natural electrical half-cell potential of the steel by a few millivolts (± 20 mV) is proportional to the natural corrosion of the steel. If a high current is required, the corrosion [current density] is high; and vice versa. The development of this technique was based on the Stern-Geary equation [57].

Table 2.2 was presented by McDonald *et al.* [58] to show the typical range values of current corrosion density, I_{corr} (measured in unit of $\mu A/cm^2$) and its equivalent corrosion penetration rate (μm/yr) which is the rate of metal loss per unit time (usually in year) while Clear [59] presented the likely time of severity of damage against the values of I_{corr} in Table 2.3. The experience on real structures [60] has confirmed the ranges of values previously recorded in laboratory experiments [61] as shown in Table 2.4.

Table 2.2: Corrosion rates of steel in concrete [58].

Rate of Corrosion	Corrosion Current Density (I_{corr}) $\mu A/cm^2$	Corrosion penetration rate (μm/yr)
High	10-100	100-1000
Medium	1-10	10-100
Low	0.1-1	1-10
Passive	< 0.1	< 1

Table 2.3: Corrosion rate and remaining service-life prediction [59].

I_{corr} ($\mu A/cm^2$)	Severity of Damage
< 0.5	No corrosion damage expected
0.5-2.7	Corrosion damage possible in 10 to 15 years
2.7-27	Corrosion damage expected in 2 to 10 years
> 27	Corrosion damage expected in 2 years or less

Table 2.4: Ranges of corrosion rate and risk levels [60].

I_{corr}, $\mu A/cm^2$	P_r, μm/yr	Interpretations
≤ 0.2	< 2	Negligible
$0.2 < I_{corr} < 0.5$	$2 < Pr < 5$	Low
$0.5 < I_{corr} < 1$	$5 < Pr < 10$	Moderate
> 1	> 10	High

In general, values of corrosion rates higher than 1 $\mu A/cm^2$ are seldom measured, while values between 0.1-1 $\mu A/cm^2$ are the most frequent. When the steel is passive, very low values (less than 0.05-0.1 $\mu A/cm^2$) are recorded.

2.5 FACTORS AFFECTING SERVICE-LIFE OF RC MEMBERS

The useful service-life of RC structures in the aggressive environments of coastal regions (such as the Arabian Gulf region) is considerably reduced due to the severe climatic and geomorphic conditions that cause noticeable accelerated structural deterioration, the degree of which is often extensive and irreparable [62].

In a new structure with good-quality concrete, the concrete can protect the steel reinforcing bars from corrosion for the service-life of the structure. For steel embedded in uncarbonated concrete or in sound un-cracked with little or no chloride, the steel is passivated, and no or low corrosion can be expected. Any corrosion-induced concrete deterioration is not likely to reach a point where repair or rehabilitation will be required during the expected service-life of the structure.

However, the concrete quality can be compromised by either chemical or mechanical means. Chemical means are chloride diffusion and carbonation, and the primary mechanical means is cracking. Cracks in concrete allow water, oxygen and chlorides to enter the concrete at a faster rate, and to reach the reinforcing steel sooner than by the diffusion process alone [63,64].

The deterioration of RC structures in aggressive corrosive regions is predominately exhibited in the form of reinforcement corrosion accompanied by severe spalling of cover concrete. Therefore, concrete structures should be designed with design requirements for structural durability specified as a priority to ensure an acceptable useful service-life of a RC structure in view of the factors affecting service-life [65].

Further, the material variables to be considered should include: cement type, mineral admixture, fine aggregate, coarse aggregate, and water-to-cementitious materials ratio, while the measured variables include: rapid chloride permeability, compressive strength, electrical resistivity, corrosion rate, and finally the chloride concentration at the reinforcing steel surface resulting from diffusion through the concrete. The major factors affecting the service-life of RC members are briefly outlined in the following sections.

2.5.1 Water-to -Cementitious Material Ratio (w/cm)

The depth of chloride penetration increases with an increase in the w/cm [66], while carbonation depth and oxygen diffusion into the concrete was also found to be increasing with it [67]. Permeability of concrete, which is mainly affected by the w/cm, is considered to be the pre-eminent criterion governing its durability [68]. Concrete permeability plays an important role in the deterioration of concrete when it is exposed to aggressive agents. Changes in the w/cm do not significantly influence resistivity at an earlier stage. The electrical resistance of concrete at 28 days with w/cm varying from 0.30 to 0.50 has been shown in tests to be similar, but significantly altered at 90 days [69]. The resistivity of concrete with a w/cm value of 0.3 is much higher than the resistivity of concretes with values of 0.4 or 0.5 at 90 days [69].

The Federal Highway Administration (FHWA) [69] report on “Material and Method for Corrosion Control of Reinforced and Prestressed Concrete Structures in New Construction” states that a w/cm generally makes concrete less permeable. In addition, a reduced w/cm only is not enough to produce concrete with low permeability, the proper gradation and type of fine and coarse aggregates and mineral admixtures that have a higher

resistance to chloride penetration are equally indispensable in ensuring that concrete is less permeable. A reduction in w/cm and the use of latex polymer modifiers or mineral admixtures, especially silica fume, are very effective strategies for reducing the permeability of the hardened concrete. With adequate cover, concrete with lower value of w/cm perform better than those with a higher value.

Clear [70] reported the adverse effect of increasing w/cm on the chloride penetration deeper within the concrete matrix as indicated in Figure 2.5. It was observed that a low w/cm is not, however, sufficient to ensure low permeability. The concrete should be equally well cured and consolidated. Figure 2.6 shows the importance of proper consolidation at different w/cm on the concrete permeability.

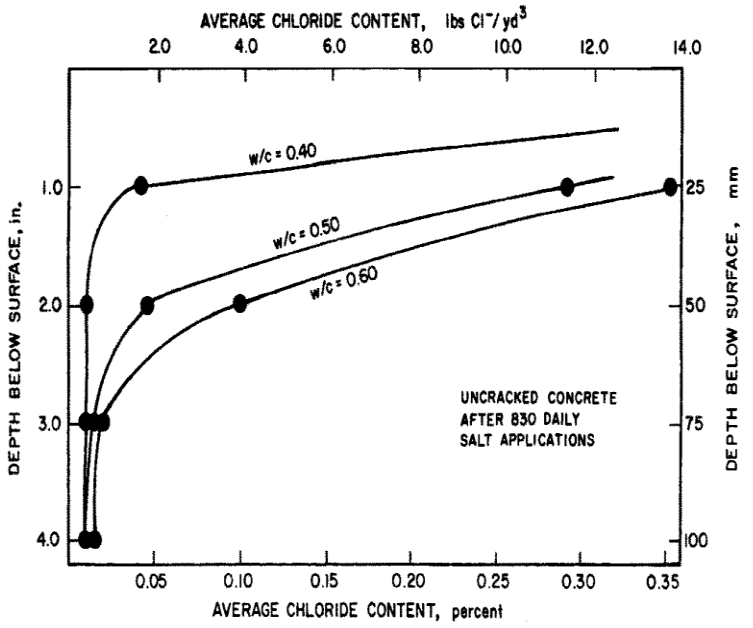

Figure 2.5: Effect of water-cementitious material ratio (w/cm) on salt penetration [70].

For instance, concrete with a w/cm ratio of 0.32 but with poor consolidation is less resistant to chloride-ion penetration compared to good consolidated concrete with a value

of 0.60. Goto and Roy [71] have found a 100-fold increase in the permeability of hardened cement paste when the w/cm was increased from 0.35 to 0.45. Al-Saadoun *et al.* [72] have observed that *the time to initiation of reinforcement corrosion in concrete* with a w/cm ratio of 0.4 was 2.15 to 1.77 times that noted in concrete with a value of 0.55, under the same accelerated corrosion environment.

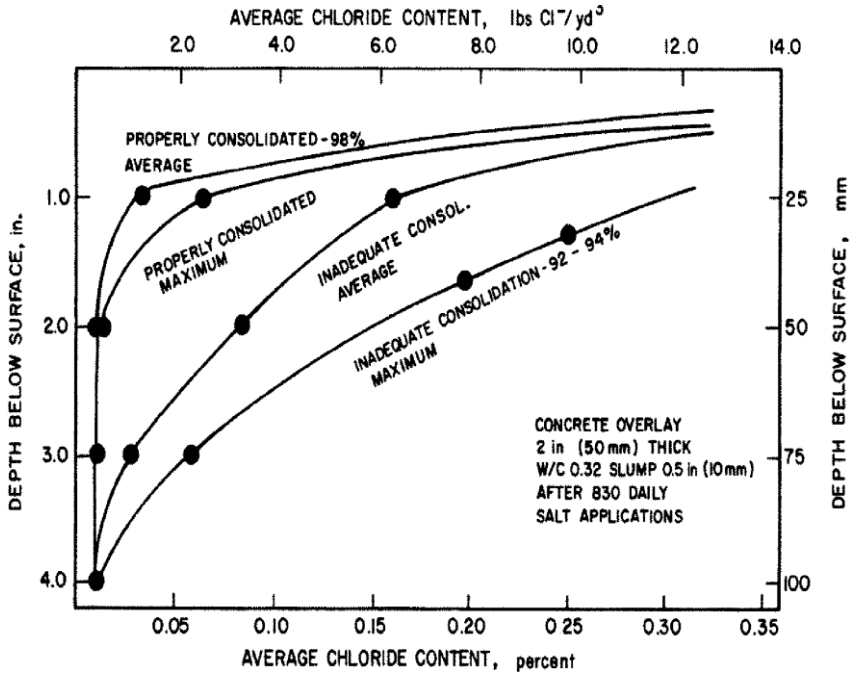

Figure 2.6: Effect of inadequate consolidation on salt penetration [70].

Al-Amoudi [73] also reported that the permeability is significantly reduced for a w/cm below 0.45. It is particularly noted that the w/cm should be less than 0.45 and preferably around 0.40 to obtain a durable concrete and a suitable percentage of admixtures may be added to obtain the desired workability. The relatively low w/cm improves the concrete impermeability, which in turn reduces the chloride penetration, carbonation penetration, and oxygen diffusion in concrete.

ACI 222 [8] pointed out that the porosity and the rate of penetration of deleterious species are directly related to the w/cm, and for high performance concrete, the ratio is generally less than 0.40 and can be as low as 0.3 with the use of suitable water-reducing admixtures. ACI 201.1 [74] and ACI 211.1 [75] contain recommended values for water-cementitious material ratio. The two documents recommended that w/cm ratio should not exceed 0.40 for concrete exposed to chlorides from seawater, deicing salts, and other sources.

2.5.2 Cementitious Material Content

The cementitious content in concrete has a significant effect on its durability. Inadequate amounts of cement may result in loss of strength, and the development of honeycombs within the concrete microstructure as a result of improper bonding of the concrete constituents. The honeycombs worsen the penetration and diffusion of corrosion-causing agents (i.e. Cl^-, H_2O, O_2, CO_2, etc.) in concrete [76]. This initiates the reinforcement corrosion due to the formation of differential cells. Further, the concrete with low cement content has a lack of plastic consistency and alkalinity. The formation of a stable passive layer against corrosion on the surface of the reinforcing bars is retarded [77].

Moreover, the cement paste formed by the hydration reactions contains pores of different sizes. These include the gel and capillary pores. The interlayer spacing within the calcium silicate hydrate (C-S-H) (gel pores) have a volume equal to about 28% of the gel and dimensions ranging from a few fractions of a nanometer (nm) to several millimeters (mm). These effects do not affect the durability of concrete and its protection of the reinforcement, because they are too small to allow the significant transport of aggressive

species. The capillary pores are voids not filled by the solid products of hydration of hardened cement paste. They have dimensions of 10-50 nm if the cement paste is well hydrated and produced with low water-cementitious material ratios but they can reach 3-5 μm if the concrete is made with high water-cementitious material ratios or is not well hydrated. Capillarity is relevant to the durability of the concrete and its protection of the rebars [13].

There is increasing evidence to show that the reaction of C_3A with chloride is only one of the several mechanisms for effective removing chloride ions from solution. This reaction removes chlorides from the porewater, and it reduces the amount of free chlorides available to participate in the depassivation and corrosion processes. The amount of free chloride ions in the porewater is more important than the amount of total chloride ions [69]. In ordinary Portland cements (OPC), there is no direct relationship between the concentration of chloride ions and C_3A content. There is, however, a qualitative relationship with the combination of both tricalcium aluminate (C_3A) and tetracalcium aluminoferrite content (C_4AF) and pH of the pore solution [78].

Mehta [79] has cited several examples of concrete sea structures built with high C_3A cements that showed excellent durability performance because they were prepared with rich mixes in conjunction with attendant low w/cm. On the other hand, structures prepared with lean mixes deteriorated prematurely. Therefore, due to the beneficial role of C_3A in binding chlorides and reducing the chloride ion diffusivity, as stated above, the cement with high C_3A content is preferred from the durability point of view. The beneficial effect

of C_3A content of cement on the chloride binding was also reported by Maslehuddin [80] and Hussain [81].

Page *et al.* [82,83] reported 2.5 times higher diffusivity of chloride ions in hardened cement paste prepared with Type V cement compared to that prepared with Type I cement. Thus, the conjoint effect of higher chloride complexing ability and of the reduced chloride ion diffusivity of high C_3A cements enables them to perform better than low C_3A cements in terms of corrosion protection.

While high C_3A cements are preferred from the reinforcement corrosion point of view, such cements are susceptible to sulfate damage when exposed to soil and ground water contaminated with chloride/sulfate soils [84,72]. In such situations, the use of Type V cement does usually provide adequate protection against sulfate attack, but it would fail to remove free chlorides to any extent, for the simple reason that up to 8% C_3A in the cement is preferentially consumed by the 4 to 5% gypsum typically added to all Portland cements to regulate the setting time. In such situations, a useful approach would be to generally specify, for both substructures and superstructures, a moderate C_3A (8 to 9%) cement modified with suitable supplementary cementing materials. Such cement would be simultaneously resistant to sulfate attack and chloride-induced reinforcement corrosion.

Rasheeduzaffar *et al.* [85] evaluated the effect of cement content on concrete durability and they recommended the minimum cement contents for foundation structures and superstructures (not exposed to direct sulphate/chloride attack) and for superstructure (exposed to direct marine influence) to be 325-350 kg/m^3 and 350-375 kg/m^3 respectively. The importance of minimum cement content for the production of durable concrete is now

recognized by the international codes of practices, and limits on these values based on the service environment are recommended [65].

2.5.3 Supplementary Cementing Materials

ACI 116 [86] defines the term admixture as “a material other than water, aggregate and hydraulic cement and fiber reinforcement, used as an ingredient of a cementitious mixture to modify its freshly mixed, setting, or hardened properties, and that is added to the batch before or during its mixing”. In ACI 212.3R [87], it is stated: “chemical admixtures are used to enhance the properties of concrete and mortar in the plastic or hardened state. These properties may be modified to increase the compressive and flexural strength at all stages, decreasing permeability and improve durability, inhibit corrosion, reduce shrinkage, accelerate or retard initial set, increase slump and workability, increase finishability and pumpability [88].

The pozzolanic materials (mineral admixtures), when added to concrete, improve the workability by reducing segregation and bleeding, and they reduce the heat of hydration as well as the damaging expansion resulting from sulfate attack and cement-aggregate reactivity. The effect of fly-ash addition on the corrosion-resisting characteristics of concrete was evaluated by Maslehuddin *et al.* [89]. They indicated that 20% cement-replaced fly-ash concrete performed better in resisting reinforcement corrosion compared to plain cement concrete. Moreover, chloride binding is enhanced by the presence of fly-ash even if the fly-ash does not contain C_3A. Mineral admixtures can be used to enhance the corrosion-control potential of the concrete by reducing permeability. Some commonly

used admixtures include fly-ash, blast furnace slag, and silica fume. The additional calcium silicate hydrate (C-S-H) that the mineral admixtures contribute leads to a reduction in the permeability and in the chloride diffusion rate. The availability of hydroxyl ions (OH^-) is typically expected to decrease [69].

The FHWA in America defined silica fume as a by-product of silicon metal and ferrosilicon alloy production. Silica fume consists of fine glassy spheres with a specific surface area of 20,025 m^2/kg. The specific surface area of Portland cement is 300 to 400 m^2/kg. The particle size of silica fume allows it to fit into the small spaces usually occupied by water, which results in a denser matrix [69]. The literature reports contradictory results on the effect of silica fume on chloride binding [90], but there is a general consensus that limited amounts of silica fume are beneficial in providing resistance to chloride-induced corrosion, primarily by reducing the permeability of concrete [8].

Gjrov [14] reported that silica fume additions consistently and significantly reduce the concrete permeability, and the most significant improvement was observed in low cement content concrete. Hussain [81] showed that the average pore radius is reduced from 285 Å to 181 Å with 10% silica fume blending. Similar results were obtained by Kumar *et al.* [91] for a paste prepared with 0.4 water-to-solid ratio. The median pore size was reduced from 15 nm to 7.5 nm and the coefficient of chloride diffusion was reduced from 227 x 10^{-13} m^2/s to 22 x 10^{-9} m^2/s for 10% silica-fume blended cement paste.

2.5.4 Aggregate Quality, Size and Grading

According to ACI Education Bulletin E1-99 [92] aggregate may be broadly classified as natural and artificial or synthetic, with respect to both source and method of preparation. Natural sand and gravel are the products of weathering, and the action of wind or water, while stone sand and crushed stones are produced by crushing natural stone. Screening and washing may be used to produce aggregates from either of these categories. Aggregate may be produced from igneous rock, sedimentary or metamorphic rocks, but the presence or absence of any geological type does not, by itself, make an aggregate suitable or unsuitable for use in concrete. The acceptance of aggregate for use in concrete on a particular job should be based upon specific information obtained from tests used to measure the aggregate quality, or upon its service record or both.

A typical consensus specification for concrete aggregates, both fine and coarse is ASTM C33 [93]. Synthetic aggregates may be either by-products of an industrial process such as blast furnace slag (BFS) or products of processes developed to manufacture aggregate with special properties, such as expanded clay, shale or slate that are used for lightweight aggregates. Some lightweight aggregates, such as pumice or scoria, also occur naturally.

Aggregates composed mainly of coarse-grained silicate minerals, such as quartz and feldspar, are known to produce weaker bonds with cement paste than calcareous rocks, such as limestone and dolomite. Differential thermal expansion and stiffness characteristics between the cement paste and aggregate contribute to the development of micro-cracking at the interface, leading to more permeability of concrete. This mainly results from the thermal incompatibility of the concrete constituents when there are large fluctuations in the

daily temperature and humidity. Such conditions typically prevail in the Arabian Gulf regions.

The aggregate shape also influences the concrete permeability. The use of elongated and flaky aggregates significantly increases the permeability by trapping sizeable mobile bleed water and air bubbles under their flat surfaces, thereby producing very porous under-aggregate fissures and zones. This results in a weak transition zone, in which micro-cracks can easily form. These micro-cracks are influential contributing factors that unfavorably increase the permeability of concrete [94].

Both the aggregate size and grading affect concrete durability. The maximum size of the aggregate is of considerable significance, as the mix water decreases with its increase due to a reduction in the surface area. Keeping this in view, Cordon and Gillespie [95] have recommended the following maximum size of aggregates:(i) 37.5 mm (1½ inch) for 35 MPa (5000 psi) concrete; (ii) 19 mm (¾ inch) for 42 MPa (6000 psi) concrete, and (iii) 10 mm to 12 mm (⅜ to ½ inch) for concrete of strength above 42 MPa (6000 psi).

Aggregates of different sizes may give different concrete strengths for the same w/cm ratios. Concrete with smaller maximum size aggregate has higher compressive strength. If compressive strength in excess of 35 MPa is required, an aggregate having a maximum size of 19 mm or smaller may be the most efficient in that its use will require the least amount of cement to produce the required strength [87]. For a given w/cm, coefficient of permeability of concrete increases considerably with the increasing size of aggregates, due to the increase in the transition zone [96].

The proportioning of coarse and fine aggregates is also important for the production of a workable and durable concrete. The aggregate proportioning for this purpose consists of fixing the optimum volume fraction of sand in the total aggregate content. Maslehuddin [97] revealed that both "too high" and "too low" sand reduces the workability of concrete. The optimum proportioning for a maximum workability was reported to correspond to a specific surface area of the combined aggregates in the range of 70 to 75 cm^2/cm^3 for concrete with a cement content in the range of 300 to 390 kg/m^3 [97]. This enhanced workability, on account of an optimum aggregate grading, allows a reduction in the water-cementitious material ratio, resulting in increased strength and durability of the concrete.

2.5.5 Concrete Cover over Reinforcing Bars

Cover thickness is an important major factor to reduce or delay the initiation and corrosion time in RC in an aggressive environment, provided the concrete is of good quality. By implication, it will take a longer time for the aggressive substances, such as chloride, moisture or carbondioxide, to migrate to the rebar surface. In RC structural members, exposed to chlorides and subjected to intermittent wetting, the degree of protection against corrosion is determined primarily by the depth of concrete cover to the reinforcing steel and the permeability of concrete [98]. The concrete-cover depth has a significant effect on corrosion either due to carbonization or penetration of chlorides or [99]. This effect is limited, within the time of casting, to the time at which the rebar is depassivated, after which the rebar corrosion is initiated. Once it has started, the rate of corrosion is independent of the cover thickness [100].

The concrete cover significantly influences the time-to-corrosion of the steel reinforcing bars, and its quality influences the diffusion rate of chloride ions through the concrete. Since this diffusion is non-linear with increasing cover thickness, there is a significant increase in the time required for chloride ions to reach the steel reinforcing bars [69]. Estimates of the increase in corrosion protection provided by an increase in concrete cover have ranged between slightly more than a linear relationship [to as much as the square of the cover [101].

Corrosion protection by concrete cover is a function of both depth of concrete cover and w/cm. McDonald [102] observed that a concrete cover of 25 mm (1 in.) is inadequate in severe environments, even with a w/cm as low as 0.30. Adding silica fume, however, made the 25 mm (1 in.) concrete cover more effective for corrosion prevention. The time to spalling after the initiation of corrosion is a function of the ratio of concrete cover to bar diameter, the reinforcement spacing, and the concrete strength [98].

One of the easiest methods of improving corrosion protection of steel reinforcement is to increase the amount of concrete cover. The minimum cover for reinforcement in most concrete structures not exposed to weather is 19 mm (3/4 in.). As the risk of corrosion increases, so does the required concrete cover. Because development length of reinforcing bars is known to be a function of cover [103], larger than minimum concrete cover may be desirable, even if there is little risk of corrosion. Where concrete will be exposed to external sources of chlorides in service or to other aggressive environments, however, a minimum concrete cover of 50 mm (2 in.) for walls and slabs and 64 mm (2-1/2 in.) for other members is required by ACI 318 for corrosion protection.

Since 1974, the American Standard Highway Transport Officials (AASHTO) standard specifications for Highway Bridges has required a minimum concrete cover for reinforcing steel embedded in concrete with direct exposure to seawater to be 100 mm (4 in.), and to be 75 mm (3 in.) for concrete cast against the earth [104]. The significance of concrete cover thickness in concrete durability can be better understood from the Table 2.5 generated by Bertolini *et al.* [13].

Table 2.5: Recommended minimum values of concrete cover thickness [13].

Exposure condition		Minimum cover thickness, mm	
		Reinforced Concrete	Prestressed concrete
No risk of corrosion or other attacks		10	10
Carbonation-induced corrosion	Dry or permanent wet	15	25
	Wet, rarely dry, moderate humidity	25	35
	Cyclic wet and dry	30	40
Chloride-induced corrosion	Exposed to air borne salt but not in direct contact with sea water, moderate humidity	35	45
	Permanently submerged, wet. Rarely dry	40	50
	Tidal, splash and spray zones, cyclic wet and dry	45	55

2.6 REINFORCED CONCRETE CONSTRUCTION PRACTICES

2.6.1 Mixing and Transporting Concrete

Fresh concrete used in structures containing embedded metals at the time of placement should be a homogeneous mixture of the concreting materials specified in the mixture design. The measuring, mixing, and transporting of the concrete should be in accordance with ACI 301 [105] and the procedures outlined in ACI 304R [106]. To ensure the accurate measurement of materials, batching equipment should meet the requirements of ASTM C 94 [107].

2.6.2 Placement of Concrete and Steel

a) Formwork

Concrete formwork should be designed with sufficient strength and rigidity to support loadings and lateral pressures caused by the concrete, equipment, and workers. Not only should the formwork have the strength to support the concrete during construction and maintain its configuration, but it should also have sufficient strength to maintain tolerances for the reinforcing steel cover or resist excessive deflections that can cause cracking. For example, excessive deflections in slab formwork can create areas of low concrete cover that will be more susceptible to cracking above the low-cover reinforcing bars. The cracks would be potential entry points for water and chloride-ion that could lead to extensive corrosion in a period of few years in a corrosive environment.

The concrete formwork should be mortar-tight to avoid leakage of cement paste during consolidation. In regions of congested steel, the spaces between bars should be designed to allow the concrete to be placed while reducing the possibility of honeycombing [8].

b) Reinforcing Steel

Reinforcing steel bars should be placed to the configuration shown in the design drawings. The specified tolerances should be followed, with particular attention paid to concrete cover and closely spaced reinforcing. The cover requirements specified in ACI 318 and ACI 201.2R [74] are the minimum.

c) Concrete Placement

Concrete should be properly placed to protect the steel components from future corrosion. Workmanship is important, and a worker's attention to the concrete placement will have a great effect on the quality and performance of the concrete member. The guidelines for cold-weather (ACI 306R) or hot-weather protection (ACI 305R) should be considered before any concrete is placed. During placement, the concrete should be placed so that segregation of aggregate and mortar is minimized. The formation of voids should be avoided as they can lead to cracking and loosely placed concrete, resulting in a high porosity. Voids can be avoided with advance planning, proper mixture proportioning, and proper placement techniques.

d) Influence of Consolidation on Permeability

Properly consolidated concrete is better able to resist the penetration of moisture, ions, gases, and other deleterious substances than in concrete that has been poorly consolidated.

Strength does not contribute to the corrosion-resistant properties of concrete, but a weak concrete may fail to sustain loads for which the structure was initially designed, leading to cracking, spalling, and disruption of protective cover, thereby exposing embedded metals to corrosive agents. A number of studies, for instance Kaplan [108], and Whiting and Kuhlman [109] have demonstrated that compressive strength is reduced by 30% for only a 5% decrease in the degree of consolidation. Bond to reinforcing steel is reduced even more dramatically and a loss of approximately 50% in bond strength results from a 5% reduction in consolidation.

An example of the effect of consolidation on permeability of concrete to chloride ions is shown in Figure 2.7. The figure represents three mixtures with cement contents ranging from 310 to 360 kg/m^3 (520 to 610 lb/yd^3) that were consolidated on a laboratory vibrating table. The group labelled “100” was consolidated in accordance with procedures described in ASTM C 192 [110]. Those labelled “102” were given an extended period of vibration. Those mixtures given less consolidation (96 and 92) showed an increase in coulomb charge passed as measured by AASHTO T277 [111].

Clear and Hay [112] showed that the performance of mixtures specifically designed to have low permeability, such as low slump dense concrete (LSDC), can be compromised if full consolidation is not achieved, because much greater amounts of chloride ions would penetrate into the concrete, compared with a properly consolidated mixture.

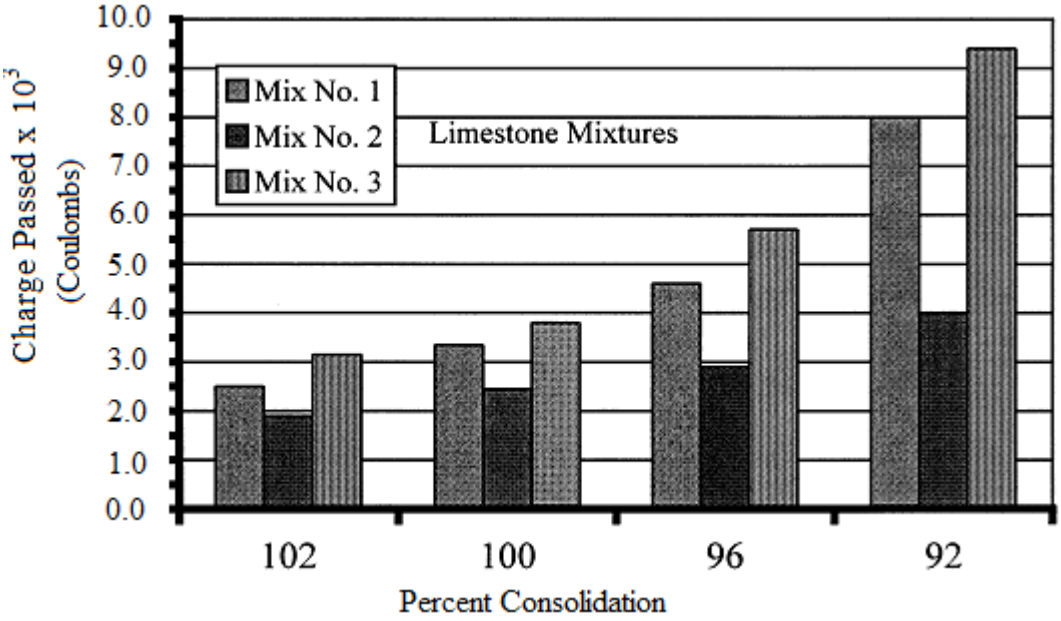

Figure 2.7: Effect of degree of consolidation on rapid chloride permeability of limestone concrete mixtures [109].

The increase in permeability to chloride ions brought about by poor consolidation would make it easier for moisture and oxygen to enter the concrete, thus promoting rapid onset and progress of corrosion. In extreme cases, honeycombing that extends to the level of the reinforcement, or large voids in the vicinity of the reinforcement, would remove virtually all protection offered by the concrete to the steel, and corrosion would proceed as if the steel was not embedded in the concrete at all.

2.6.3 Influence of Curing on the Corrosion of Reinforcing Steel

ACI Committee 308 has proposed the following definition: "Curing is the maintaining of a satisfactory moisture content and temperature in concrete during its early stages so that desired properties may develop" [113]. In normal construction, the desired properties usually include strength, elastic modulus, and freezing-and-thawing resistance. Adequate

curing brings about improvement of porosity and pore-size distribution. This enhances prevention and delay of onset of the corrosion of reinforcing steel. The concrete properties that develop as a consequence of curing include high electrical resistivity and impermeability to liquid water, water vapour, chloride ions in solution, oxygen, and carbon dioxide.

With adequate and continued temperature and moisture control, not only does the strength of concrete increase but the porosity decreases, the remaining pores become increasingly smaller, the electrical resistivity becomes higher, and the permeability to both liquids and gases becomes lower. Therefore, through proper curing, the internal resistance that concrete provides against corrosion of reinforcing steel is enhanced.

Similarly, the corrosion-resisting properties of concrete will not develop to their expected values if adequate curing is not provided. Whiting and Kuhlmann [109] demonstrated that chloride permeability, as measured by AASHTO T 277 [111], was strongly influenced by the curing duration. Their tests also demonstrated that "measurements of permeability of concretes cured under standard laboratory conditions may be optimistic, and the permeability of field-cured concrete is significantly greater than that of comparable laboratory specimens."

Saricimen *et al.* [114] evaluated the effect of curing on the permeability of plain and pozzolanic concrete. They reported that continuous water curing is necessary for reducing the permeability of both plain and pozzolanic concretes. The fly-ash concrete exhibited lower permeability than the plain concrete after about a week of curing [114]. Powers *et al.* [115] studied the relationship between curing and permeability. In laboratory tests, they

evaluated the duration of continuous wet curing required to develop cement pastes to the point of being essentially impervious to water under low pressure because the capillary system had become discontinuous, as shown in Table 2.6.

Table 2.6: Wet-curing duration time to achieve capillary discontinuity [115].

W/cm ratio of cement paste	Duration of wet-curing for Type I cement at 23 °C (73 °F) to achieve capillary discontinuity
0.40	3 days
0.45	7 days
0.50	14 days
0.60	6 months
0.70	1 year
Greater than 0.70	Impossible

2.7 SERVICE-LIFE PREDICTION MODELS

During the past decades, many investigations have been conducted to evaluate the chloride diffusion parameters in concrete, and some mathematical and empirical models have been introduced to estimate the time to corrosion initiation and propagation [116]. The first numerical model was developed by Collepardi, who used Fick's second law of diffusion and suggests that the *diffusion coefficient* (D_{app}) is one of the most important parameters in the service-life prediction [117]. Tutti's model was one of the first attempts to predict the service-life of RC structures. The main idea of this model, as shown in Figure 2.8, is to divide the service-life of the structure into two life spans: the time to corrosion initiation (t_{init}); and the time for corrosion propagation before repair (t_{prop}) [118].

In Europe, a highly developed service-life design model, *DuraCrete*, has been developed that uses a probabilistic approach for durability-based design [119]. *Condur* and *Stadium* are examples of more sophisticated durability models developed in North America [120].

The *former* considers the coupling effect of heat, moisture, and chloride transfer in concrete simultaneously, while the *latter* is based on the ionic interaction of various substances in concrete pore solution and their corresponding effect on chloride penetration through concrete [121].

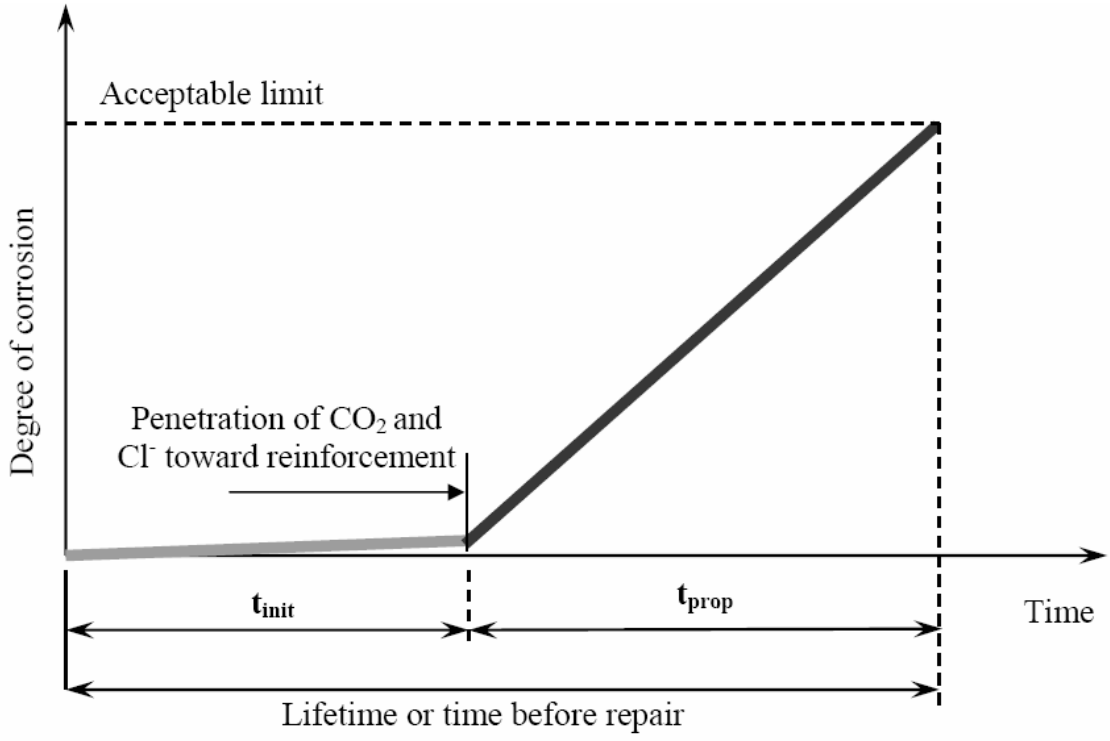

Figure 2.8: Schematic illustration of Tutti's model [118].

2.7.1 Chloride-Induced Corrosion Models

Browne [122] proposed a basis for design that takes into account chloride diffusion and steel corrosion. He cited two critical times, t_1 and t_2, in the life of a structure, where t_1 is the time from new concrete to the onset of corrosion, and t_2 is the time from corrosion onset to the occurrence of damage. In other words, reinforcement corrosion takes place in two main stages: initiation stage (t_p) and propagation stage (t_{corr}). The *initiation stage* of reinforcement corrosion is the time period, during which the aggressive species (i.e.,

carbonation or chloride or both) from the exposure environment penetrate into the concrete cover, thus causing destruction of the passivity layer of rebars against corrosion and thereby resulting in the initiation of reinforcement corrosion. *The propagation stage* starts after initiation of reinforcement corrosion and counts the time period during which various damage consequently takes place. These damages include: cracking; spalling and delamination of the concrete cover; collapse due to the combined effect of reduction in steel cross-sectional area; and loss in bond between steel and concrete. A simplified model for reinforcement corrosion, comprising initiation and propagation stages is graphically shown in Figure 2.9 [123].

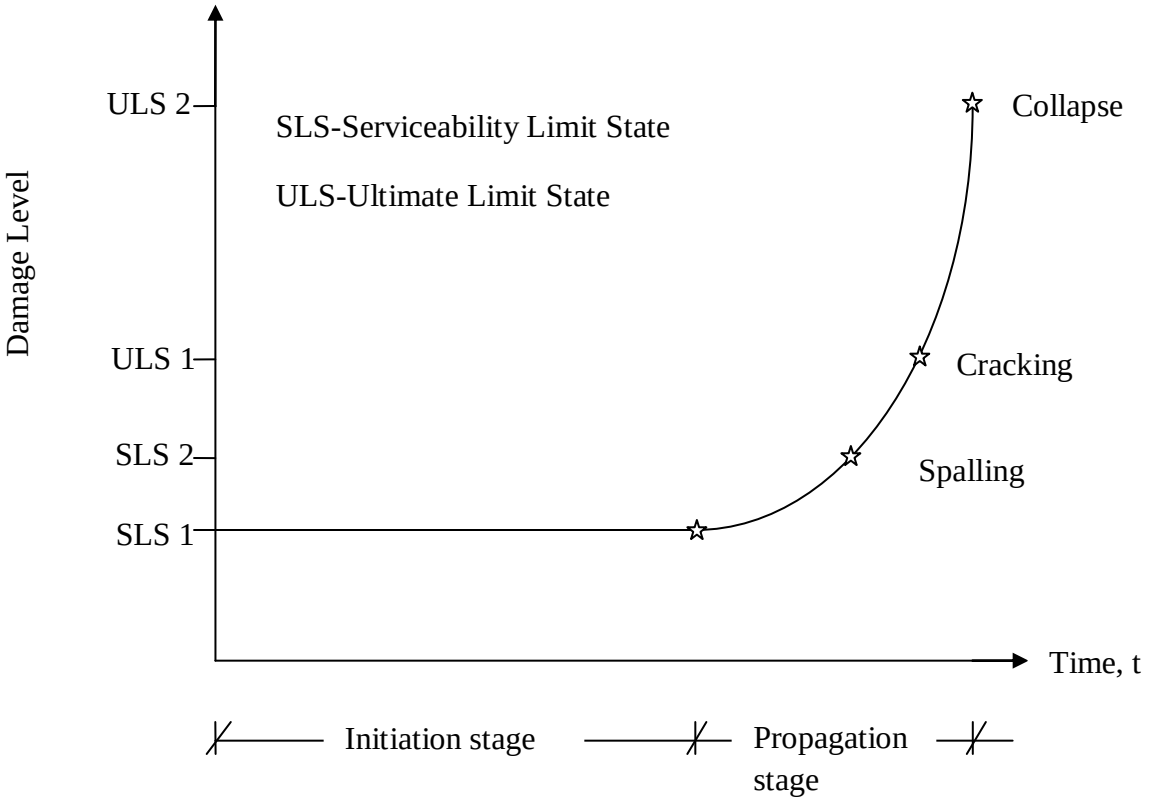

Figure 2.9: Simplified corrosion model for steel in concrete [123].

a) Chloride Penetration Modelling

The chloride penetration rate, C(x,t) as a function of depth from the concrete surface and time can reasonably be represented by Fick's second law of diffusion, according to the following partial differential equation. [124]:

$$\frac{\partial C}{\partial t} = D_c \frac{\partial^2 C}{\partial x^2} \quad \text{... (2.12)}$$

Considering the following initial boundary conditions:

C(x,t=0)=0

C(x=0, t>0) =C_s

C(x=∞, t>0) =0,

the solution for this differential equation is expressed in terms of chloride ions content of concrete surface and the error function *erf (z),* such that:

$$C(x,t)=C_s\left[1-erf\left[\frac{x}{2(D_{app}t)^{0.5}}\right]\right] \quad \text{... (2.13)}$$

where: C(x, t) = Cl^- content (% by mass of cement or concrete) at time, *t* (sec) and at depth x (m) from the surface of concrete

C_s = Cl^- content at surface of concrete (% by mass of cement or concrete)

D_{app}= apparent diffusion coefficient for chloride (m^2/s)

$$z = \frac{x}{2(D_{app}t)^{0.5}}$$

$$erf(z) = \frac{2}{\sqrt{\pi}} \int_0^z e^{-t^2} dt$$

The above model for chloride penetration may be simplified by using a parabola function, as follows:

$$C(x, t) = C_s \left[1 - \frac{x}{2(3D_{app}t)^{0.5}} \right]^2 \quad \text{.... (2.14)}$$

Equation 2.14 is an approximation to simplify Fick's model analytical solution. The two solutions are compared in Figure 2.10 for different depth of chloride penetration inside the concrete matrix.

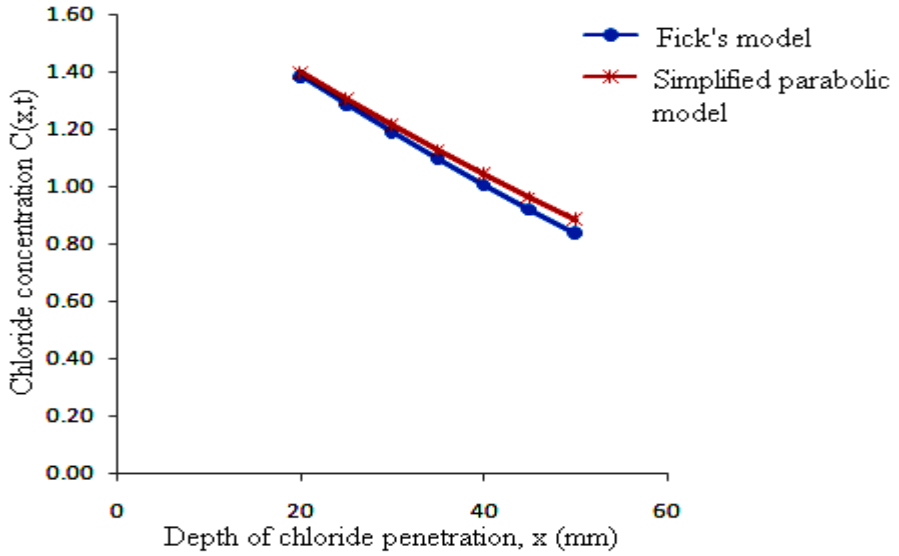

Figure 2.10: Relationship between Fick's model analytical solution and simplified parabolic model at constant time, t and diffusion coefficient, D_{app}.

The model developed by Al-Kutti [125] for diffusion coefficient (D_{app}) for silica fume blended concrete can be used to determine the value of chloride diffusion coefficient, D_{app}, as given by Eq. 2.15:

$$D_{app} = 5.73R_{w/cm} - 0.006Q_C + 1.29 \quad \text{... (2.15)}$$

where: D_{app} = chloride diffusion coefficient of silica fume concrete in 10^{-12} m^2/s

$R_{w/cm}$ = w/cm ratio (by mass)

Q_C = cementitious materials content in kg/m^3

b) Model for Time of Corrosion Initiation Due to Chloride Penetration

From Eq. 2.14, the *model for the time to corrosion initiation* (t_p) may be obtained by using the chloride penetration model, in which t may be equated to t_p in the Eq.(2.14) to simplify the expression for the calculation of time of corrosion initiation, t_p.

x = cover thickness (cv), and

$C(x, t)$ = threshold chloride concentration (C_{th}), as follows:

$$t_p = \frac{1}{12D_{app}}\left[\frac{cv}{1-(C_{th}/C_s)^{1/2}}\right]^2 \text{ (parabolic chloride penetration model)} \quad \text{...(2.16)}$$

In Eq. (2.16), the following "normal values" of D_{app}, C_s, and C_{th} may be used:

D_{app} = 10^{-12} to 10^{-11} m^2/s

C_s = 0.3 to 0.4% of Cl^- by weight of concrete

C_{th} = 0.05 to 0.07% of Cl^- by weight of concrete

Once the time to corrosion initiation is known, the time of corrosion propagation (t_{corr}) may be given by Eq. 2.17

$$t_{corr} = \text{design service life} - t_p \quad \text{... (2.17)}$$

for specified target service life

c) Corrosion Rate Modelling (I_{corr})

Ahmad and Bhattacharjee [126] developed the following empirical model for corrosion current density, I_{corr}, for rebars embedded in chloride-admixed concrete ($CaCl_2$ admixed at the time of casting):

$$I_{corr}(nA/cm^2) = 37.73 + 6.12C - 2.23B^2D + 2.72D^2C \quad \text{…(2.18)}$$

where: B = coded level of cement content $= \dfrac{cement\ content\ kg/m^3 - 300}{50}$

C = coded level of admixed $CaCl_2$ content = $\dfrac{\%\ CaCl_2\ by\ cement\ weight - 2.5}{1.25}$

D = coded level of water-cementitious material, w/cm, ratio= $\dfrac{w/cm\ by\ mass - 0.65}{0.075}$

The coded values-scaling was used to minimize the variables deviations and to improve the fitted data accuracy.

2.7.3 Determination of the rate of Loss of Concrete and Steel

a) Model for Concrete Rate of Loss of Concrete

The model for evaluating the rate of deterioration of surface concrete subjected to aggressive exposure conditions, excluding frost attack, is given as follows [127];

$$C_r = \frac{C_{env}.C_{cur}}{f_{ck}^{3.3}} \qquad ...(2.19)$$

where: C_r = the rate of loss of structurally effective concrete (mm/year)

C_{env} = the environmental coefficient

C_{cur} = the curing coefficient

f_{ck} = the characteristic cubic compressive strength of concrete at 28 days (MPa)

The C_{env} in the Gulf region within latitude 10^o-30^o can be assumed to be within the range of 0.1 x 10^5 to 5 x 10^5 [127]. The curing coefficient, c_{cur}, may be calculated by using the following equation [128].

$$c_{cur} = \frac{1}{0.85 + 0.17\log_{10}(d)} \qquad ...(2.20)$$

where: d = the curing time (days)

The rate of loss of structurally effective concrete, C_r, is calculated by using Eq. 2.19. Then loss of surface concrete, $\Delta c(t)$, leading to reduced cross-sectional area of concrete, at any exposure time, *t*, may be calculated by using Eq. 2.21, as follows:

$$\Delta c(t) = C_r.t \quad \text{... (2.21)}$$

By using $\Delta c(t)$ calculated from Eq. 2.21, the residual width $b'(t)$ and the residual depth $h'(t)$ of the concrete member at any exposure time, *t*, may be calculated by using Eqns. 2.22 and 2.23, respectively, as follows:

$$b'(t) = b_0 - 2\Delta c(t) \quad \text{... (2.22)}$$

$$h'(t) = h_0 - 2\Delta c(t) \quad \text{... (2.23)}$$

where: b_o and h_o are the original width and depth of the member, respectively.

b) Model for calculating reinforcement corrosion penetration rate:

The corrosion rate expressed as corrosion penetration per unit time, termed as corrosion penetration rate (P_r) can be determined by using the corrosion current density, I_{corr}, as follows [129]:

$$P_r = \left(\frac{W}{F \rho_{st}} \right) I_{corr} \quad \text{... (2.24)}$$

where:

W = equivalent weight of steel = 55.85/2 = 27.925 g

F = Faraday's constant = 96500 Coulombs = 96500 Amp-s

ρ_{st} = density of steel (7.85 g/cm^3)

I_{corr} = corrosion current density (usually expressed as μA/cm^2)

The P_r, is calculated by using Eq. 2.24, the loss of the rebar diameter $\Delta\phi(t)$ leading to a reduced cross-sectional area of steel at any exposure time *t* may be calculated by using Eq. 2.25,

$$\Delta\phi(t) = P_r.t \quad \text{... (2.25)}$$

By using $\Delta\phi(t)$ calculated from Eq. 2.25, the reduced diameter of rebar $\phi'(t)$ at any exposure time *t* may be calculated by using Eq. 2.26,

$$\phi'(t) = \phi_0 - 2\Delta\phi(t) \quad \text{... (2.26)}$$

where ϕ_0 is the original diameter of rebar.

2.8 STRUCTURAL DURABILITY DESIGN

Sarja and Vesikari [130] have proposed methods for structural durability design of RC members. In these methods, the loss of concrete and steel sections due to deterioration was considered for a given design service-life of the concrete structures. The cross-sections of concrete and steel, required to satisfy serviceability requirements, were increased to satisfy durability requirements.

CHAPTER 3

METHODOLOGY OF RESEARCH

3.1 EXPERIMENTAL PROGRAM

The primary objective of this work is two-fold: (i) to develop models for strength of concrete and rate of loss of bar diameter due to corrosion by using the experimental data obtained through testing concrete specimens prepared with aggregates from two different sources within in Saudi Arabia (*namely*: Western province-Taif quarries and Eastern province-Riyadh road), and (ii) to utilize these models for an optimal design of RC beams and columns. An experimental program was designed to achieve those two objectives through the following five main steps:

1. Cast several cylindrical concrete specimens, with/without centrally placed 16 mm reinforcement, with different cover, fine to total aggregate ratio and w/cm, with additional 8% silica fume.

2. Conduct the compression test on the plain cylindrical concrete specimens, and determine the corresponding elastic modulus, by simultaneously measuring the failure loads and corresponding strains.

3. Measure the current density by using linear polarization on cylindrical RC specimens in several rounds.

4. Statistically analyze the performance of the test specimens prepared from the two aggregates. The analysis of the data is obtained from compressive strength tests and electrochemical corrosion measurements compiled in steps 2 and 3.

5. Study the compiled experimental data closely, to develop models for strength of concrete and for rate of loss of the rebar diameter due to corrosion, in order to achieve a durable RC structure for a target service-life.

3.2 MATERIALS

The test specimens were prepared with aggregates procured from two different national quarries (Riyadh road and Taif). Figure 3.1 shows the typical samples of the two aggregates tested and used in the experimental program [131]. Table 3.2 shows the chemical composition of the Portland cement and silica fume used in the preparation of the concrete specimens.

	Dammam (H)	Taif quarries (T)
Coarse aggregates		
Fine aggregates	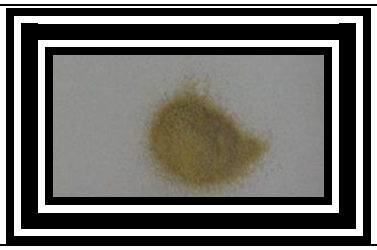	

Figure 3.1: Samples of Taif and Dammam aggregates.

The specific gravity and absorption conducted based on ASTM C128 [132] and abrasion test results of the coarse aggregates in accordance with ASTM C131 are tabulated in Table 3.1. The specific gravity and absorption of fine aggregate (Dune sand) was found to be 2.6 and 0.57%, respectively. Table 3.2 shows the chemical composition of the Portland cement and silica fume used in the preparation of the concrete specimens. Potable water was used for mixing the constituents of all the specimens.

Table 3.1: Specific gravity, absorption and abrasion test results of the coarse aggregates.

Aggregate source	**Specific gravity**	**Water Absorption (%)**	**Abrasion loss (%)**
Dammam (H)	2.55	1.75	28.86
Taif (T)	2.82	1.27	37.84

Table 3.2: Chemical composition of Portland cement and silica fume.

Constituent (wt %)	Type I cement	Silica fume
Silica (SiO_2)	19.92	98.7
Alumina (Al_2O_3)	6.54	0.21
Ferric oxide (Fe_2O_3)	2.09	0.046
Lime (CaO)	64.70	0.024
Magnesia (MgO)	1.84	-
Silicate (SO_3)	2.61	0.015
Potassium Oxide (K_2O)	0.56	0.048
Sodium Oxide(Na_2O)	0.28	0.085
Tricalcium Silicate (C_3S)	55.9	-
Dicalcium silicate (C_2S)	19	-
Tricalcium aluminate (C_3A)	7.5	-
Tetracalcium aluminoferrite (C_4AF)	9.8	-

3.3 CONCRETE SPECIMENS

Un-reinforced cylindrical concrete specimens (size: 75 mm diameter and 150 mm high) were prepared to evaluate compressive strength. For corrosion testing, cylindrical RC specimens with a height of 150 mm and diameters 66 mm, 91 mm and 116 mm, with three different covers thickness (25, 37.5 and 50 mm) were cast including centrally placed steel reinforcing bar and were immersed in a 5% NaCl solution as electrolyte throughout the period of corrosion testing. To avoid crevice corrosion, the bottom and the concrete-air interface of the specimens were coated with an epoxy-coating to 25 mm depth, as shown in Figure 3.2 [133].

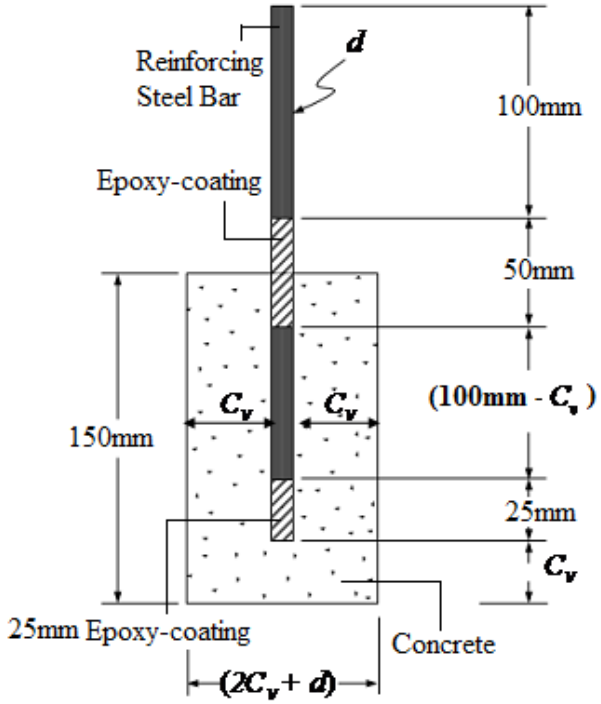

Figure 3.2: Schematic diagram of a typical test specimen used for corrosion assessment.

3.4 PREPARATION OF CONCRETE SPECIMENS

3.4.1 Concrete Mix Design

Concrete mixes were designed according to the *absolute volume method*, and proportioning of materials was carried out on a weight basis. The concrete mixes were prepared with cementitious materials contents of 350, 375 and 400 kg/m^3, with effective w/cm ratios of 0.40, 0.45 and 0.5 and with fine-to-total aggregate ratios of 0.35, 0.4 and 0.45. All the concrete specimens were prepared with 8% silica fume. The following concrete specimens were cast from each concrete mix.

- Un-reinforced cylindrical concrete specimens (size: 75 mm diameter and 150 mm high) for determination of compressive strength.
- Cylindrical specimens with centrally placed 16 mm diameter rebar and geometric dimension of 150 mm height and diameter (2*cover+16) mm for reinforcement corrosion rate measurements.

Superplasticizer was used to improve the workability of concrete mixes, as the w/cm ratio became very low. The variables considered for preparing the cylindrical concrete test-specimens for compressive strength on one hand and corrosion rate on the other, are as shown in Tables 3.3 and Table 3.4 respectively. The total number of unreinforced cylindrical concrete specimens for compressive strength was 162 (that is: [3*3*3*2*1*1]*3 replicates). The total number of the other cylindrical concrete specimens for corrosion rate determination was 1,458 (that is: [3*3*3*2*3*3*1]*3 replicates). Each test specimen had a centrally placed 16 mm-diameter steel bar.

All the concrete specimens were cured in water tanks for a period of 28 days. After that, the compressive strength test specimens were taken out for *test*ing, and the corrosion test specimens were partly submerged in chloride solutions to allow corrosion to take place. Next, the electrochemical technique (Linear Polarization Method) was used to determine the corrosion rate by using a potentiostat (PARSTAT 2273) [134].

3.4.2 Mixing of Concrete and Specimen Casting

Mixing was done systematically. Fine and coarse aggregates were first mixed separately. Silica fume and cement were mixed separately. Then both constituents were mixed with the addition of potable water (mixed uniformly with superplasticizer) to ensure a homogenous mixture of concrete constituents. The constituents were mixed in a revolving drum type of mixer for one minute, after the completion of mixer charging, to obtain uniform consistency and cohesiveness without segregation. After mixing and discharging, the concrete was poured into the oil-applied cylindrical moulds in three layers and the moulds were vibrated over a vibrating table to remove the entrapped air. After casting, the concrete specimens were cured for 28 days in a curing tank under laboratory conditions.

Table 3.3: Variables for compressive strength of concrete test specimens.

Mix Parameter	Levels	No. of Case studies
Effective water/cementitious materials ratio* (by mass)	0.38, 0.43, 0.48 (*H*-aggregate)	3
	0.42, 0.47, 0.52 (*T*- aggregate)	
Cementitious materials content	350, 375, 400 kg/m^3	3
FA/TA ratio (by mass)	0.35, 0.40, 0.45	3
Aggregate type	2 (H and T aggregates)	2
Cement type	1 (Type - I)	1
Mineral admixture	1 (8% Silica fume by weight of cement) (28, 30, 32 kg/m^3)	1

Table 3.4: Variables for reinforced concrete specimens for corrosion rate measurements.

Parameter	Levels	No of case studies
Effective water/cementitious materials ratio* (by mass)	0.4, 0.45, 0.50	3
Cementitious materials content	350, 375, 400 kg/m^3	3
FA/TA ratio (by mass)	0.35, 0.40, 0.45	3
Aggregate types	2 (H and T aggregates)	2
Cement type	1 (Type-1)	1
Mineral admixtures	1 (8% silica fume by weight) of cement) (28, 30, 32 kg/m^3)	1
Cover thickness	25 mm, 37.5 mm, 50 mm	3
Chloride exposure concentration	3%, 7% and 12% NaCl	3

**Note: Considering water absorption of aggregates, gross w/cm 0.38, 0.43 and 0.48 and 0.42, 0.47, and 0.52, for H-aggregate and T-aggregates respectively for were converted into effective w/cm of, respectively of 0.40, 0.45 and 0.50.*

3.5 EXPERIMENTAL TECHNIQUES

3.5.1 Compressive strength

The specimens were capped prior to testing them in compression. Capping the surface of the cast plain concrete shown in Figure 3.3 is an essential preparation of the specimen for the compressive strength to ensure the smooth loading surface and the uniform load distribution. Sulfur was used for concrete capping in accordance with ASTM C617 [*135*]. This included preparing sulfur mortar as shown in Figure 3.4 for use by heating to about 265°F (130°C). Fresh sulfur mortar was dried at the time of placement in the melting point (dampness will cause foaming) while the flash point of sulfur mortar was maintained at approximately 440°F (225°C). The capping plate was oiled slightly prior to the pouring of well stirred molten sulfur before the concrete specimen was placed on it. A thickness of 5

mm [136] was maintained. Figure 3.5 shows the sulfur capped specimen prior to testing it in compression.

Figure 3.3: Un-reinforced concrete specimens prior to capping.

Figure 3.4: Molten sulfur poured into oiled capping plate.

Figure 3.5: Sulfur-capped specimens.

The compressive strength of concrete is the most common performance measure used by engineers in designing buildings and other structures. The *test* method consists of applying a compressive axial load to molded cylinders (or cores) at a rate which is within a prescribed range until failure occurs. The compressive strength (f'_c) of the specimen is calculated by dividing the maximum load attained during the test by the cross-sectional area of the specimen resisting the load. Compressive strength is reported in units of pound-force per square inch (psi) in US customary units or megapascals (MPa) or N/mm^2 in SI units. A test result is the average of two to three specimens made from the same concrete specimen and tested at the same age.

Cylindrical concrete specimens were *test*ed in accordance with ASTM C39 [136], by using the 300 kN capacity INSTRON machine. Strain gauges were attached to the specimens and connected to a data logger to record the accompanying strain, as shown in Figure 3.6, for recording strains at different levels of the applied load, so that the modulus

of elasticity could also be determined from stress-strain plots by using the secant modulus simultaneously with the compressive strength of the concrete. The typical stress-strain curves for each specimen tested in compression are presented in Appendix-1. The secant modulus of elasticity was calculated by using a stress-strain diagram for each concrete mix [136]. A sample photograph of a test specimen that typically failed in compression is shown in Figure 3.7.

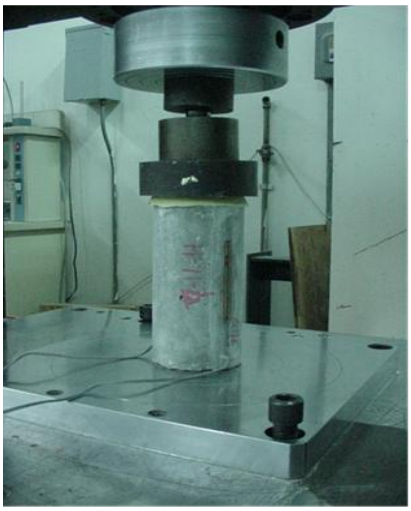

Figure 3.6: Specimen attached with strain gauge.

Figure 3.7: A concrete specimen that failed in compression.

3.5.2 Corrosion Current Density Measurements

All the 1458 RC test specimens belonging to 27 mixes of the two aggregate sources were partly submerged as shown in Figure 3.8 in chloride solutions with three different concentrations (3%, 7% and 12% NaCl) for allowing simulated corrosion conditions to take place. The corrosion current density was measured after three, six, and nine months of exposure to the chloride solution.

Figure 3.8: Cylindrical reinforced concrete specimen exposed to chloride solutions.

The corrosion current density on steel embedded in the cylindrical concrete specimens was measured by using the Linear Polarization Resistance (LPR) method [137]. A typical LPR set-up is shown in Figure 3.9. The equipment-PARSTAT 2273 potentiostat that was used is manufactured by PRINCETON (USA) [134]. The principle involves application of 10 mV above and below corrosion potential value (E_{corr}). Equivalent current is recorded within the machine while the slope of potential difference (abscissa) and current (mantissa) is taken as the polarization resistance (R_p). The corrosion current density is obtained by taking the ratio of the Stern-Geary constant, β, (100 mV) and polarization resistance (R_p).

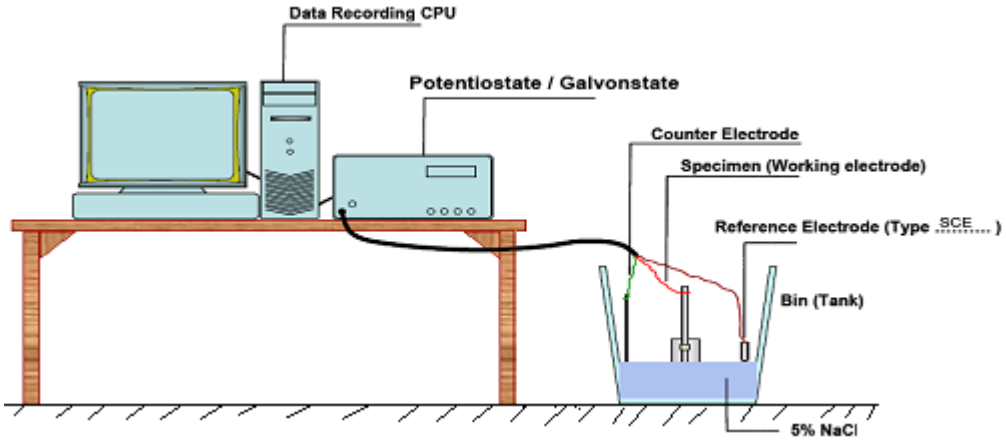

Figure 3.9: Typical set-up for I_{corr} measurement by using polarization

The linear polarization resistance (LPR) method is confined to a small magnitude of the overpotentials, ε_a and ε_c, respectively, using linear coordinates. This technique allows the determination of I_{corr} using a potential range of ±10mV from the E_{corr}. Prior to determining I_{corr}, the polarization resistance, R_p is estimated from the linear slope of the curve as:

$$R_p = \frac{\Delta E}{\Delta i} \quad \text{.... (3.1)}$$

The corresponding corrosion current density depends on kinetic parameters since $I_{corr} = f(B,R_p)$. Thus the simple linear relation from Butler Volmer kinetic relations that defines the corrosion current density is of the form [138].

$$I_{corr} = \frac{B}{R_p} \quad \text{... (3.2)}$$

Detail of Butler-Volmer equation is shown in Appendix IV. The magnitude of polarization resistance is mainly controlled by the corrosion current density, I_{corr}.

$B = f(\beta_a, \beta_c)$, while β_a , β_c are taken as positive kinetic parameter for determining I_{corr} of corroding metallic materials.

$$B = \frac{\beta_a \beta_c}{2.303(\beta_a + \beta_c)} \quad \text{... (3.3)}$$

where: B is the Stern-Geary constant and it is derived from the basic equations for a polarization curve. The value of Stern-Geary constant (B) is determined by using the values of the coefficients (β_a and β_c) obtained from the Tafel plot. In the absence of this plot, the value of B may be assumed as 52 mV for passive (non-active) corrosion and 26 mV for active corrosion [139]. The polarization resistance (R_p) is determined by using the slope of the linear portion of the polarization curve, as shown in Figure 3.10 [140].

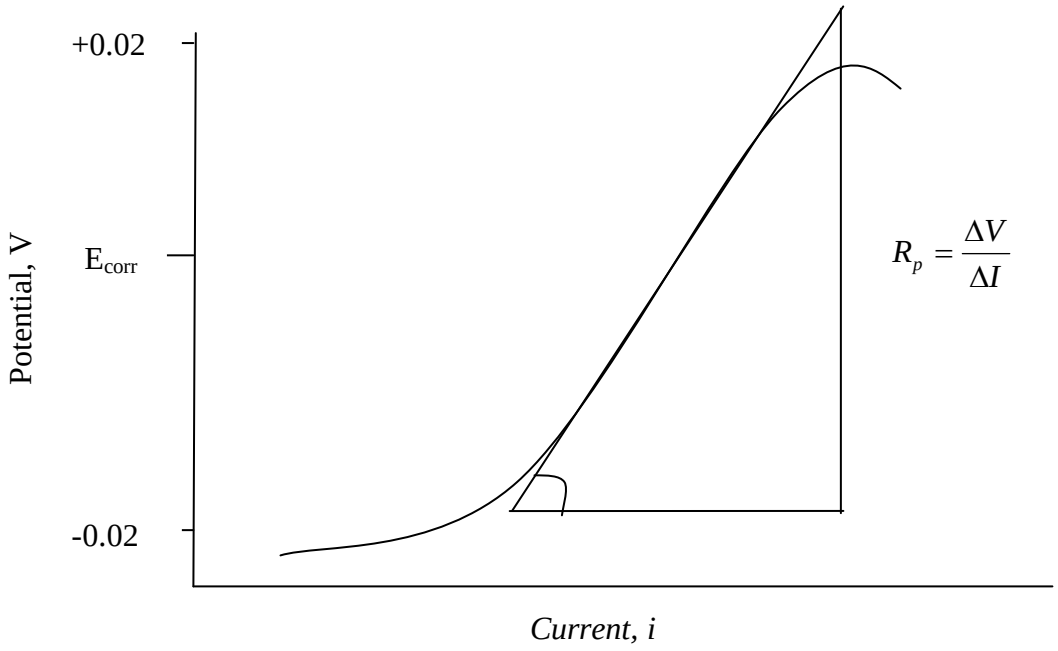

Figure 3.10: Typical polarization curve [140]

where: $\Delta V/\Delta I$ = slope of the linear portion of the polarization curve

$$R_p = \frac{\Delta V}{\Delta I} \quad \text{… (3.4)}$$

3.6 QUANTITATIVE ESTIMATION OF REBAR DIAMETER LOSS

A quantitative estimation of corrosion propagation is usually given in terms of the *corrosion penetration rate*, which is defined as the loss of metal per unit of surface area per unit of time. Most non-destructive techniques currently used for monitoring corrosion are based on electrochemical measurements, with the corrosion rate estimated in terms of a corrosion current density, I_{corr}. In the case of general corrosion, the corrosion current density I_{corr} can be transformed directly into the loss of metal by the use of Faraday's law of electrochemical equivalence, which indicates that a constant corrosion current density of 1 μA/cm^2 corresponds to a uniform corrosion penetration of 11.7 μm/yr [141].

For the 243 mixes in triplicate (729 specimens) the data for each aggregate type monitored were recorded in *Excel* format and then averaged to obtain 243 data, shown in Tables 4.3 and 4.4, for *H*-test specimens and *T*-test specimens, respectively. The data were analyzed by plotting the rebar diameter loss, $\Delta\phi(t)$ (micron) which was obtained by multiplying the corrosion penetration rate, P_r, obtained from the measured I_{corr} by the time, *t*, through the following relations [129]:

$$P_r = \frac{W}{F\rho_{st}} \mathrm{I}_{\mathrm{corr}}$$

$$\Delta\phi(t) = P_r t \qquad \text{...(3.5)}$$

$$P_r = 11.7 I_{corr} \ (\mu m/year)$$

$$t = \frac{T_m - \mathrm{T_c}}{365} \qquad \text{... (3.6)}$$

where: $\Delta\phi$(t)= cumulative rebar loss

t = time in years

T_m = Corrosion monitoring data in days

T_d = Specimen initial date of dipping in an aqueous NaCl solution in days

W= equivalent weight of steel = 55.85/2 = 27.925 g

F= Faraday's constant = 96500 Coulombs = 96500 Amp-s

ρ_{st} = density of steel (7.85 g/cm^3) =0.212 tonnage/ft^3

I_{corr}= corrosion current density (usually expressed as (μA/cm^2)

Thus, assuming a constant corrosion rate, the reduction in the diameter (2 Radii) of a corroding reinforcing bar $\Delta\phi$ after t years since corrosion initiation can be estimated in millimetres by Eq. 3. 7:

$$\Delta\varphi(t) = 2(11.7 I_{corr} t)\ (\mu m)$$

$$\Delta\phi(t) = 0.0234\, I_{corr} t\ (mm) \qquad \text{... (3. 7)}$$

Then with the cumulative rebar loss, $\Delta\phi$ plotted against time, the slope of the curve is taken as the penetration rate of corrosion, P_r as will be outlined in section 4.2 of chapter 4. A typical curve generated is shown in Figure 4.1.

If it is to be assumed that the corrosion current density is the same for a group of n reinforcing bars of the same diameter ϕ_o, their cross-sectional area after t years of general corrosion will be:

$$A_s = n\frac{\pi[\phi_o - \Delta\phi(t)]^2}{4} \geq 0 \qquad \text{... (3. 8)}$$

CHAPTER 4

RESULTS AND DISCUSSION

In this chapter, experimental *test* results obtained used in this study are presented separately for the two types of aggregates (*namely*: Dammam (H) and Taif (T) aggregates). *Test* results were first analyzed statistically by using software to pinpoint the effects of variable factors on strength and elasticity of concrete and corrosion rate of rebars. Based on the results of *ANALYSIS OF VARIANCE* (ANOVA) of the data, models for strength, elasticity, and corrosion rate were developed. Utilization of these models in optimal design of RC members is described at the end of this chapter.

4.1 COMPRESSIVE STRENGTH AND ELASTIC MODULUS TEST RESULTS

The cylindrical concrete specimens cast by using 27 mixtures in triplicate with varied w/cm ratio (0.38, 0.43 and 0.48) and (0.42, 0.47 and 0.52) for *H-test* specimens and *T-test* specimens respectively. In addition, cementitious materials content (350, 375 and 400 kg/m^3), and fine to total aggregate (FA/TA) ratios (0.35, 0.40, and 0.45), are the same for the two types of aggregates (*H* and *T*). Concrete from both mixtures was tested for compressive strength and modulus of elasticity. Results of these tests, conducted after 28-days of curing on concrete specimens prepared with *H*-type and *T*-type aggregate, are presented in Tables 4.1 and 4.2 respectively.

Table 4.1 Compressive strength and modulus of elasticity results of H-test specimens.

Mix #	Water-cementitious material ratio ($R_{w/cm}$)	Cementitious material content, Q_C (kg/m^3)	Fine/Total aggregate ratio ($R_{FA/TA}$)	28-day compressive strength, f'_c (MPa)	28-day modulus of elasticity, E_c (GPa)
1	0.38	350	0.35	39.7	36.5
2			0.40	38.8	39.4
3			0.45	39.1	34.7
4		375	0.35	34.1	31.4
5			0.40	38.2	36.5
6			0.45	40.6	38.6
7		400	0.35	34.2	28.6
8			0.40	39.3	38.4
9			0.45	39.8	38.3
10	0.43	350	0.35	27.9	32.7
11			0.40	37.4	37.4
12			0.45	38.5	35.0
13		375	0.35	31.9	31.9
14			0.40	37.1	33.5
15			0.45	33.9	33.9
16		400	0.35	26.5	29.6
17			0.40	30.7	31.3
18			0.45	36.5	30.8
19	0.48	350	0.35	30.0	25.9
20			0.40	32.1	31.5
21			0.45	30.5	31.3
22		375	0.35	20.7	28.0
23			0.40	27.5	27.5
24			0.45	29.9	31.6
25		400	0.35	25.4	26.3
26			0.40	31.0	31.8
27			0.45	25.3	27.7

Table 4.2 Compressive strength and modulus of elasticity results of *T*-test specimens.

Mix #	water-cementitious materials ratio ($R_{w/cm}$)	Cementitious materials content Q_C (kg/m^3)	Fine/Total aggregate. ratio ($R_{FA/TA}$)	28-day compressive strength, f'_c (MPa)	28-day modulus of elasticity, E_c (GPa)
1	0.42	350	0.35	21.6	22.03
2			0.40	25.3	26.2
3			0.45	31	25.78
4		375	0.35	23.3	17.5
5			0.40	27	28.26
6			0.45	30.7	25.36
7		400	0.35	24.6	21.27
8			0.40	27	24.64
9			0.45	28.9	30.93
10	0.47	350	0.35	20.3	23.27
11			0.40	22.8	22.53
12			0.45	25.4	25.4
13		375	0.35	20.8	18.45
14			0.40	26.1	25.95
15			0.45	30.4	30.23
16		400	0.35	22.9	20.94
17			0.40	23.7	22.03
18			0.45	26.5	28.06
19	0.52	350	0.35	19.1	20.86
20			0.40	27.9	26.78
21			0.45	30.9	29.37
22		375	0.35	16.6	17.2
23			0.40	24	21.73
24			0.45	25.8	23.58
25		400	0.35	16	15.56
26			0.40	21.6	19.3
27			0.45	25.2	21.4

4.2 CORROSION PENETRATION RATE

The concrete test specimens (corresponding to 27 mixtures) of varying cover thickness cast by using both aggregate types were exposed to chloride salt solutions of three different concentrations. Corrosion penetration rates of rebars, P_r were determined for *H*-test specimens and *T*-test specimens. The results are presented in Tables 4.3 and 4.4, respectively. The corrosion penetration rate was calculated by using values of the corrosion current density I_{corr} obtained during three rounds of corrosion monitoring on samples continuously exposed to chloride solutions. The procedure for calculation of corrosion penetration rate P_r by using the corrosion current density I_{corr} is shown in Fig. 4.1.

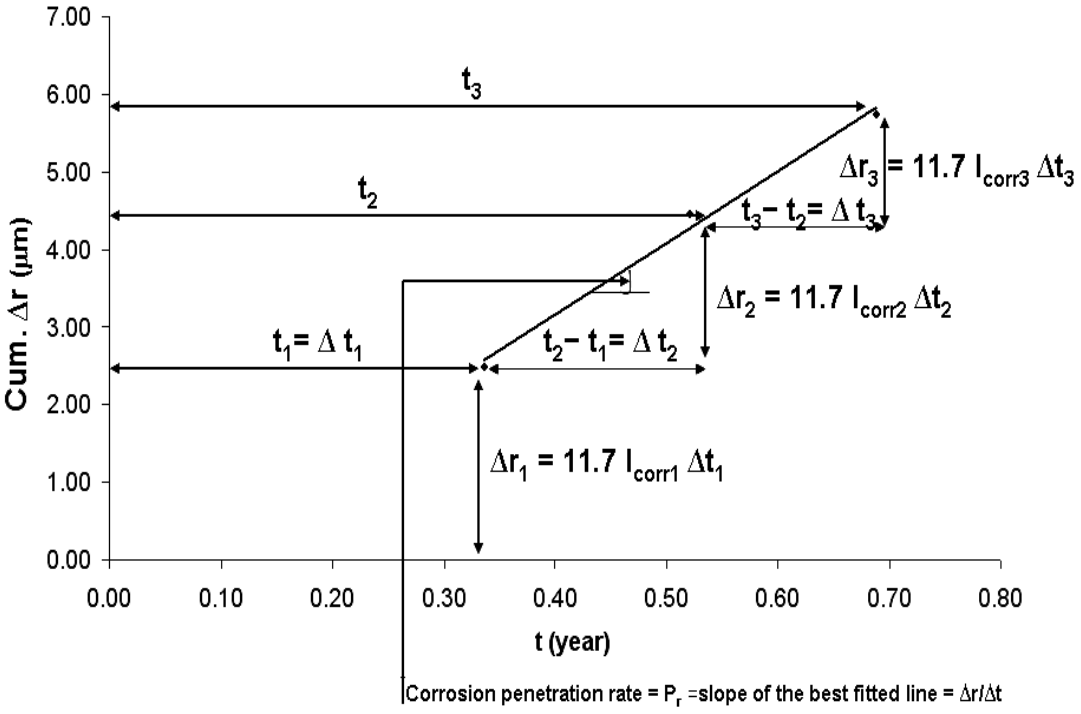

Figure 4.1: Procedure for calculation of corrosion penetration rate, P_r.

Table 4.3: Corrosion Penetration rate data for H-test specimens.

Cem. mat content (Q_C)	w/cm ratio by mass ($R_{w/cm}$)	FA/TA ratio by mass ($R_{FA/TA}$)	Corrosion penetration rate, Pr (μm/yr) for H-Test Specimens								
			3% NaCl solution exposure (C_{CHL})			7% NaCl solution exposure (C_{CHL})			12% NaCl solution exposure (C_{CHL})		
			25 mm Cover (T_{CV})	37.5 mm Cover (T_{CV})	50 mm Cover (T_{CV})	25 mm Cover (T_{CV})	37.5 mm Cover (T_{CV})	50 mm Cover (T_{CV})	25 mm Cover (T_{CV})	37.5 mm Cover (T_{CV})	50 mm Cover (T_{CV})
350	0.38	0.35	5.87	5.29	4.05	9.73	7.93	7.79	10.67	8.47	8.07
		0.40	6.89	6.58	5.12	8.89	7.06	5.68	9.63	9.13	3.73
		0.45	5.02	4.28	4.19	7.32	5.95	4.43	11.02	9.23	7.01
375		0.35	5.58	4.96	4.56	6.84	5.49	4.00	8.63	7.69	6.80
		0.40	5.95	4.04	3.14	6.60	4.21	3.46	9.90	4.39	3.94
		0.45	5.37	4.29	3.81	6.87	5.00	4.85	9.11	4.56	4.03
400		0.35	5.96	4.13	3.69	6.28	4.48	3.88	7.76	4.73	4.21
		0.40	5.11	4.95	4.81	5.92	5.45	4.39	8.45	7.20	4.52
		0.45	5.25	4.23	3.94	6.51	4.80	4.45	9.27	6.78	4.53
350	0.43	0.35	11.44	8.98	7.84	16.53	13.70	9.37	18.52	16.19	10.49
		0.40	13.81	11.52	9.08	18.29	14.20	8.57	18.48	14.04	9.28
		0.45	14.53	10.16	5.18	17.27	13.50	7.57	20.62	16.17	8.49
375		0.35	14.54	10.04	9.35	19.55	16.04	8.62	25.77	19.78	10.82
		0.40	13.63	11.85	10.99	21.92	16.88	10.71	27.05	17.90	9.30
		0.45	14.91	14.29	11.72	19.03	18.10	11.38	23.14	15.00	9.63
400		0.35	13.00	12.68	10.18	16.03	12.94	10.79	18.34	14.07	8.91
		0.40	13.06	12.56	9.94	15.04	11.93	9.65	18.52	13.47	9.30
		0.45	13.64	11.91	9.60	14.96	11.65	9.72	18.27	12.81	8.99
350	0.48	0.35	24.34	16.57	14.48	28.57	18.68	14.34	30.67	20.72	15.93
		0.40	22.18	14.25	13.68	25.09	17.52	12.78	28.79	18.58	15.42
		0.45	20.33	11.00	9.67	24.73	15.64	11.17	25.42	16.95	13.37
375		0.35	25.15	18.44	15.52	27.68	19.57	13.90	30.23	18.80	16.28
		0.40	25.39	13.85	12.48	26.07	17.76	15.14	27.83	18.14	15.42
		0.45	24.98	13.20	10.37	25.93	15.52	10.46	28.05	21.43	16.77
400		0.35	25.09	19.05	9.84	27.58	17.28	13.47	29.09	18.91	16.64
		0.40	25.34	12.61	8.24	26.17	14.84	13.66	28.48	16.32	15.63
		0.45	24.96	13.24	9.88	26.94	14.64	12.45	27.51	17.91	15.46

Table 4.4: Corrosion penetration rate for T-test specimens.

Cem. mat content (Q_C)	w/cm ratio by mass ($R_{w/cm}$)	FA/TA ratio by mass ($R_{FA/TA}$)	Corrosion penetration rate, Pr (μm/yr) for T-Test Specimens								
			3% NaCl solution exposure (C_{CHL})			7% NaCl solution exposure (C_{CHL})			12% NaCl solution exposure (C_{CHL})		
			25 mm Cover (T_{CV})	37.5 mm Cover (T_{CV})	50 mm Cover (T_{CV})	25 mm Cover (T_{CV})	37.5 mm Cover (T_{CV})	50 mm Cover (T_{CV})	25 mm Cover (T_{CV})	37.5 mm Cover (T_{CV})	50 mm Cover (T_{CV})
350	0.42	0.35	7.55	7.48	3.01	12.72	11.68	3.63	10.14	7.66	5.92
		0.40	9.09	8.22	4.47	10.21	7.35	6.27	12.70	11.35	5.80
		0.45	8.28	8.08	6.19	10.49	8.91	6.43	14.50	13.67	6.70
375		0.35	9.39	8.22	6.54	9.13	8.12	8.97	13.08	11.30	6.74
		0.40	9.54	6.58	5.10	10.69	7.67	6.60	11.80	9.57	7.06
		0.45	10.73	8.94	6.26	10.80	8.83	7.67	13.83	10.01	7.49
400		0.35	12.60	11.59	8.14	11.90	9.06	5.96	13.85	10.74	7.93
		0.40	13.28	12.19	8.64	12.67	9.42	6.76	14.63	11.30	8.41
		0.45	14.62	10.52	9.70	13.80	12.08	6.97	16.20	12.85	8.80
350	0.47	0.35	17.43	14.47	10.85	17.52	15.85	8.06	21.70	19.76	12.80
		0.40	19.38	16.77	12.80	19.11	17.55	10.12	21.95	19.72	14.22
		0.45	23.32	17.88	13.53	21.18	19.46	11.66	22.82	23.28	11.81
375		0.35	23.97	19.25	14.34	28.00	22.83	12.33	32.58	28.44	12.29
		0.40	29.87	24.94	15.67	30.06	25.48	11.43	33.91	26.94	11.66
		0.45	33.96	32.77	16.22	34.97	26.44	12.50	40.26	37.32	11.37
400		0.35	39.57	35.33	23.16	31.64	28.16	17.98	55.15	34.68	12.25
		0.40	39.11	34.08	21.91	34.45	34.06	18.09	36.11	32.79	20.84
		0.45	38.98	35.92	21.68	40.91	35.46	19.86	38.35	29.79	19.42
350	0.52	0.35	44.52	30.26	23.07	41.82	33.84	18.40	43.93	34.79	21.40
		0.40	44.91	38.11	26.44	54.52	38.66	19.81	43.47	37.40	23.43
		0.45	56.19	48.85	25.30	55.41	35.42	21.66	42.56	38.46	24.19
375		0.35	50.40	47.38	27.13	57.19	35.89	23.73	52.88	40.96	24.07
		0.40	52.06	45.77	27.96	58.19	37.73	24.53	51.50	45.18	25.59
		0.45	52.19	43.36	28.61	59.19	35.77	24.14	52.94	45.75	27.44
400		0.35	57.65	45.59	29.77	63.94	38.67	28.29	65.44	44.03	35.05
		0.40	70.25	42.59	32.14	66.89	45.65	32.28	64.72	49.64	38.37
		0.45	70.29	56.36	38.15	65.27	48.10	35.51	71.35	50.51	38.89

4.3 DATA SCALING

If the data are not in the same range, there may be a larger error due to data deviation, especially when these widely varied data interact with one another in a model prediction. In this light, each element of the data set is expressed as the ratio of the largest value in the data set through a simple mathematical manipulation so as to reduce the variable deviation and to improve the model accuracy [142]. This was done for all the results obtained from the experiments on both *H*-test specimens and *T*-test specimens.

$$\bar{f}(x_i) = \frac{f(x_i)}{f^o}; \qquad i = 1\ 2.....n \qquad \ldots (4.1)$$

where n is the number of elements in the data set

$\bar{f}(x_i)$ is the normalized individual element in the data set,

f^o is the maximum value in the data set, $f^o \neq 0$

The variables considered were then scaled, as shown in Table 4.5, for both *H*-test specimens and *T*-test specimens.

Table 4.5: Data scaling for H-test specimens and T-test specimens.

Experimental variables	H-test specimen		T-test specimen	
	Actual values	Scaled values	Actual values	Scaled values
Cement. material content, Q_C (kg/m3)	300,350,400	0.88,0.94,1.00	300,350,400	0.88,0.94,1.00
w/cm ratio, Rw/cm (by mass)	0.38,0.43, 0.48	0.79, 0.90, 1.00	0.42,0.47, 0.52	0.81, 0.90, 1.00
FATA ratio, R_{FATA} (by mass)	0.35, 0.40, 0.45	0.78, 0.89, 1.00	0.35, 0.40, 0.45	0.78, 0.89, 1.00
Cover , T_{CV} (by mass)	25.0, 37.5, 50.0	0.5, 0.75, 1.00	25.0, 37.5, 50.0	0.5, 0.75, 1.00
Chloride conc. (decimal)	0.03, 0.07, 0.12	0.25, 0.58, 1.00	0.03, 0.07, 0.12	0.25, 0.58, 1.00

4.4 STATISTICAL ANALYSIS OF TEST RESULTS AND MODEL FITTING

Descriptive statistical analysis of the test results was carried out to determine the minimum, maximum, and mean of the data population. Analysis of variance (ANOVA) was also carried out to pinpoint the individual and interactive effects of variable factors on the dependent variable. The procedure for ANOVA is outlined in Appendix II. ANOVA analysis of the test results in the present study was done with software named *MINITAB* [143]. A sample of the ANOVA results by *MINITAB* is given in Appendix III. Based on the ANOVA results, the regression models for compressive strength, elastic modulus, and corrosion penetration rate corresponding to *H*-test specimen and *T*-test specimens was fit by the *least square error* method. In the ANOVA as well as in the regression models, the notations used for independent variables are as follows:

$\boldsymbol{Q_C}$: cementitious materials content in kg/m^3

$\boldsymbol{R_{w/cm}}$: water/cementitious materials ratio by mass

$\boldsymbol{R_{FA/TA}}$: fine/total aggregate ratio by mass

$\boldsymbol{T_{CV}}$: cover thickness in mm

$\boldsymbol{C_{CHL}}$: chloride salt concentration in percentage by decimal

4.4.1 Statistical Analysis for Compressive Strength, Elastic Modulus, and Corrosion Penetration Rate

The minimum, maximum, and mean of compressive strength, elastic modulus, and corrosion penetration rate data obtained from H-test specimens and T-test specimens are presented in Table 4.6, Table 4.7 and Table 4.8, respectively.

Table 4.6: Descriptive statistics table of compressive strength data (data size: 27).

Concrete type	Minimum (MPa)	Maximum (MPa)	Mean (MPa)
H-test specimens	20.7	40.6	33.21
T-test specimen	16.0	31.0	24.64

Table 4.7: Descriptive statistics table of modulus of elasticity data (data size: 27).

Concrete type	Minimum (GPa)	Maximum (GPa)	Mean (GPa)
H-test specimens	25.9	39.4	32.6
T-test specimen	15.6	30.9	23.5

Table 4.8: Descriptive statistics table of corrosion penetration rate data (data size: 243).

Concrete type	Minimum (μm/y)	Maximum (μm/y)	Mean (μm/y)
H-test specimens	3.14	30.67	12.79
T-test specimen	3.00	71.35	24.644

It is observed from the results of the descriptive statistics that the *H*-test specimens have compressive strengths in the range of about 20 to 40 MPa, whereas the compressive strength of *T*-test specimens varies from 16 to 31 MPa. This shows that the strength performance of *T*-type aggregate is about 25% less than the *H*-aggregate. Lower

performance of the *T*-type aggregate is observed also in the case of elastic modulus and reinforcement corrosion. The maximum elastic modulus of *T*-test specimens is found to be around 25% less than that of *H*-test specimens. Maximum corrosion penetration rate of *T*-test specimens is found to be more than double that for the *H*-test specimens. These observations reveal that performance of the commonly used *T*-aggregate is significantly less than that of *H*-aggregate both in case of strength as well as durability.

4.4.2 Analysis of Variance (ANOVA) of the Test Results

a) ANOVA and Regression Models for Compressive Strength ($f_c^{'}$)

The results of ANOVA for compressive strength of *H* and *T* mixtures are presented in Table 4.9 and Table 4.10 while the relationships between the experimental and fitted data are shown in Figure 4.2 and 4.3 respectively.

A response variable (dependent variables) has significant contribution to its predictor (independent variable) if the equivalent level of variable significance designated *P*-values is less than 0.05 (95% confidence level). The *P*-value is obtained from Fisher's distribution table which depends on error degree of freedom (df) and the ratio of predictor variables and error (residual) mean squares. Table 4.9, shows that the w/cm ($R_{w/cm}$) and fine to total aggregate ratio ($R_{FA/TA}$) make significant contributions as their levels of significance, P-values, are less than 0.05. Therefore, these two significant variables are considered for obtaining the regression model for compressive strength, f_c'.

Although the effect of cementitious materials content (Q_C) on compressive strength is found to be insignificant because it varies within a close range of 350 to 400 kg/m^3, yet it is

considered in the regression analysis as cement remains an indispensable material in concrete production.

Table 4.9: ANOVA for compressive strength of *H*-test specimens.

Factors	Type	Level	Scale values			
Qc	Fixed	3	0.875	0.938	1.000	
Rw/cm	Fixed	3	0.792	0.896	1.000	
RFATA	Fixed	3	0.778	0.889	1.000	
Source	DF	Seq SS	Adj MS	F	P	Comment
Qc	2	39.672	19.380	1.990	0.199	No
Rw/cm	2	464.501	232.250	23.260	0.000	Yes
RFATA	2	135.281	67.640	6.770	0.019	Yes
Qc*Rw/cm	4	23.686	5.921	0.590	0.678	No
Qc*RFA/TA	4	4.993	1.248	0.120	0.969	No
Rw/cm*RFA/TA	4	22.437	5.609	0.560	0.697	No
Error	8	79.890	9.986			
Total	26	770.456				

Table 4.10: ANOVA for compressive strength of *T*-test specimens.

Factors	Type	Level	Scale values			
Q_C	Fixed	3.000	0.875	0.938	1.000	
$R_{w/cm}$	Fixed	3.000	0.808	0.904	1.000	
$R_{FA/TA}$	Fixed	3.000	0.778	0.889	1.000	
Source	DF	Seq SS	Adj MS	F	P	Comment
Q_C	2	4.869	2.434	1.750	0.235	No
$R_{w/cm}$	2	59.362	29.681	213.000	0.001	Yes
$R_{FA/TA}$	2	271.280	135.640	97.400	0.000	Yes
Q_C * $R_{w/cm}$	4	51.362	12.841	9.220	0.004	Yes
Q_C * $R_{FA/TA}$	4	10.338	2.584	1.860	0.212	No
$R_{w/cm}$ * $R_{FA/TA}$	4	20.911	5.228	3.750	0.053	No
Error	8	11.144	1.393			
Total	26	429.3				

The regression model equations for compressive strength of *H*-test specimens are presented as follows:

Model generated in terms of scaled variables

(R^2=0.80): $f_c^{'} = -61.24 - 22.50Q_C - 19.87\,Exp(R_{w/cm}) + 166.79R_{FA/TA}^{0.119}$ ...(4.1)

Model generated in terms of actual (un-scaled) variables (R^2 =0.80):

$f_c^{'} = -61.24 - 0.056\,Q_C - 19.87\,Exp(2.083R_{w/cm}) + 183.45R_{FA/TA}^{0.119}$ ... (4.2)

The ANOVA for compressive strength $f_c^{'}$ for *T*-test specimens presented in Table 4.10, shows that the w/cm ($R_{w/cm}$), fine to total aggregate ratio ($R_{FA/TA}$) and the interaction of cementitious materials content (Q_C) with water-cementitious material ratio ($R_{w/cm}$) have a significant effect on $f_c^{'}$ as their *P*-values are less than 0.05. Thus, these significant individual and interactive variables were considered in the regression model for compressive strength $f_c^{'}$. As in the case of *H*-test specimens, cementitious materials content (Q_C) is insignificant in the case of *T*-test specimens, also but it is considered in the regression analysis. The regression model equations for compressive strength of *T*-test specimens are presented as follows:

Model generated in terms of scaled variables (R^2=0.84):

$f_c^{'} = -339.12 + 157.67Q_C + 61.43Exp(R_{w/cm}) + 178.34R_{FA/TA}^{0.1766} - 139.14(Q_C R_{w/cm})^{1.3951}$ ...(4.3)

Model generated in terms of actual (un-scaled) variables (R^2=0.84):

$f_c^{'} = -339.12 + 0.39Q_C + 61.43Exp(1.923R_{w/cm}) + 205.37R_{FA/TA}^{0.17663} - 0.08(Q_C R_{w/cm})^{1.3951}$ ... (4.4)

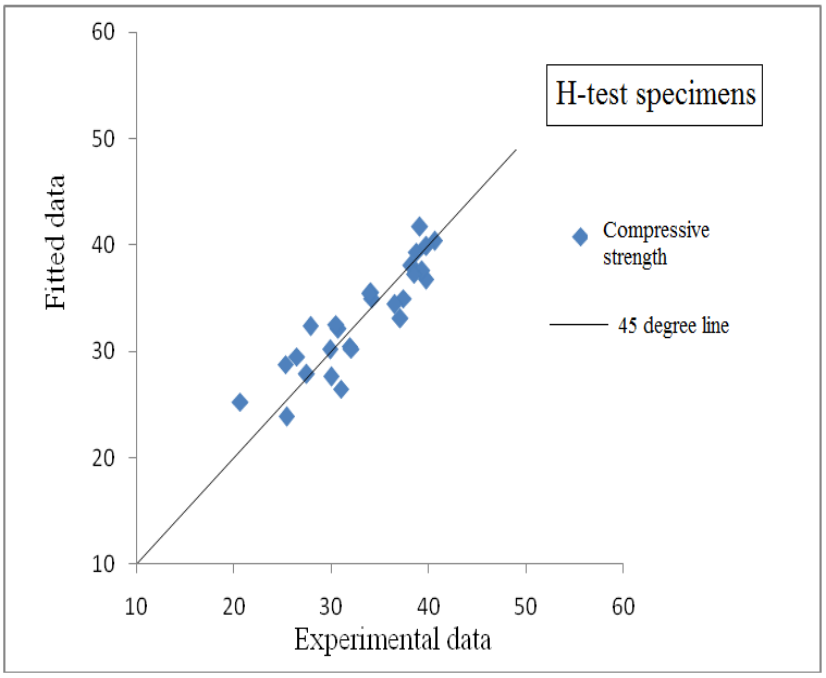

Figure 4.2: Correlation graph of compressive strength $f_c^{'}$ for *H*-test specimen (Experimental data vs. model data).

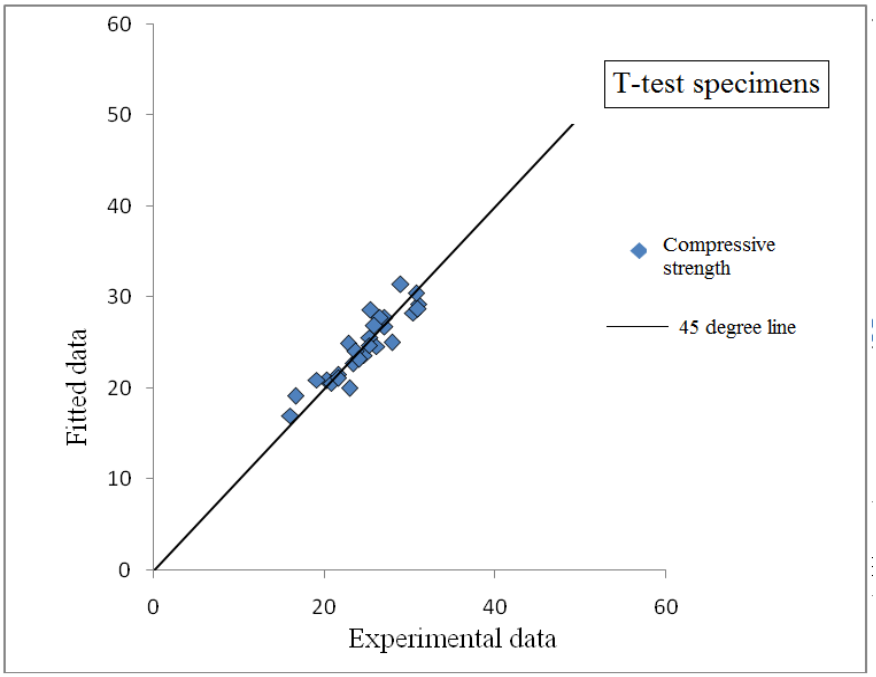

Figure 4.3: Correlation graph of compressive strength $f_c^{'}$ for *T*-test specimens. (Experimental data vs. model data).

b) ANOVA and Regression Models for Elastic Modulus (E_C)

The results of ANOVA for elastic modulus of H and T Mixtures are presented in Table 4.11 and Table 4.12, respectively while the relationship between the experimental and fitted data are shown in Figure 4.4 and 4.5 respectively.

Table 4.11: ANOVA for elastic modulus of *H*-test specimens.

Factors	Type	Level	Scale values			
Q_C	Fixed	3.000	0.875	0.938	1.000	
$R_{w/cm}$	Fixed	3.000	0.792	0.896	1.000	
$R_{FA/TA}$	Fixed	3.000	0.778	0.889	1.000	
Source	DF	Seq SS	Adj MS	F	P	Comment
Q_C	2	25.956	12.978	2.340	0.158	No
$R_{w/cm}$	2	206.614	103.307	18.700	0.001	Yes
$R_{FA/TA}$	2	85.745	42.873	7.750	0.013	Yes
Q_C*$R_{w/cm}$	4	10.706	2.676	0.480	0.748	No
Q_C*$R_{FA/TA}$	4	22.095	5.524	1.000	0.462	No
$R_{w/cm}$*$R_{FA/TA}$	4	11.277	2.819	0.510	0.731	No
Error	8	44.276	5.535			
Total	26	406.670				

Table 4.12: ANOVA for elastic modulus of *T*-test specimens.

Factors	Type	Level	Scale values			
Q_C	Fixed	3.000	0.875	0.938	1.000	
$R_{w/cm}$	Fixed	3.000	0.808	0.904	1.000	
$R_{FA/TA}$	Fixed	3.000	0.778	0.889	1.000	
Source	DF	Seq SS	Adj MS	F	P	Comment
Q_C	2	19.97	9.985	2.39	0.154	No
$R_{w/cm}$	2	42.829	21.415	5.12	0.037	Yes
$R_{FA/TA}$	2	226.479	113.239	27.1	0	Yes
Q_C*$R_{w/cm}$	4	63.775	15.944	3.81	0.051	No
Q_C*$R_{FA/TA}$	4	30.587	7.647	1.83	0.217	No
$R_{w/cm}$*$R_{FA/TA}$	4	12.141	3.035	0.73	0.599	No
Error	8	33.476	4.185			
Total	26	429.261				

From Table 4.11, it can be seen that the w/cm ($R_{w/cm}$) and fine to total aggregate ratio ($R_{FA/TA}$) are variables which significantly contribute to elastic modulus, and therefore these variables are considered in the regression analysis. Although, cementitious materials content (Q_C) is found to be insignificant, because of its close range of variation, it is also considered in the regression analysis. The regression model equations for elastic modulus of *H*-test specimens are presented as follows:

Model generated in terms of scaled variables (R^2=0.71):

$$E_c = -49.10 - 19.19Q_C - 13.23\,Exp(R_{w/cm}) + 133.86R_{FA/TA}^{0.106} \quad ...(4.5)$$

Model generated in terms of actual (un-scaled) variables (R^2=0.71):

$$E_c = -49.10 - 0.0048Q_C - 13.23\,Exp(2.083R_{w/cm}) + 145.68R_{FA/TA}^{0.106} \quad ...(4.6)$$

The ANOVA for elastic modulus of *T*-test specimens, presented in Table 4.12 shows that the variables significantly affecting elastic modulus of *T*-test specimens are the same as those of *H*-test specimens. However, the interactive effect of cementitious materials content (Q_C) and water-cementitious material ratio ($R_{w/cm}$) may also be considered marginally. For regression analysis of elastic modulus of *T*-test specimens, Q_C, $R_{w/cm}$, $R_{FA/TA}$, and Q_C $R_{w/cm}$ are considered as independent variables. The model regression equations for elastic modulus of *T*-test specimens are presented as follows:

Model generated in terms of scaled variables (R^2 = 0.72):

$$E_c = -330.77 + 71.27Exp\ (Q_C) + 83.74\,Exp(R_{w/cm}) + 161.78R_{FA/TA}^{0.1768} - 229.08Q_C R_{w/cm} \quad ...(4.7)$$

Model generated in terms of actual (un-scaled) variables (R^2 = 0.72):

$$E_c = -330.77 + 71.27Exp(0.0025Q_C) + 83.74Exp(1.932R_{w/cm}) + 186.30R_{FA/TA}^{0.1768} - 1.10Q_C R_{w/cm} \quad ... (4.8)$$

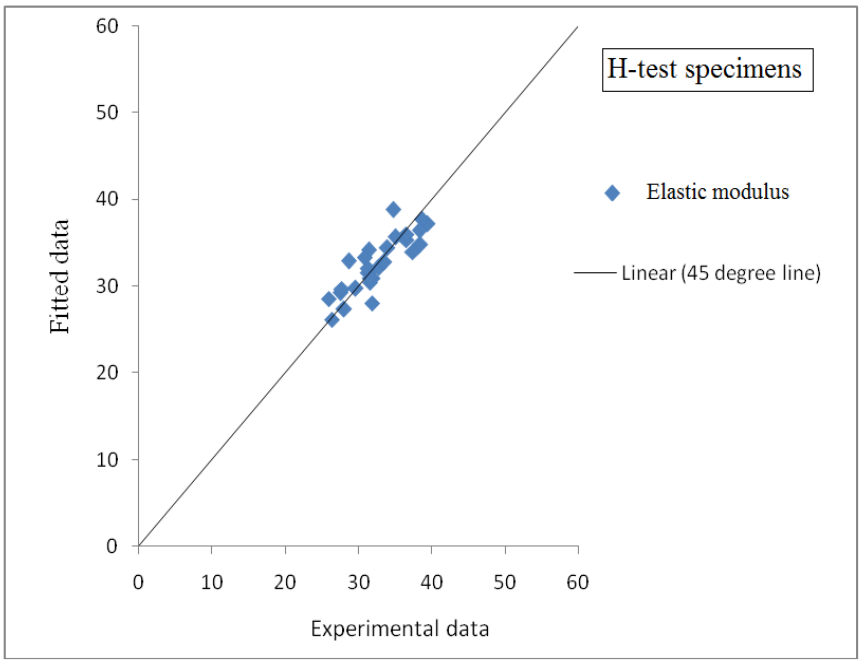

Figure 4.4: Correlation graph of elastic modulus E_c for H-test specimens (Experimental data vs. model data).

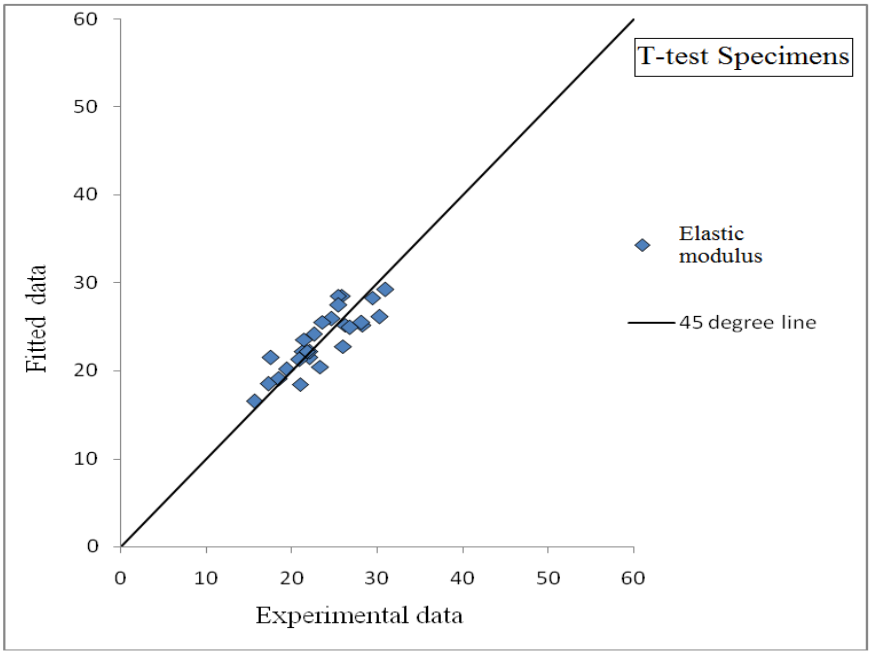

Figure 4.5: Correlation graph of elastic modulus E_c for *T*-test specimens (Experimental data vs. model data).

4.4.3 ANOVA and Regression Models for Corrosion Penetration Rate (P_r)

The results of ANOVA for corrosion penetration rate of H and T Mixtures are presented in Table 4.13 and Table 4.14 while the relationships between the fitted and experimental data are shown in Figure 4.6 and 4.7 respectively.

From ANOVA analysis for corrosion penetration rate (Table 4.13) of *H*-test specimens, it can be observed that all the individual variables (Q_C, $R_{w/cm}$, $R_{FA/TA}$, T_{CV}, and C_{CHL}) were found with significant effects on corrosion penetration rate (P_r). Out of ten interactive variables, five were found with significant effect on corrosion penetration rate, but the other five including $Q_CR_{FA/TA}$, Q_CT_{CV}, Q_CC_{CHL}, $R_{FA/TA}C_{CHL}$, and $R_{FA/TA}C_{CHL}$ were found to be insignificant. Accordingly, Q_C, $R_{w/cm}$, $R_{FA/TA}$, T_{CV}, C_{CHL}, Q_C $R_{w/cm}$, $R_{w/cm}$ $R_{FA/TA}$, $R_{w/cm}$ T_{CV}, $R_{w/cm}$ C_{CHL}, and $T_{CV}C_{CHL}$ were considered for regression analysis of corrosion penetration rate P_r. The regression models for corrosion penetration rate of *H*-test specimens are as follows:

Model generated in terms of scaled variables (R^2=0.92):

$$P_r = \sqrt{\begin{aligned} &38.31 - 138.4Q_C + 0.68Exp(-1.442R_{w/cm}) + 3.07R_{FA/TA}^{3.6076} + 61.147T_{CV}^{1.341} \\ &+ 0.19Exp(-4.14C_{CHL}) + 149.65(Q_CR_{w/cm}) - 14.37(R_{w/cm}R_{FA/TA}) \\ &- 96.25(R_{w/cm}T_{CV}) + 8.25Exp(0.76R_{w/cm}C_{CHL}) - 5.82(T_{CV}C_{CHL}) \end{aligned}} \quad ...(4.9)$$

Model generated in terms of actual (un-scaled) variables (R^2=0.92):

$$P_r = \sqrt{\begin{aligned} &38.31 - 0.35Q_C + 0.68Exp(-3.01R_{w/cm}) + 54.68R_{FA/TA}^{3.6076} + 0.32T_{CV}^{1.341} \\ &+ 0.19Exp(-34.53C_{CHL}) + 0.78(Q_CR_{w/cm}) - 66.54(R_{w/cm}R_{FA/TA}) \\ &- 4.01(R_{w/cm}T_{CV}) + 8.25Exp(13.20R_{w/cm}C_{CHL}) - 0.97(T_{CV}C_{CHL}) \end{aligned}} \quad ...(4.10)$$

Table 4.13: ANOVA for corrosion penetration rate of H-test specimens.

Factors	Type	Level	Scale values			
Q_C	Fixed	3	0.875	0.938	1.000	
$R_{w/cm}$	Fixed	3	0.792	0.896	1.000	
R_{FATA}	Fixed	3	0.778	0.889	1.000	
T_{CV}	Fixed	3	0.500	0.750	1.000	
C_{CHL}	Fixed	3	0.250	0.583	1.000	
Source	DF	Seq SS	Adj MS	F	P	Comment
Q_C	2	56.370	28.180	14.040	0.000	Yes
$R_{w/cm}$	2	6795.210	3397.610	1692.420	0.000	Yes
R_{FATA}	2	42.340	21.170	10.550	0.000	Yes
T_{CV}	2	2570.940	1285.470	640.320	0.000	Yes
C_{CHL}	2	470.330	235.170	117.140	0.000	Yes
$Q_C * R_{w/cm}$	4	118.830	29.710	14.800	0.000	Yes
$Q_C * R_{FATA}$	4	11.200	2.800	1.390	0.237	No
$Q_C * T_{CV}$	4	11.130	2.780	1.390	0.240	No
$Q_C * C_{CHL}$	4	19.270	4.820	2.400	0.051	No
$R_{w/cm} * R_{FATA}$	4	52.380	13.100	6.520	0.000	Yes
$R_{w/cm} * T_{CV}$	4	837.470	209.370	104.290	0.000	Yes
$R_{w/cm} * C_{CHL}$	4	28.600	7.150	3.560	0.008	Yes
$R_{FATA} * T_{CV}$	4	3.650	0.910	0.450	0.769	No
$R_{FATA} * C_{CHL}$	4	3.650	0.910	0.450	0.769	No
$T_{CV} * C_{CHL}$	4	76.550	19.140	9.530	0.000	Yes
Error	192	385.450	2.010			
Total	242	11483.380				

Table 4.14: ANOVA for corrosion penetration rate of *T*-test specimens.

Factors	Type	Level	Scale values			
Q_C	Fixed	3	0.875	0.938	1.000	
$R_{w/cm}$	Fixed	3	0.808	0.904	1.000	
R_{FATA}	Fixed	3	0.778	0.889	1.000	
T_{CV}	Fixed	3	0.500	0.750	1.000	
C_{CHL}	Fixed	3	0.250	0.583	1.000	
Source	DF	Seq SS	Adj MS	F	P	Comment
Q_C	2	3976.500	1988.200	119.090	0.000	Yes
$R_{w/cm}$	2	42731.200	21365.600	2139.430	0.000	Yes
R_{FATA}	2	366.300	183.200	18.340	0.000	Yes
T_{CV}	2	10995.500	5497.800	550.510	0.000	Yes
C_{CHL}	2	139.600	69.800	6.990	0.001	Yes
$Q_C * R_{w/cm}$	4	1156.000	289.000	28.940	0.000	Yes
$Q_C * R_{FATA}$	4	14.300	3.600	0.360	0.839	No
$Q_C * T_{CV}$	4	312.100	78.000	7.810	0.000	Yes
$Q_C * C_{CHL}$	4	32.700	8.200	0.820	0.515	No
$R_{w/cm} * R_{FATA}$	4	107.100	26.800	2.680	0.033	Yes
$R_{w/cm} * T_{CV}$	4	3785.400	946.400	94.760	0.000	Yes
$R_{w/cm} * C_{CHL}$	4	77.100	19.300	1.930	0.107	No
$R_{FATA} * T_{CV}$	4	23.700	5.900	0.590	0.668	No
$R_{FATA} * C_{CHL}$	4	38.800	9.700	0.970	0.425	No
$T_{CV} * C_{CHL}$	4	99.200	24.800	2.480	0.045	Yes
Error	192	1917.400	10.000			
Total	242	65772.900				

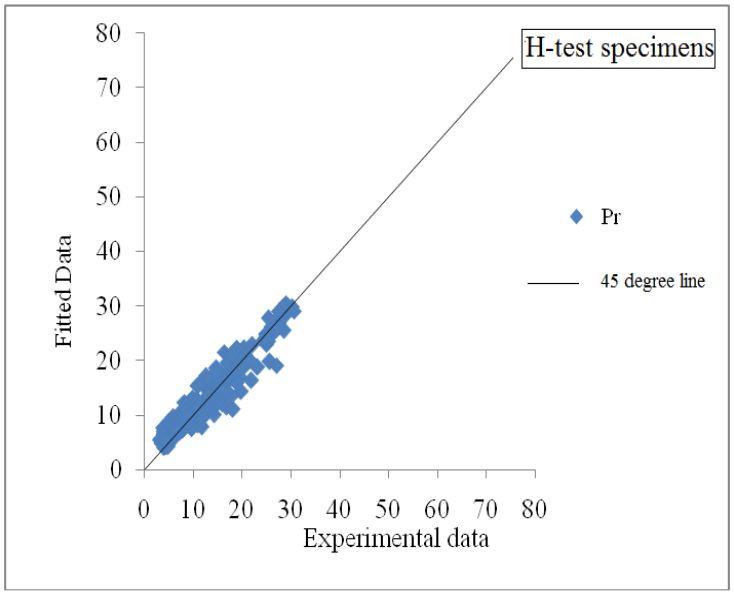

Figure 4.6: Correlation graph of corrosion penetration rate P_r for *H*-test specimens (Experimental data vs. model data).

From Table 4.14 for corrosion penetration rate of *T*-test specimens, it can be observed that like the case of *H*-test specimens all the individual variables (Q_C, $R_{w/cm}$, $R_{FA/TA}$, T_{CV}, and C_{CHL}) were found with significant effects on corrosion penetration rate (P_r). Out of ten interactive variables, five were found with significant effect on corrosion penetration rate and rest five including $Q_CR_{FA/TA}$, Q_CC_{CHL}, $R_{w/cm}C_{CHL}$, $R_{FA/TA}T_{CV}$, and $R_{FA/TA}C_{CHL}$ were found to be insignificant. Accordingly, Q_C, $R_{w/cm}$, $R_{FA/TA}$, T_{CV}, and C_{CHL}, Q_C $R_{w/cm}$, Q_CT_{CV}, $R_{w/cm}$ $R_{FA/TA}$, $R_{w/cm}T_{CV}$, and $T_{CV}C_{CHL}$ were considered for regression analysis of corrosion penetration rate (P_r). The results of the regression model equation for the corrosion penetration rate of *T*-test specimens are presented as follows:

Model generated in terms of scaled variables (R^2=0.93):

$$P_r = -71.35 - 173.60Q_C + 4.38Exp(1.046R_{w/cm}) + 4.57R_{FA/TA}^{-0.0097} + 9.15T_{CV}^{-1.046} + 13.81Exp(-7.30C_{CHL}) + 226.72Q_C R_{w/cm} + 63.40Q_C T_{CV} + 20.75(R_{w/cm}R_{FA/TA})^{0.703} - 59.731(R_{w/cm}T_{CV})^{2.271} + 4.890(T_{CV}C_{CHL}) \quad \text{...(4.11)}$$

Model generated in terms of actual (un-scaled) variables (R^2=0.93):

$$P_r = -71.35 - 0.43Q_C + 4.38Exp(2.011R_{w/cm}) + 4.54R_{FA/TA}^{-0.0097} + 547.95T_{CV}^{-1.046} + 13.81Exp(-60.83C_{CHL}) + 1.09Q_C R_{w/cm} + 0.0032Q_C T_{CV} + 57.65(R_{w/cm}R_{FA/TA})^{0.703} - 0.037(R_{w/cm}T_{CV})^{2.271} + 0.82(T_{CV}C_{CHL}) \quad \text{... (4.12)}$$

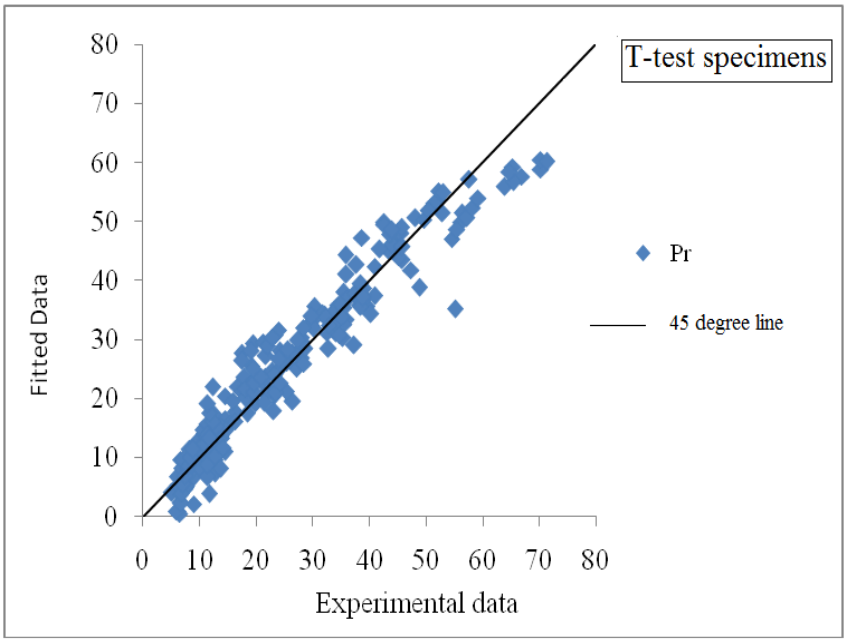

Figure 4.7: Correlation graph of corrosion penetration rate P_r for *T*-test specimens (Experimental data vs. model data).

4.5 EFFECT OF AGGREGATE QUALITY FACTOR ON STRENGTH

For comparing the effect of quality of *H*-type and *T*-type aggregates on strength, the compressive strengths of concrete belonging to both types of aggregate were calculated by using the respective models listed previously (*namely*: Eq. 4.1 and Eq. 4.3) corresponding to water to cementitious materials ratio, $R_{w/cm}$ of 0.40, 0.45, and 0.50 at various combinations of cementitious materials contents, Q_C and fine-to-total aggregate ratios, $R_{FA/TA}$. Calculated values of compressive strength were divided into nine groups, and $f_c^{'}$ versus $R_{w/cm}$ curves were plotted for both types of aggregates, as shown in Fig. 4.8 through 4.16.

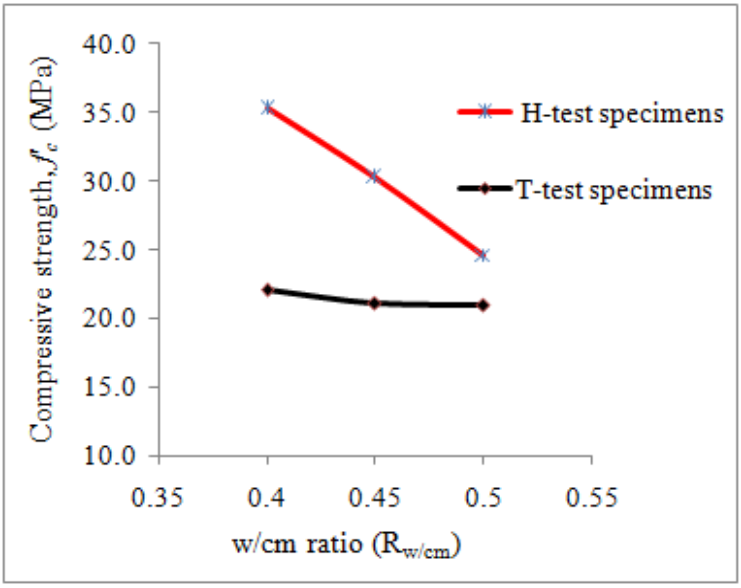

Figure 4.8: Compressive strength relatioship between *H*-test specimen and *T*-test specimens at $R_{FA/TA}$= 0.35 and Q_C= 350 kg/m^3.

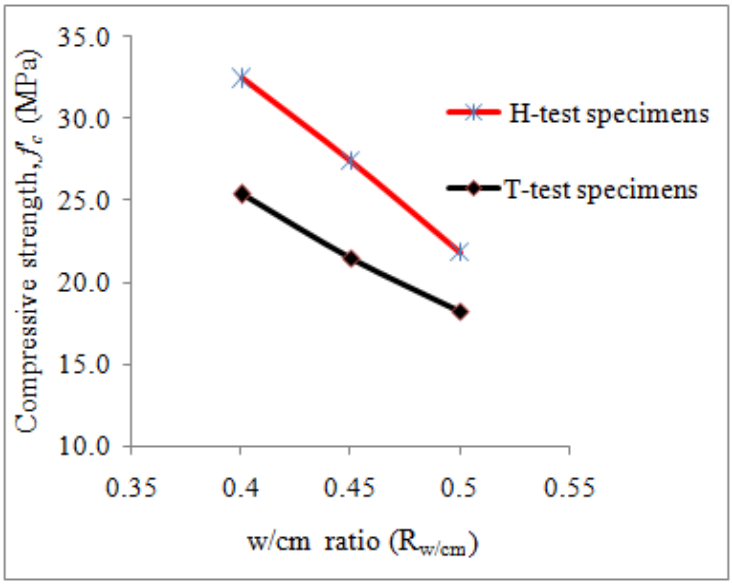

Figure 4.9: Compressive strength relationship between *H*-test specimens and *T*-test specimens at $R_{FA/TA}$= 0.35 and Q_C = 375 kg/m^3.

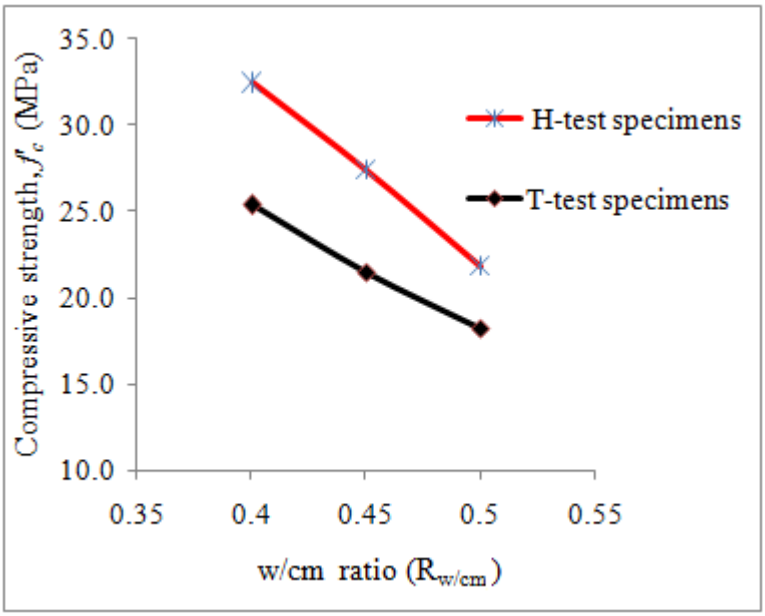

Figure 4.10: Compressive strength relationship between *H*-test specimens and *T*- test specimens at $R_{FA/TA}$= 0.35 and Q_C = 400 kg/m^3.

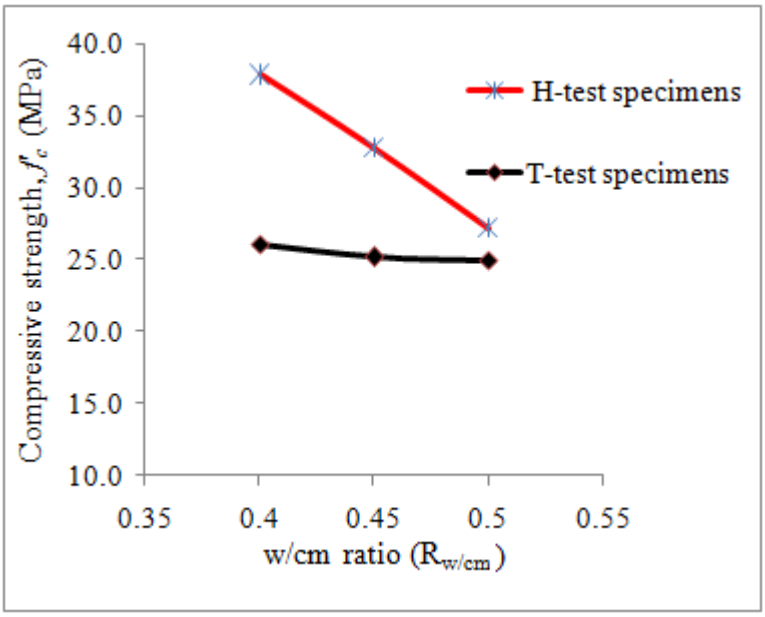

Figure 4.11: Compressive strength relationship between *H*-test specimens and *T*-test specimens at $R_{FA/TA=}$ 0.4 and Q_C= 350 kg/m^3.

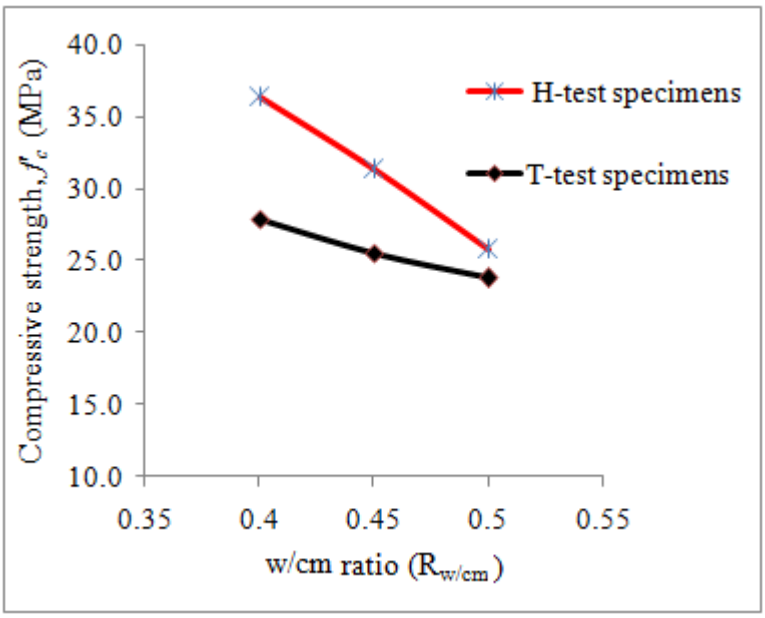

Figure 4.12: Compressive strength relationship between *H*-test specimens and *T*-test specimens at $R_{FA/TA}$ = 0.40 and Q_C = 375 kg/m^3.

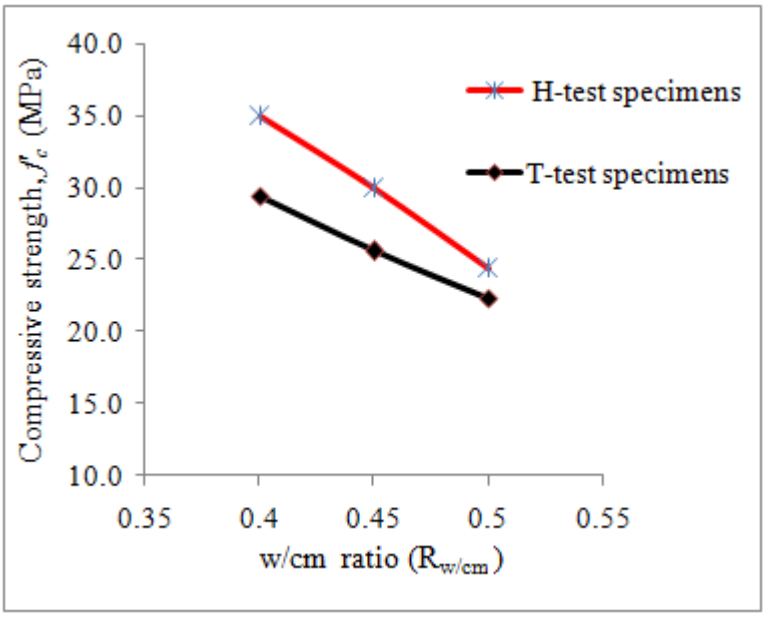

Figure 4.13: Compressive strength relationship between *H*-test specimens and *T*-test specimens at $R_{FA/TA}$= 0.4 and C_{CHL}= 400 kg/m^3.

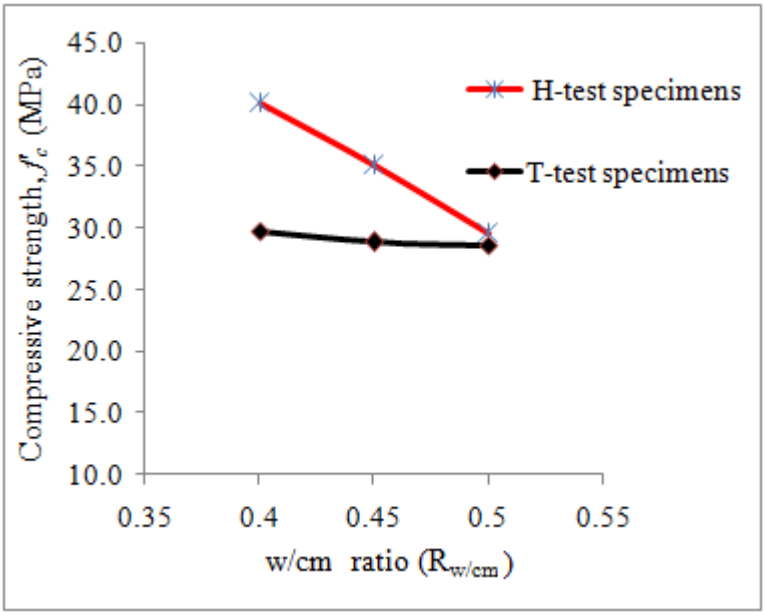

Figure 4.14: Compressive strength relationship between *H*-test specimens and *T*-test specimens at $R_{FA/TA}$=0.45 and C_{CHL}= 350 kg/m^3.

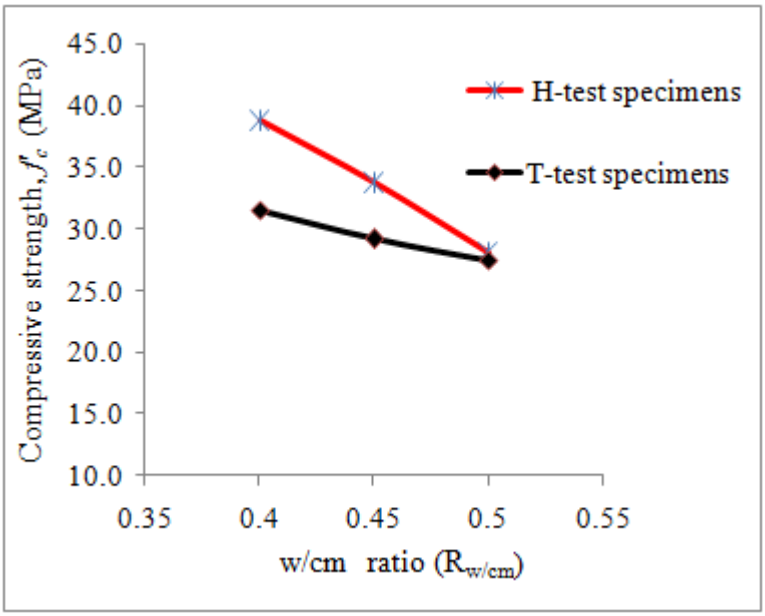

Figure 4.15: Compressive strength relationship between *H*-test specimens and *T*-test specimens at $R_{FA/TA}$=0.45 and C_{CHL}= 375 kg/m^3.

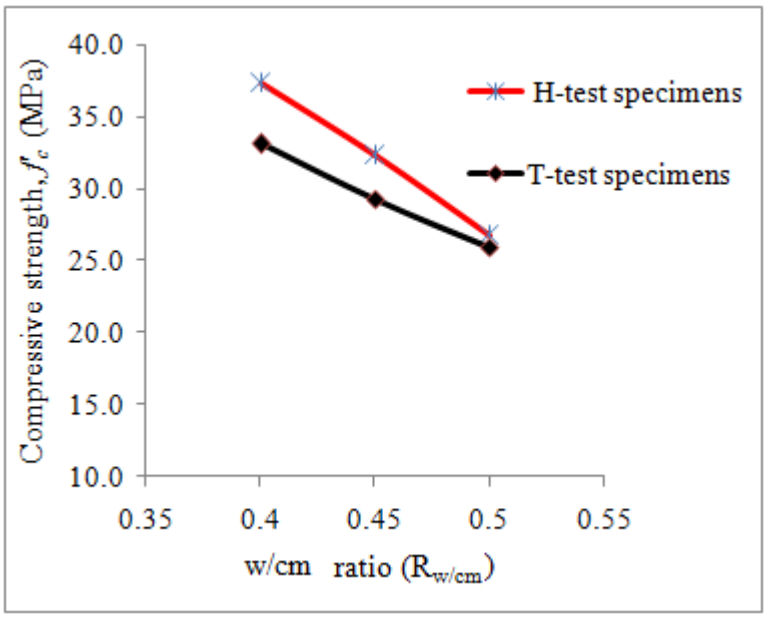

Figure 4.16: Compressive strength relationship between *H*-test specimens and *T*-test specimens at $R_{FA/TA}$=0.45 and C_{CHL}= 400 kg/m^3.

The following points may be noted from Figures 4.8 through 4.16:

- For a given $R_{w/cm}$, Q_C, and $R_{FA/TA}$, the compressive strength of concrete by using *H*-aggregate is higher than that of concrete with *T*-aggregate (i.e., concrete produced with *H*-aggregate performed better than that by using *T*-aggregate).
- Effect of w/cm ratio ($R_{w/cm}$) on compressive strength for concrete by using *T*-aggregate is insignificant at lower cementitious materials content but with increase in cement content the effect of w/cm on compressive strength increases
- The effect of quality of aggregate is more at lower w/cm (i.e. the difference of compressive strengths of concretes made by using two types of aggregates is more at lower w/cm than that at higher w/cm).
- With an increase in the fine to total aggregate ratio (i.e., decrease in the coarse aggregate content), the compressive strength of concrete by using *T*-aggregate increases.

4.6 EFFECT OF AGGREGATE QUALITY FACTOR ON REBAR CORROSION

For comparing the effect of quality of *H* and *T* aggregates on reinforcement corrosion, the corrosion penetration rates of rebar in concrete belonging to both types of aggregate were calculated by using the respective models (Eq. 4.9 and Eq. 4.11) corresponding to w/cm ratio, $R_{w/cm}$ of 0.40, 0.45, and 0.50 at various combinations of cementitious materials contents, Q_C and fine to total aggregate ratios, $R_{FA/TA}$. Calculated values of corrosion penetration rate were divided into nine groups, and P_r versus $R_{w/cm}$ curves were plotted for both types of aggregates, as shown in Fig. 4.17 through 4.25.

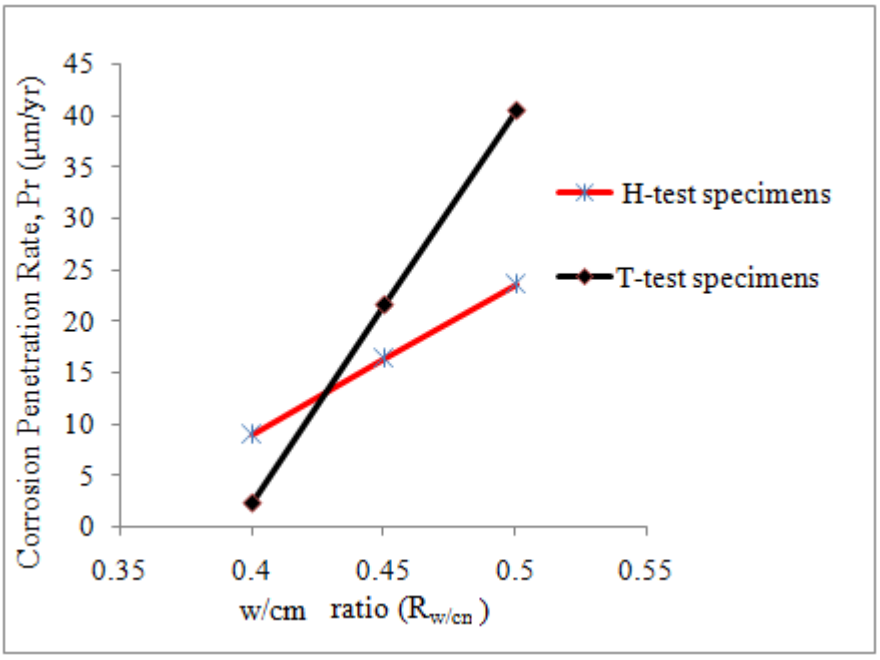

Figure 4.17: Corrosion penetration rate for H-test specimens and T-test specimens at Q_C=350 kg/m^3 $R_{FA/TA}$ =0.35, C_{CHL}=3 % and T_{CV}=25 mm.

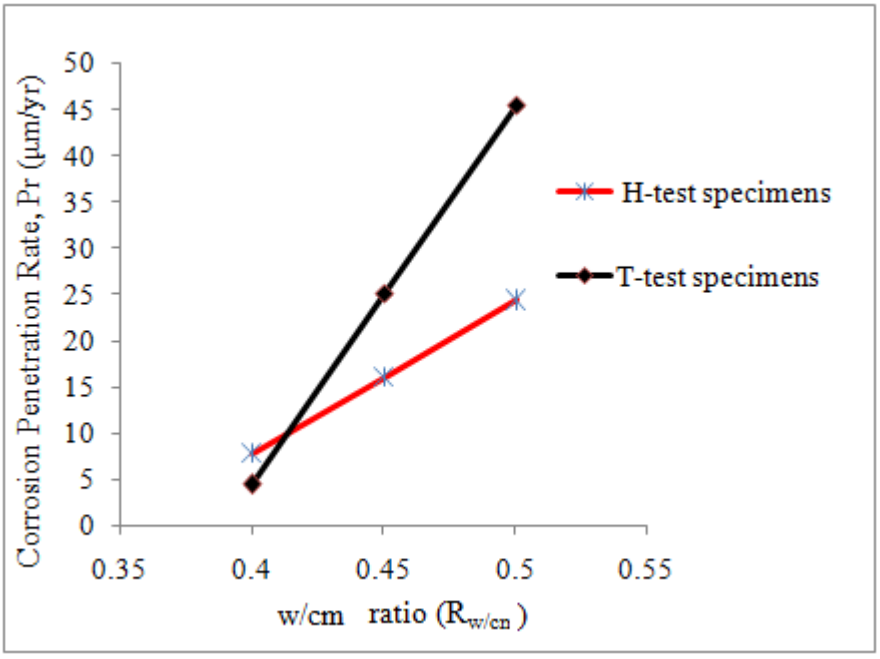

Figure 4.18: Corrosion penetration rate for *H*-test specimens and *T*-test specimens at Q_C=375 kg/m^3 $R_{FA/TA}$ =0.35, C_{CHL}=3 % and T_{CV}=25 mm.

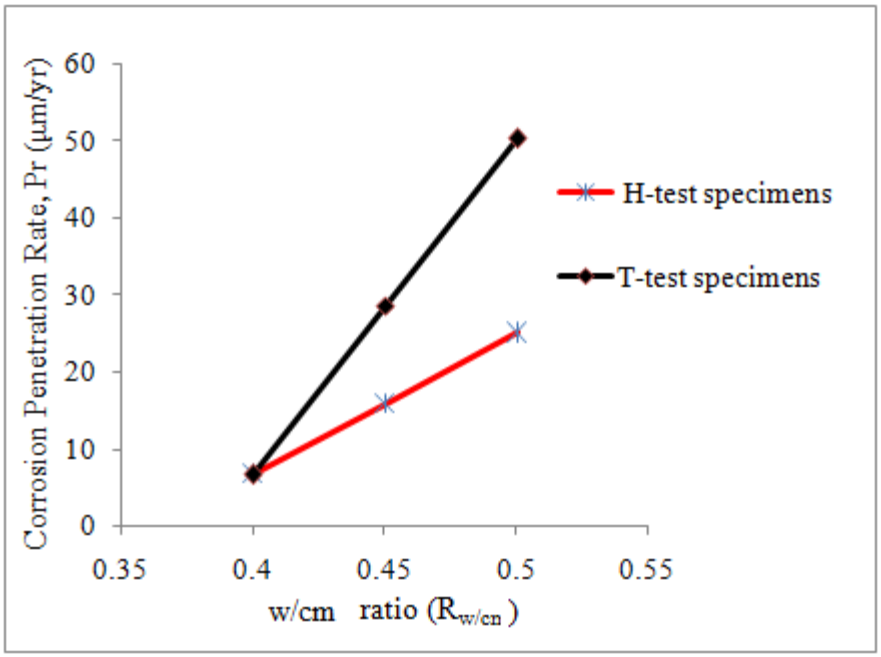

Figure 4.19: Corrosion penetration rate for *H*-test specimens and *T*-test specimens at Q_C=400 kg/m^3 $R_{FA/TA}$ =0.35, C_{CHL}=3 % and T_{CV}=25 mm.

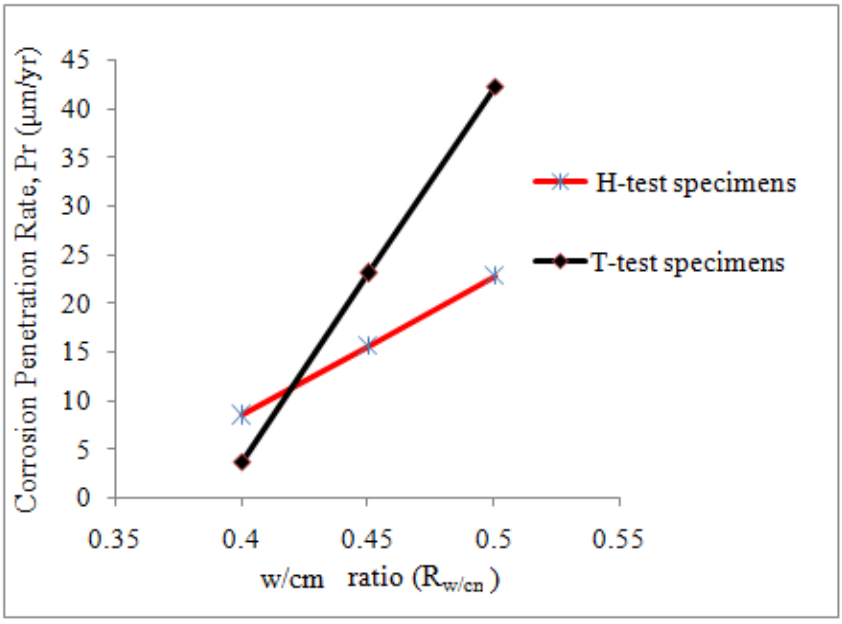

Figure 4.20: Corrosion penetration rate for H-test specimens and T-test specimens at Q_C =350 kg/m3, $R_{FA/TA}$ =0.40, C_{CHL}=3 % and T_{CV} = 25 mm.

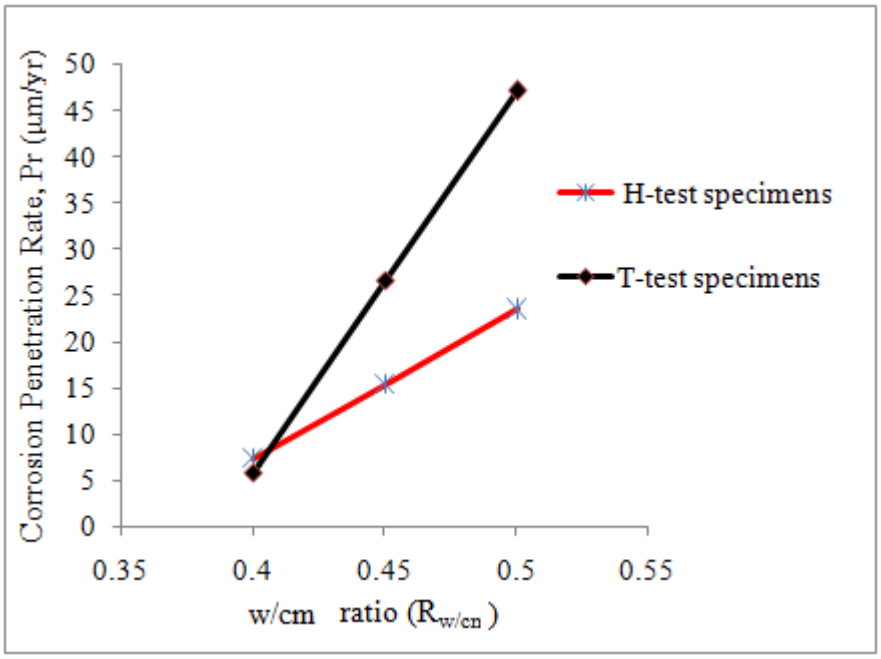

Figure 4.21: Corrosion penetration rate for *H*-test specimens and *T*-test specimens at Q_C =375 kg/m^3, $R_{FA/TA}$ =0.40, C_{CHL}=3 % and T_{CV} =25 mm.

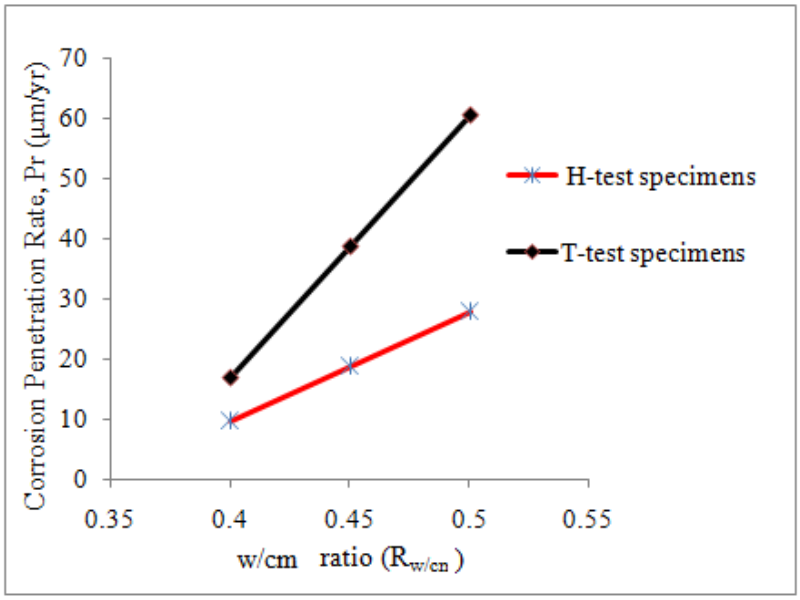

Figure 4.22: Corrosion penetration rate for *H*-test specimens and *T*-test specimens at Q_C = 400 kg/m^3 ,$R_{FA/TA}$ = 0.40, C_{CHL}= 3 % and T_{CV} = 25 mm.

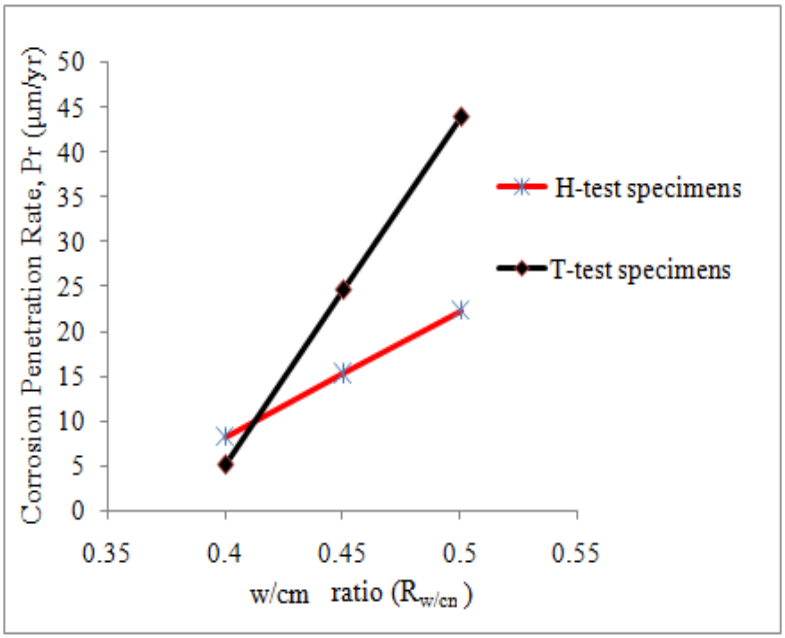

Figure 4.23: Corrosion penetration rate for *H*-test specimens and *T*-test specimens at Q_C = 350 kg/m^3 , $R_{FA/TA}$ = 0.45, C_{CHL}= 3 % and T_{CV}= 25 mm.

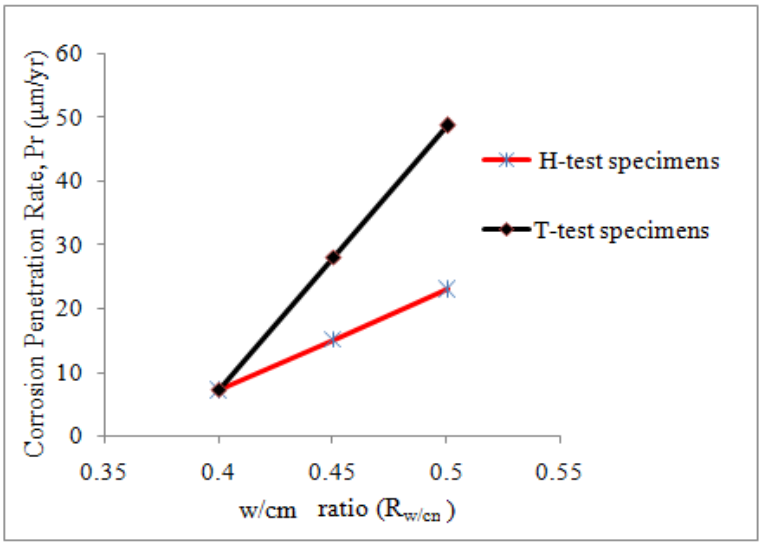

Figure 4.24: Corrosion penetration rate for *H*-test specimens and *T*-test specimens at Q_C = 375 kg/m^3 , $R_{FA/TA}$ = 0.45, C_{CHL}= 3 % and T_{CV}= 25 mm.

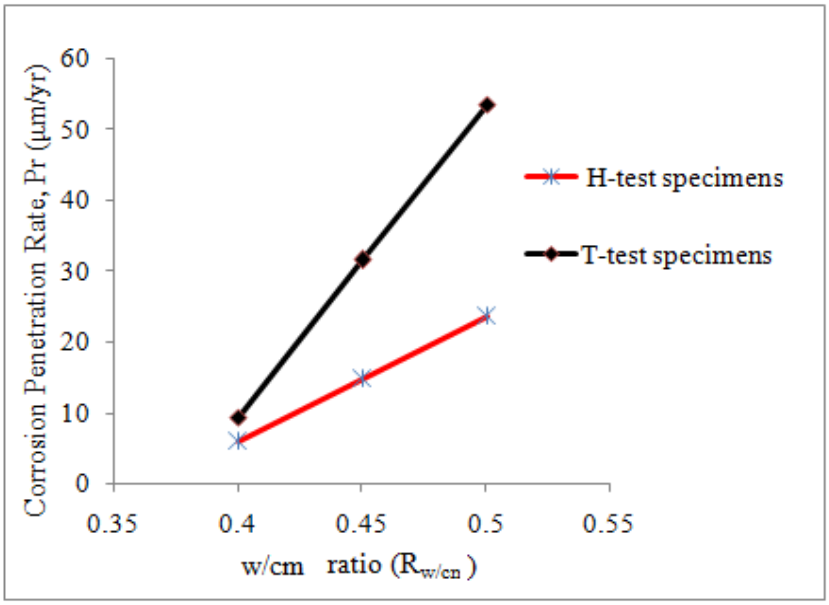

Figure 4.25: Corrosion penetration rate for *H*-test specimens and *T*-test specimens at Q_C = 400 kg/m^3 , $R_{FA/TA}$ =0.45, C_{CHL}=3 % and T_{CV}= 25 mm.

A close inspection of Figs. 4.17 through 4.25 indicates the following points:

- For a given $R_{w/cm}$, Q_C, and $R_{FA/TA}$, the corrosion penetration rate in concrete with *H*-aggregate is lower than that with *T*-aggregate (i.e., concrete produced with *H*-aggregate performed better than that with *T*-aggregate).
- For both types of aggregates (*namely*: *T*-type and *H*-type), the corrosion penetration rate increases linearly with the $R_{w/cm}$.
- Effect of w/cm ($R_{w/cm}$) on corrosion penetration rate for concrete with *T*-aggregate is lower at lower Q_C and vice versa.
- Effect of quality of aggregate is greater at higher $R_{w/cm}$ (i.e. the difference between corrosion penetration rate of rebar in concretes made by using two types of aggregates is lesser at lower $R_{w/cm}$ than that at higher values).

4.7 SUMMARY AND UTILIZATION OF REGRESSION MODELS

The models for strength, elastic modulus, and corrosion penetration rate obtained through ANOVA (using *MINITAB*) and regression analysis (using *Microsoft Excel Solver)* of the experimental data generated in the present study for both *H*-type and *T*-type aggregates are summarized in Table 4.15.

Table 4.15: Models obtained for compressive strength, elastic modulus and corrosion penetration rate.

	Models obtained for concrete using H-type aggregate	Models obtained for concrete using T-type aggregate
$f_c^{'}$	Compressive strength model: $= \left[-61.24 - 0.056\,Q_C - 19.87\,Exp(2.083R_{w/cm}) + 183.45(R_{FA/TA})^{0.119}\right]$ (in MPa)	Compressive strength model: $= \left[\begin{array}{l} -339.12 + 0.39Q_C + 61.43Exp(1.923R_{w/cm}) \\ +205.37(R_{FA/TA})^{0.1766} - 0.081(Q_C R_{w/cm})^{1.3951} \end{array}\right]$ (in MPa)
E_c	Elastic modulus model: $E = \left[-49.1 - 0.048Q_C - 13.23Exp(2.083R_{w/cm}) + 145.68(R_{FA/TA})^{0.106}\right]$ (in GPa)	Elastic modulus model: $= \left[\begin{array}{l} -330.77 + 71.27Exp(0.0025Q_C) + 83.74Exp(1.932B) \\ +186.30(R_{FA/TA})^{0.1768} - 1.101(Q_C R_{w/cm}) \end{array}\right]$ (in GPa)
P_r	Corrosion penetration rate model: $= \left[\begin{array}{l} -71.35 - 0.43Q_C + 4.38Exp(2.011R_{w/cm}) + 4.54(R_{FA/TA})^{-0.0097} \\ +547.95T_{CV}^{-1.046} + 13.81Exp(-60.83C_{CHL}) + 1.09Q_C R_{w/cm} \\ +0.0032Q_C T_{CV} + 57.65(R_{w/cm}R_{FA/TA})^{0.703} \\ -0.037(R_{w/cm}T_{CV})^{2.271} + 0.82(T_{CV}C_{CHL}) \end{array}\right]$ (in μm/year)	Corrosion penetration rate model: $= \left[\begin{array}{l} -71.35 - 0.43Q_C + 4.38Exp(2.011R_{w/cm}) + 4.54(R_{FA/TA})^{-0.0097} \\ +547.95T_{CV}^{-1.046} + 13.81Exp(-60.83C_{CHL}) + 1.09Q_C R_{w/cm} \\ +0.0032Q_C T_{CV} + 57.65(R_{w/cm}R_{FA/TA})^{0.703} \\ -0.037(R_{w/cm}T_{CV})^{2.271} + 0.82(T_{CV}C_{CHL}) \end{array}\right]$ (in μm/year)

where:
Q_C = cementitious materials content in kg/m^3,
$R_{w/cm}$ = water-cementitious material ratio (by mass),
$R_{FA/TA}$ = Fine to total aggregate ratio (by mass),
T_{CV} = Cover thickness (mm), and
C_{CHL} = Percentage chloride concentration (decimal).

The developed models were utilized to determine optimal values of mixture parameters and cover thickness at a given chloride exposure corresponding to a maximum compressive strength and minimum reinforcement corrosion penetration rate. For this purpose, *Microsoft Excel Solver* was used in the procedures explained as follows:

1. Maximize the compressive strength and get the corresponding values of mixture parameters, cover thickness, and corrosion penetration rate;
2. Minimize the corrosion penetration rate, and get the corresponding values of mixture parameters, cover thickness, and compressive strength;
3. Optimize compressive strength and corrosion penetration rate simultaneously, and get the corresponding values of mixture parameters and cover thickness;
4. Finally, choose the optimal value out of the above three options

The optimization of compressive strength and corrosion penetration rate, by using the developed models and the approach outlined above, is shown separately for H and T aggregates in Tables 4.16 and 4.17 respectively. The optimization results obtained in Tables 4.16 and 4.17 are utilized for optimal design of RC beams and columns in Chapter 5.

Table 4.16: Optimization of compressive strength and corrosion penetration rate for concrete with *H*-aggregate at 3% chloride exposure.

Optimization option	$f_c^{'}$ (MPa)	P_r (µm/y)	Q_C (kg/m^3)	$R_{W/CM}$ (by mass)	$R_{FA/TA}$ (by mass)	T_{CV} (mm)
I. Maximize compressive strength	42.00	6.09	350	0.38	0.45	50.00
II. Minimize corrosion penetration rate	39.21	3.04	400	0.38	0.45	38.00
III. Simultaneous optimization of strength and corrosion rate	39.20	3.01	400	0.38	0.45	40.32
Finally selected optimization option: **III**	**39.20**	**3.01**	**400**	**0.38**	**0.45**	**40.32**

Table 4.17: Optimization of compressive strength and corrosion penetration rate for concrete with *T*-aggregate at 3% chloride exposure.

Optimization option	$f_c^{'}$ (MPa)	P_r (µm/y)	Q_C (kg/m^3)	$R_{W/CM}$ (by mass)	$R_{FA/TA}$ (by mass)	T_{CV} (mm)
I. Maximize compressive strength	31.38	17.51	400	0.42	0.45	50.00
II. Minimize corrosion penetration rate	21.49	5.70	350	0.42	0.32	50.00
III. Simultaneous optimization of strength and corrosion rate	24.94	6.93	350	0.42	0.39	50.00
Finally selected optimization option: **III**	**24.94**	**6.93**	**350**	**0.42**	**0.39**	**50.00**

CHAPTER 5

OPTIMAL DESIGN OF REINFORCED CONCRETE BEAM AND COLUMN

5.1 INTRODUCTION

The regression models developed and listed in chapter 4 obtained for strength, elastic modulus and reinforcement corrosion penetration rate may be utilized in the optimal design of reinforced concrete members. The cost of a reinforced concrete member can be minimized through optimization at two levels as explained next.

Table 4.15 gives the appropriate regression models which can be optimized to obtain optimum values for strength, elastic modulus and corrosion penetration rate. In the *first level* of optimization, optimum levels of cementitious materials content (Q_C), w/cm ratio ($R_{w/cm}$), fine to total aggregate ratio ($R_{FA/TA}$), and cover thickness (T_{CV}) can be determined for a given chloride concentration (C_{CHL}) corresponding to maximum compressive strength ($f_c^{'}$), maximum elastic modulus (E_c), and minimum reinforcement corrosion penetration rate (P_r). The loss of concrete and steel over design service-life can be predicted by using the optimum values of $f_c^{'}$ and P_r, and other durability parameters as was explained in Chapter 3.

In the *second level* of optimization, a cross-section of the reinforced concrete member can be optimized corresponding to the minimum overall cost in view of the *first level* optimum values of $f_c^{'}$, E_c, and P_r. The predicted values of losses in concrete and steel can be determined from the C_r (concrete loss rate) and the optimized P_r respectively. The details are outlined in Figure 5.1.

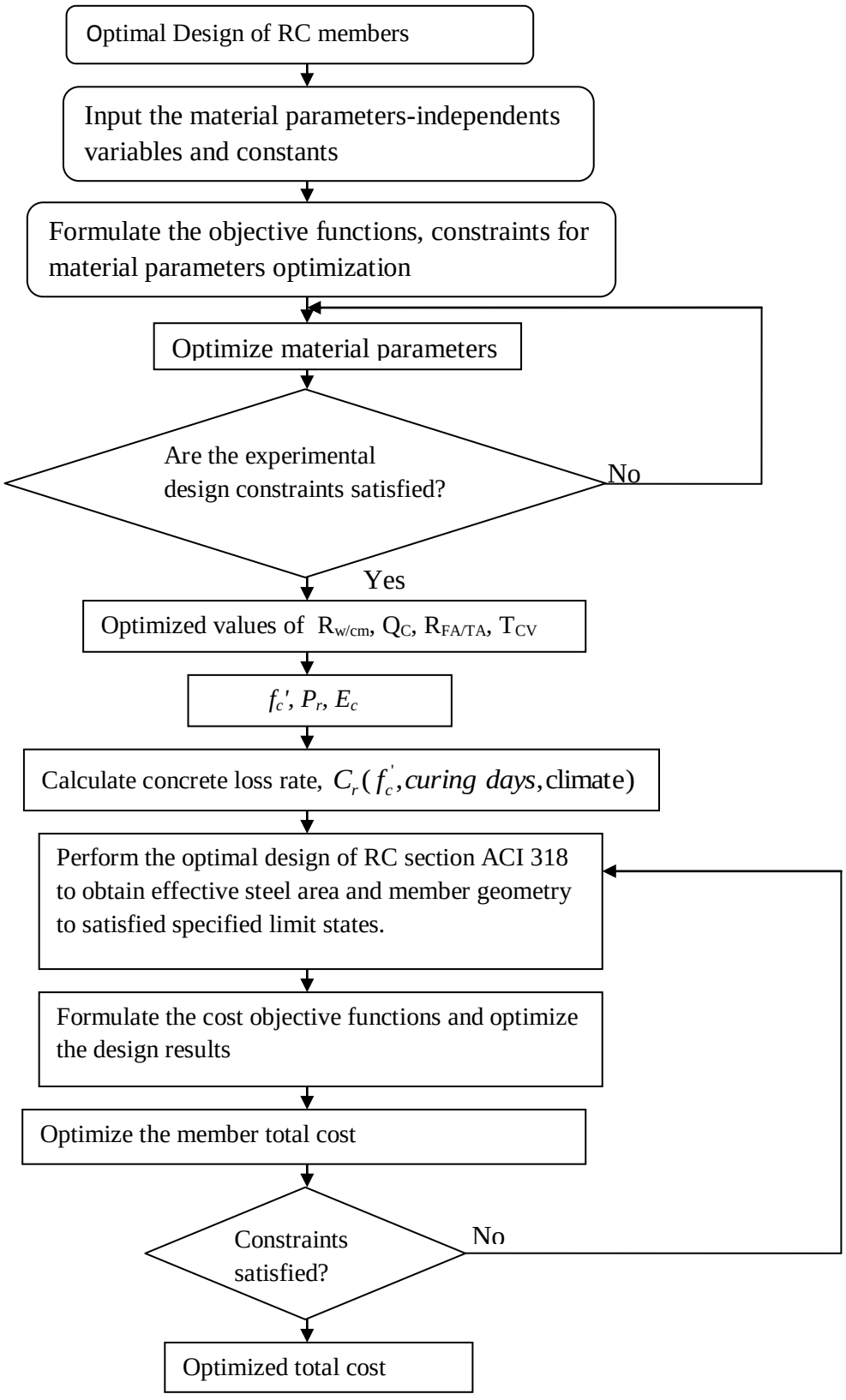

Figure 5.1: Flow chart for structural design of RC members with durability consideration.

5.2 OBJECTIVE FUNCTION, DECISION VARIABLES AND CONSTRAINTS

5.2.1 Objective Function

The overall cost of the member including costs of concrete, steel, and formworks is set as an objective function, given by Eq. 5.1 as follows:

$$F(x) = C_{con} V(x)_{concrete} + \rho_s C_s V(x)_{steel} + C_f A(x)_{formwork} \quad \text{... (5.1a)}$$

or expressed simply as:

$$F(x) = C_{tcon} + C_{ts} + C_{tf} \quad \text{... (5.1b)}$$

where:

$F(x)$ = objective function expressing the overall cost of the reinforced concrete member

C_{con} = unit cost of concrete per unit volume

$V(x)_{concrete}$ = volume of concrete for given values of decision variables (x)

ρ_s = density of steel

C_s = unit cost of steel per unit mass

$V(x)_{steel}$ = volume of steel for given values of decision variables (x)

C_f = unit cost of formwork per unit surface area of the reinforced concrete member

$A(x)_{formwork}$ = surface area of the member for given values of decision variables (x)

C_{ts}= total cost of steel

C_{tcon}= total cost of concrete

C_{tf} = total Cost of formwork

The objective function, as given by Eq. 5.1, is used to minimize the overall cost to achieve the optimal durable design for the reinforced concrete member under consideration.

5.2.2 Decision Variables

In optimization, the parameters, which if they significantly change the value of the objective function are considered as decision variables. For reinforced concrete members such as beams and columns, a change in width and depth of section will change the volume of concrete, volume of steel, and area of the formworks, and therefore the overall cost of the member. Thus, in the geometry of the cross-section of the reinforced concrete member, the defining width and depth, (b_o and h_o), may be considered as the decision variables. If x is the vector containing the decision variables then:

$$x = [b_o, h_o] \qquad ...(5.2)$$

If the geometry of the reinforced concrete member is fixed for any reasons the percentage of steel (ρ) may be considered as a decision variable within its minimum and maximum limits, as specified by the ACI code [103] for strength and durability requirements.

5.2.3 Constraints

Constraints are the restrictions that must be satisfied for ensuring the acceptability of the optimal solutions obtained through objective functions. For optimal design of a reinforced concrete member, the constraints may be considered as the restrictions on minimum and maximum values of geometric dimensions of the cross-section from practical

considerations (practical range of the variation of percentage of steel in a reinforced concrete section, maximum limits of deflection, etc).

5.3 OPTIMAL DESIGN OF RC BEAMS

5.3.1 Objective Function

For a typical reinforced concrete beam, as shown in Figure 5.2, the objective function is formulated to include the cost of concrete, steel and formwork, as given by Eq. 5.3:

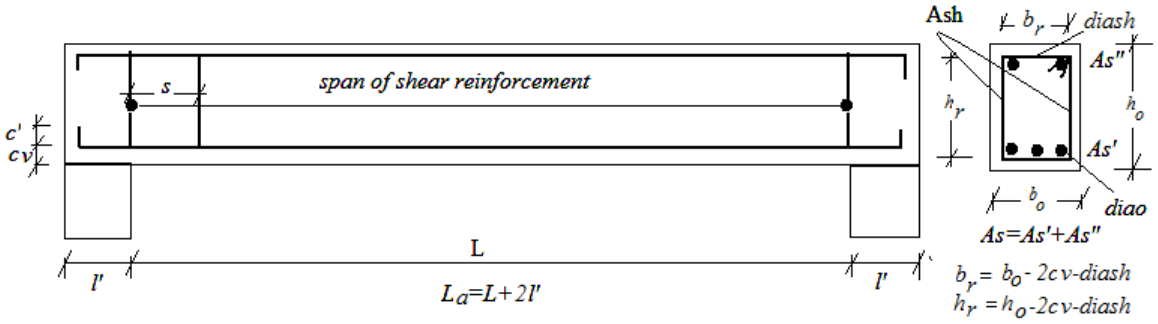

Figure 5.2: Geometric and reinforcement layout of a typical beam.

$$F(x) = b_o h_o L_a C_{con} + \left\{ A_s L' + 2A_{sh}\left(\frac{L}{s}+1\right)(b_r + h_r) \right\} \rho_s C_s + (b_o + 2h_o) L_a C_f \qquad ...(5.3)$$

where:

b_o = width of beam

h_o = depth of beam

b_r= width of shear stirrups

h_r= depth of shear stirrups

l' = adjacent column thickness

L= clear span of the beam

cv = cover to the reinforcement

l = effective span of the beam= $L+ l'$

L' = effective span of the longitudinal reinforcement= $L+2(l'- cv)+2c$

s = spacing of shear stirrups

c = Longitudinal reinforcement anchorage length

L' = effective span of the longitudinal reinforcement= $L+2(l'- cv)+2c$

A_s = cross-sectional area of main steel bars

A_{sh} = cross-sectional area of one two-legged shear stirrup

ρ_{steel} = density of steel =7.85g/cm^3

C_s = unit cost of the steel per tonnage

C_{con} = unit cost of the concrete per volume

C_f = unit cost of the formwork per area.

5.3.2 Constraints

Considering the stress-strain diagram as shown in Figure 5.3, the following constraints can be set for optimizing the objective function given by Eq. 5.3 for optimum design of a reinforced concrete member:

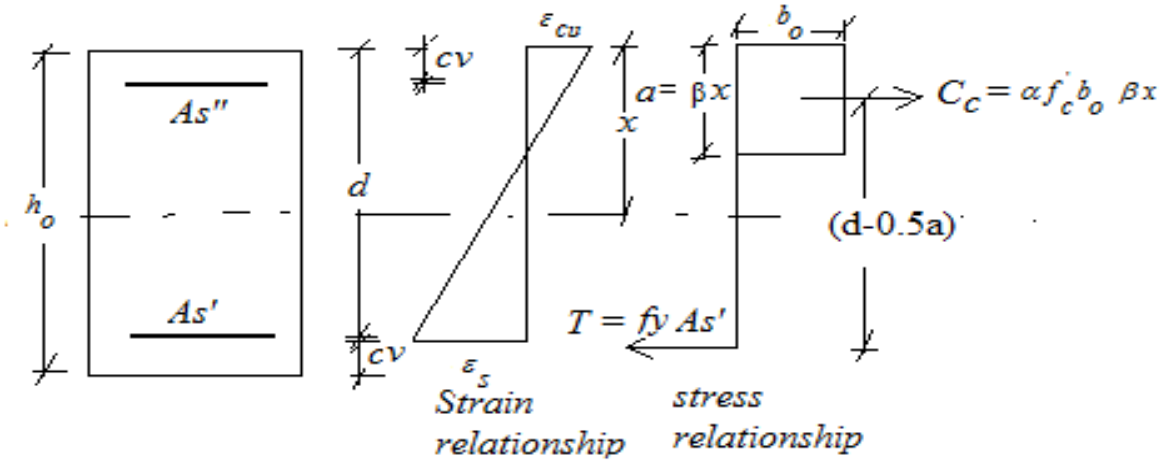

Figure 5.3: Stress-strain diagram of a typical beam.

a) Geometry Constraints

Typical constraints on geometry are: (i) the minimum and maximum acceptable widths as 200 mm and 250 mm (8-in and 10-in), respectively; (ii) the minimum and maximum acceptable depths as: 300 mm and 625 mm (12-in and 25-in), respectively; (iii) the depth to width ratio in the range of 1 to 3.5; and (iv) the span to depth ratio to be less than or equal to 30. The constraints pertaining to beam geometry can be expressed in mathematical inequality form, as given by Eq. 5.4 through 5.7. These constraints are specified for practicality and serviceability reasons.

Width constraints

$$1 - \frac{b_o}{8} \leq 0 \qquad \text{...(5.4a)}$$

$$\frac{b_o}{10} - 1 \leq 0 \qquad \text{...(5.4b)}$$

Depth constraints

$$1-\frac{h_o}{12}\le 0 \qquad ...(5.5a)$$

$$\frac{h_o}{25}-1\le 0 \qquad ...(5.5b)$$

Depth-to-width constraints

$$1-\frac{h_o}{b_o}\le 0 \qquad ...(5.6a)$$

$$\frac{h_o}{3.5b_o}-1\le 0 \qquad ...(5.6b)$$

Span-to-depth ratio constraints

$$\frac{l}{30h_o}-1\le 0 \qquad ...(5.7)$$

b) Shear Force Constraints

These constraints are specified for practicality and serviceability considerations. The combined maximum shear V_R includes the strength provided by concrete V_c and the strength provided by stirrups V_s. Thus,

$$V_R = V_c + V_s \qquad \text{(ACI 11.3.1.1)} \qquad ...(5.8a)$$

$$V_R = 2b'd'\sqrt{f_c'} + \frac{A_{sh}' f_y d'}{s} \le 8b'd'\sqrt{f_c'} \qquad ...(5.8b)$$

where:

b' = residual width of beam after allowing for the loss of concrete due to deterioration

= $b_0 - 2\Delta c$, where Δc is the loss of concrete from one side

d' = residual effective depth of beam after allowing for the loss of concrete due to deterioration $= h_o - cv - 2\Delta c$

$A_{sh}^{'}$ = residual cross-sectional area of one two-legged vertical shear stir = $2 \times \frac{\pi}{4}(\phi_{sh}^{'})^2$

$\phi_{sh}^{'}$ = residual diameter of shear stirrup = $\phi_{sh} - \Delta\phi_{sh}$

ϕ_{sh} = original diameter of shear stirrup

$\Delta\phi_{sh}$ = loss of diameter of shear stirrup due to corrosion = $2P_r t_{corr}$ (with t_{corr} being the time of corrosion propagation) .

The maximum shear force at the support, V_{sd}, due to load on a simply-supported beam as an example is given as:

$$V_{sd} = 0.5 w_u l_a \qquad \ldots(5.9)$$

where: w_u is the factored load and L_a is the span of the beam

V_{sd} should not exceed Eq. 5.8b. The constraints for shear may be set as given by Eq. 5.10:

$$\frac{(V_{sd})_{ij}}{V_R} - 1 \le 0 \quad \text{(ACI318 Sec.11.1)} \qquad \ldots(5.10)$$

c) Bending Moment Constraints

For illustration purposes, a case-study of a simply-supported beam having span, l_a and a factored load w_u, the design moment is given by Eq. 5.11:

$$M_{\max} = \frac{w_u l_a^{\,2}}{8} \qquad \ldots(5.11)$$

For an assumed geometry (i.e. b and d) and given strength of concrete ($f_c^{'}$), the ultimate allowable moment can be determined by using Eq. 5.12, as follows:

$$M_u = 0.85ab'\varphi f_c'(d' - \frac{a}{2}) \quad \ldots(5.12)$$

where: a = depth of the stress block $= 0.75\beta d\left\{\frac{\varepsilon_c}{\varepsilon_c + \varepsilon_s}\right\}$

φ = flexural factor = 0.85

ε_{cu} = maximum strain in concrete = 0.003

ε_s = maxmium strain in steel = $\frac{f_y}{E_s}$

E_s = elastic modulus of steel

The factor "0.75" in the expression for the depth of the stress block a is used to ensure that the section is *designed as an under-reinforced section to satisfy the design ductility requirements*. If $M_{max} \leq M_u$, the beam will be designed as a singly-reinforced section and if $M_{max} > M_u$, it will be re-designed by either increasing the depth or by using doubly-reinforced section design. The maximum moment of resistance of a singly-reinforced beam is given by Eq. 5.13 [103]:

$$M_{res} = A_s' f_y \left\{d' - \frac{A_s' f_y}{1.7 f_c' d'}\right\} \quad \ldots(5.13)$$

MacGregor [144] gave the maximum moment of resistance of a singly-reinforced beam as Eq. (5.14).

$$M_{res} \leq \frac{1}{3} f_c' b' d'^2 \quad \ldots(5.14)$$

$$\frac{M_{\max}}{M_{res}} - 1 \leq 0 \quad \ldots(5.15)$$

If the beam is designed as *singly-reinforced section*, the area of reinforcement can be calculated by using Eq. 5.16, as follows:

$$A_s^{'} = \frac{0.85ab^{'} f_c^{'}}{f_y} \quad \ldots(5.16)$$

If the beam is designed as *doubly-reinforced section*, the area of reinforcement can be calculated by using Eq. 5.17, as follows:

$$A_s = A_s^{'} + A_s^{''} \quad \ldots(5.17)$$

where:

$A_s^{'}$ = cross-sectional area of tension reinforcement.

$A_s^{''}$ = is the cross-sectional area of compression reinforcement

The expression for $A_s^{'}$ and $A_s^{''}$ are given by Eqs. 5.18 and 5.19, respectively.

$$A_s^{'} = \frac{C_c}{f_y} \quad \ldots (5.18)$$

$$A_s^{''} = \frac{M_{\max} - M_u}{(f_y - 0.85 f_c^{'})(d - cv)} \quad \ldots (5.19)$$

where C_c is the force in concrete in compression as defined in Figure 5.3.

d) Percentage of Steel Constraints

According to the American Concrete Institution (ACI) design specification [103], the minimum $\rho_{\min}$ and maximum steel reinforcement ratio $\rho_{\max}$ required are given as follows

$$\rho_{\min} = Max\left\{\frac{200}{f_y}, \frac{3(\sqrt{f_c^{'}})}{f_y}\right\} \quad \text{(ACI 10.5.1)} \quad \ldots(5.20)$$

$$\rho_{\max} = 0.75\beta \frac{f_c^{'}}{f_y}\left\{\frac{87000}{87000 + f_y}\right\} \quad \text{(ACI 10.3.3)} \quad \ldots(5.21)$$

The required steel reinforcement ratio ρ should satisfy the following two constraints relations:

$$1-\frac{\rho}{\rho_{\min}} \le 0 \qquad \text{... (5.22a)}$$

$$\frac{\rho}{\rho_{\max}}-1 \le 0 \qquad \text{... (5.22b)}$$

e) Deflection constraint

Consideration of deflection is an important serviceability requirement for a structure. The case-study of a simply-supported beam having span as, l_a with uniformly distributed load w_u involves the maximum deflection as given by Eq. 5.23:

$$\Delta_{\lim} = \frac{5w_u l_a^4}{384E_c I} \qquad \text{...(5.23)}$$

where:

E_c = elastic modulus of concrete

$I =$ moment of inertia of the beam cross-section $= \frac{b'h'^3}{12}$, $h' = h_0 - 2\Delta c$

ACI 318 Table 9.5a [103] requires that the deflection of the beam should be expressed as:

$$\Delta = \frac{l_a}{180}$$

Thus, the beam design deflection constraint is expressed in a dimensionless form as:

$$\frac{\Delta}{\Delta_{\lim}}-1 \le 0 \qquad \text{...(5.24)}$$

5.4 OPTIMAL DESIGN OF RC COLUMNS

5.4.1 Objective Function

The objective function for an axially-loaded column is typically given by Eq. 5.25 considering overall cost of the column including the cost of concrete, steel and formwork:

$$F(x) = (b_o h_o H)C_{con} + \left\{(A_{sc}L_c^{'}) + 2A_{sh}(\frac{H}{s}+1)((b_o - 2cv) + (h_o - 2cv))\right\}\rho_s C_s + 2H(b_o + h_o)C_f$$

...(5.25)

For square column Eq. 5.25 becomes

$$F(x) = (b_o{}^2 H)C_{con} + \left\{(A_{sc}L_c^{'}) + 4A_{sh}(\frac{H}{s}+1)(b_o - 2cv)\right\}\rho_s C_s + 4Hb_o C_f \quad ...(5.26)$$

where:

b_o = width of column

h_o = depth of column

H = Height of column

$L_c^{'}$ = total length of longitudinal compression reinforcement

s = spacing of shear reinforcement

cv = cover thickness

A_{sc} = cross-sectional area of longitudinal reinforcement

A_{sh} = cross-sectional area of one tie

ρ_{steel} = specific mass of the steel=7.85g/cm^3

C_s = cost of steel per tonnage

C_{con} = cost of concrete per unit of volume

C_f = cost of formwork per unit surface area.

5.4.2 Design Constraints

a) Geometry Constraints:

Typical constraints on an axially loaded column are: (i) the minimum and maximum acceptable widths as 150 mm and 500 mm (6-in and 20-in), respectively; (ii) the minimum and maximum acceptable depths as 300 mm and 625 mm (12-in and 25-in), respectively; and (iii) width should not exceed depth. The constraints pertaining to column geometry can be expressed in mathematical inequality form, as given by Eq. 5.27 through 5.29:

Column width

$$1-\frac{b_o}{6}\le 0 \qquad \text{...(5.27a)}$$

$$\frac{b_o}{25}-1\le 0 \qquad \text{...(5.27b)}$$

Column depth

$$1-\frac{h_o}{15}\le 0 \qquad \text{...(5.28a)}$$

$$\frac{h_o}{25}-1\le 0 \qquad \text{...(5.28b)}$$

$$\frac{b_o}{h_o}-1\le 0 \qquad \text{...(5.29)}$$

b) Strength Constraints

The ultimate strength of an axially-loaded column (R_u) given by Eq. 5.30:

$$R_u = 0.87 f_y A_{sc} + 0.67 f_c^{'} A_c \qquad \text{...(5.30)}$$

Thus,

$$R_u = W_u \quad \text{...(5.31a)}$$

$$A_{sc}^{'} = \frac{W_u - 0.67 f_c^{'} b^{'2}}{0.87 \times f_y - 0.67 \times f_c^{'}} \quad \text{...(5.31b)}$$

where:

A_{sc}= area of steel

A_c = area of concrete = $b'h' - A_{sc}$

$b^{'}$ = residual width of column after concrete deterioration during propagation time, t_{corr}

$= b_o - 2\Delta c$

$h^{'}$ = residual depth of column after concrete deterioration during propagation time, t_{corr}

$= h_o - 2\Delta c$

W_u =the ultimate imposed load ($=1.2W_L + 1.6W_D$)

$$\frac{W_u}{R_u} - 1 \le 0 \quad \text{...(5.32)}$$

Simultaneously, the imposed load of the column should also be set to be less than Euler's critical buckling load, $P_e = EI\left(\frac{\pi}{L}\right)^2$, as shown in Eq. 5.33:

$$\frac{W_u}{P_e} - 1 \le 0 \quad \text{...(5.33)}$$

The normal stress which the column can withstand should be limited to a certain value, say 15 ksi, as shown in Eq. 5.34:

$$\frac{W_u}{15 b_o h_o} - 1 \le 0 \quad \text{...(5.34)}$$

The steel area (A_s) should be limited to a minimum $A_{sc\,\min} = 0.01 b_o h_o$ and maximum $A_{sc\,\max} = 0.08 b_o h_o$ allowed steel area as per the ACI requirement [103] (ACI 318: 10.9.1), such that:

$$1 - \frac{100 A_{sc}}{b_o h_o} \le 0 \qquad \text{...(5.35a)}$$

$$\frac{12.5 A_{sc}}{b_o h_o} - 1 \le 0 \qquad \text{...(5.35b)}$$

5.5 METHODOLOGY FOR OPTIMAL DESIGN OF R.C. MEMBERS

The following four steps summarize the methodology for durable and optimal design of reinforced concrete beams and columns by using the objective functions and constraints outlined in sections 5.1 to 5.4.

Step 1:

Determine the optimum levels of cementitious materials content (Q_C), w/cm ($R_{w/cm}$), fine to total aggregate ratio ($R_{FA/TA}$), and cover thickness (T_{CV}) for a given chloride concentration (C_{CHL}) corresponding to maximum compressive strength ($f_c^{'}$), maximum elastic modulus (E_c), and minimum reinforcement corrosion penetration rate (P_r) by using their respective models given in Table 4.15.

Step 2:

Determine the durability parameters such as chloride diffusion coefficient (D_{app}) from Eq.2.15, time of corrosion initiation (t_p) from Eq. 2.16, time of corrosion propagation (t_{corr})

from Eq. 2.17, and rate of concrete loss (C_r) from Eq. 2.19 and 2.20 by using the optimum values of Q_C , $R_{w/cm}$ and T_{CV} obtained in step 1.

Step 3:

By using the values of t_{corr}, C_r, and P_r obtained in Step 2, determines the residual dimensions of the cross-section (width and depth) of the member by using Eq. 2.21 through 2.23 and the residual rebar diameter by using Eq. 2.25 through 2.26. In all these equations, t will be taken as propagation time t_{corr}.

Step 4:

Carry out the optimum design of reinforced concrete members by using the objective functions, decision variables, and constraints developed based on the ACI 318 reinforced concrete design procedure, and by considering the loss of concrete and steel due to deterioration during an assumed design service-life. The above steps are outlined in the flow-chart given in Figure 5.1.

5.6 CASE STUDY EXAMPLES ON OPTIMAL DESIGN OF RC MEMBERS

5.6.1 Case study on Optimal Design of a RC Beam

A simply supported beam having 20 ft span and subjected to a live load of 960 lb/ft and dead load of 702 lb/ft is to be designed for optimal satisfaction of strength durability and serviceability requirements. The initially specified design data are as follows:

i) Target service-life = 50 years, and service-life factor, $\gamma_s = 2$

ii) Aggregate from Dammam source

iii) Yield strength of steel, f_y = 60,000 psi

iv) Elastic modulus of steel, E_s = 29000 ksi

v) Chloride (NaCl) exposure concentration, C_{CHL} = 3% (C_s=1.8%)

vi) Chloride threshold value, C_{th} to initiate reinforcement corrosion is 0.4% by cement weight

vii) Density of steel, ρ_s=7.85 g/cm^3

viii) Unit cost of concrete, C_{con} = SR 6.75/ft^3

ix) Unit cost of steel, C_s = SR1900/tonnage

x) Unit cost of formwork, C_f = SR 3/ft^2

a) Detailed Solution Methodology and Design Steps

i) Mixture and Cover Thickness Optimization to Determine $f'_{c,\max}$, $E_{c,\max}$, $P_{r,\min}$:

The models for f'_c, E_c, P_r as given in Table 4.15 for *H*-aggregate concrete, were used to determine the optimum values of cementitious materials content (Q_C), w/cm ($R_{w/cm}$), fine to total aggregate ratio ($R_{FA/TA}$), and cover thickness (T_{CV}) for given chloride concentration

(C_{CHL}) of 3%. The *optimum results* shown in Table 4.16 were obtained by using *Microsoft Excel Solver* optimization codes and they are as follows:

Q_C = 400 kg/m^3, $R_{w/cm}$ = 0.4, $R_{FA/TA}$ = 0.45, T_{CV} = 40.32 mm (1.6125 in.)

$f'_{c,\max}$ = 39.21 MPa (5685 psi)

$E_{c,\max}$ = 36.36 GPa (5274 ksi)

$P_{r,\min}$ = 3.01 μm/year (0.0001204 in/year)

ii) Determination of Durability Parameters D_{app}, t_p, t_{corr} and C_r :

The chloride diffusion coefficient D_{app} was obtained by using Eq. 2.15 which is given as follows:

$$D_{app} = [5.73R_{w/cm} - 0.006Q_C + 1.29]10^{-12}$$
$$= [5.73\times 0.38 - 0.006\times 400 + 1.29]10^{-12} = 1.0674\times 10^{-12} \quad \text{m}^2/\text{s}$$

By using Eq. 2.16, the corrosion initiation time t_p is determined as:

$$t_p = \frac{1}{12D_{app}}\left[\frac{C_v}{1-\left(\frac{C_{th}}{C_s}\right)^{0.5}}\right]^2 = \frac{1}{12\times 1.0674\times 10^{-12}\times 3600\times 365\times 24}\left[\frac{40.32\times 0.001}{1-\left(\frac{0.4}{1.8}\right)^{0.5}}\right]^2 = 14.40 \text{ yr}$$

By using Eq. 2.17, the corrosion propagation time t_{corr} is determined as:

$$t_{corr} = Design\,life - t_p = 2\times 50 - 14.40 = 85.6 \text{ year}$$

By using Eq. 2.20, the curing coefficient c_{cur} is determined as:

$$c_{cur} = \frac{1}{0.85 + 0.17\log_{10}(d)}$$

$$= \frac{1}{0.85 + 0.17\log_{10}(28)} = 0.912$$

The rate of loss of structurally effective concrete, C_r, is determined by using Eq. 2.19.

$$C_r = \frac{c_{env}.c_{ur}}{f_{ck}^{3.3}} = \frac{10000 \times 0.912}{39.21^{3.3}}$$
$$= 0.05038 \text{ mm/yr}$$
$$= 1.259 \times 10^{-3} \text{ in/yr}$$

iii) Residual Cross-sectional Dimensions after Deterioration

The residual cross-sectional dimensions b', h', d', ϕ' and $\phi_{sh}^{'}$ after deterioration during t_{corr} are obtained as follows:

By using Eq. 2.21 loss of surface concrete Δc is determined as:

$$\Delta c = C_r t = 1.259 \times 10^{-3} \times 100 = 0.1259 in$$

By using Eq. 2.22, expression for residual width of the beam b' is determined as:

$$b^{'} = b_o - 2\Delta c = b_o - 2 \times 0.1259 = (b_o - 0.2518) \text{ in}$$

By using Eq. 2.23, expression for residual depth of the beam h' is determined as:

$$h^{'} = h_o - 2\Delta c = h_o - 2 \times 0.1259 = (h_o - 0.2518) \text{ in}$$

The expression for residual effective depth of the beam d' is determined as:

$$d^{'} = h^{'} - cv$$

By using Eq. 2.25, loss diameter of rebar $\Delta\phi$ is determined as:

$$\Delta\phi = P_r.t_{corr} = 0.0001204 \times 85.6 = 0.01030624 \text{ in}$$

By using Eq. 2.26, residual diameter of main rebars ϕ' is determined as:

$$\phi' = \phi_o - 2\Delta\phi = \phi_o - 2 \times 0.01030624 = (\phi_o - 0.0206124) \text{ in}$$

Residual diameter of shear stirrups ϕ'_{sh} is determined as:

$$\phi'_{sh} = \phi_{sh} - 2\Delta\phi = \phi_{sh} - 2 \times 0.01030624 = (\phi_{sh} - 0.0206124) \text{ in}$$

Diameter of tension (main) rebars = $\frac{3}{4}$ in,

Diameter of compression rebar = $\frac{5}{8}$ in,

Diameter of two legged vertical stirrups = $\frac{3}{8}$ in,

Effective areas of **one** tension rebar (A_{stac}) = $A'_{stac} = \frac{\pi}{4}\left[\frac{3}{4} - 0.0206124\right]^2 = 0.4116 \text{in}^2$ The

Effective areas of **one** compression rebar (A'_{scac}) = $A'_{scac} = \frac{\pi}{4}\left[\frac{5}{8} - 0.0206124\right]^2 = 0.2870 \text{in}^2$

Area of **one** leg vertical stirrup $A'_{sh} = \frac{\pi}{4}\left[\frac{3}{8} - 0.0206124\right]^2 = 0.098 \text{ in}^2$

iv) Design Moment and Shear Force:

Assuming the load factor γ_L =1.6, γ_d = 1.2 and a live load of 960 lb/ft and a dead load of 702 lb/ft, the ultimate design load is:

w_u=1.2×702+1.6×960 = (842.4+1536) =2378.4 lb/ft, (ACI 318, Sec. 9.2);

and the ultimate design moment is:

$$M_u = 0.125 w_u L^2$$

$M_u = 0.125 \times (2378.4) \times 20^2 = 44655.5 + 76800 = 118.9$ ft-kips,

and the ultimate design shear is:

$$V_{su} = \frac{w_u L}{2}$$

$$V_{su} = \frac{2378 \times 20.33}{2 \times 1000} = 24.2 \text{ kips}$$

v) Design for Moment:

Taking a starting width of beam as 8 inches

$$b' = (8 - 0.2518) = 7.7482 in$$

The maximum permissible design reinforcement is given by [103] as:

$$\rho_{\max} = \frac{0.75 \times \beta \times 0.85 f_c'}{f_y} \times \left[\frac{87000}{87000 + f_y} \right] \quad \text{(ACI 318, Sec. 10.3 \& 10.5)}$$

$$\rho_{\max} = \frac{0.75 \times 0.766 \times 0.85 \times 5685}{60000} \times \left[\frac{87000}{87000 + 60000} \right] = 0.028$$

$$\rho_{b\min} = 3 \frac{\sqrt{f_c'}}{f_y}$$

$$\rho_{b\min} = 0.0038 \geq 0.00333 \quad (\frac{200}{f_y})$$

$$\rho_{b\min} = 0.0038$$

$$m = \frac{f_y}{0.85 f_c'} = 11.67, \text{ assuming } \rho = 0.020$$

$$R_n = \rho \times f_y \times (1 - 0.5 \times \rho \times m)$$

$$R_n = 0.02 \times 60000 \times (1 - 0.5 \times 0.02 \times 11.67) = 1060 psi$$

Mn = M_u / φ =(118.9 ft-kips)/0.9 =132.11 ft-kips

$$d' = \sqrt{\frac{132.11 \times 12 \times 1000}{1060 \times 7.7482}} = 13.89\ in$$

$$h' = (h_o - 0.2518)$$

$$h_o = (h' + 0.2518) = d' + cv + 0.2518 = 13.89 + 1.6128 + 0.2518 = 15.76 in$$, say 16mm

$$d' = 16 - 0.2518 - 1.6128 = 14.13 in$$

Required $R_n = \frac{M_n}{b' d'^2}$

$$R_n = \frac{132 \times 12 \times 1000}{7.7482 \times 14.13^2} = 1023 psi$$

Recall, $m = 11.67$

$$\rho = \frac{1}{m}\left(1 - \sqrt{1 - 2 \times \frac{mR_n}{f_y}}\right)$$

$$\rho = \frac{1}{11.67}(1 - \sqrt{1 - 2 \times \frac{11.67 \times 1185}{60000}} = 0.019$$

$$\rho_{\min} = 0.0038$$

$$\rho_{\max} = 0.028$$

$$A'_{st} = \rho b' d' = 0.019 \times 7.7482 \times 14.13 = 2.08 in^2$$

Therefore, the actual area of steel to be provided, A'_{steff}, to account for reinforcement corrosion is determined as:

Number of bars required, # $= \frac{A_{st}^{'}}{A_{ac}} = \frac{2.319}{0.4116} = 5.05$, say 6 numbers

$$A_{steff}^{'} = 6 \times \frac{\pi}{4}\left(\frac{3}{4}\right)^2 = 2.65 in^2$$

It is concluded that providing 6 bars of ¾ inch diameter as main reinforcement with 3 bars of size 5/8 inch diameter as hanger bars (A_{sc} = 0.92 in^2). *The design is adequate for flexure*.

Since $\rho_{min} < \rho < \rho_{max}$

Check the design: $T = \frac{2.651 \times 60000}{1000} = 159.1 kips$

$$a = \frac{T}{0.85 f_c^{'} b^{'}} = \frac{159.1}{0.85 \times 5681 \times 7.7482} = 4.251 in$$

$$M_n = T(d^{'} - 0.5a) = \frac{159.1}{12}(14.13 - 0.5 \times 4.25) = 159.1 \, ft\text{-}kips \geq 132.11 \text{ft - kips} \ (M_u)$$

Therefore, with ϕM_n > Mu, this design is acceptable in flexure.

vi) Design for Shear:

As per the design specification of ACI 318, Sec 11.3, Eq. 11.3.1.1,

$$\varphi V_c = \varphi \times 2 \times b' d' \sqrt{f_c^{'}}$$

$$\varphi V_c = \frac{0.85 \times 2 \times \sqrt{5681} \times 7.7482 \times 14.13}{1000} = 14.03 kips$$

$$\text{Re}quired \ \varphi V_s = V_{su} - \varphi V_c = (24.2 - 14.03) = 10.17 \text{kips (ACI Eq. 11-15)}$$

$$s = \frac{\varphi A_{sh}^{'} f_y d^{'}}{\varphi V_s} = \frac{0.85 \times 0.1973 \times 60 \times 14.13}{10.17} = 13.98 \text{ in} \leq \frac{d^{'}}{2}(6 in)$$

Provide 41 stirrups @ 6 in spacing until $V_{su} < 0.5 \phi V_c$

vii) Check for Deflection:

As per ACI 318 Sec 9.5, Table 9.5b specification [103], the limiting deflection is given as:

Limiting deflection: $\Delta_{\lim} = \frac{L_a}{360} = 0.68$

$$I = \frac{b^{'}h^{'3}}{12} = \frac{7.7482 \times 15^3}{12} = 2179 in^4$$

$$\Delta = \frac{5 w_l L a^4}{384 E_c I} = \frac{5 \times 1536 \times (20 \times 12)^4}{12 \times 384 \times 5273509 \times 2179} = 0.481 < 0.68 in$$

Therefore, the design also satisfies the deflection constraint of $\frac{\Delta}{\Delta_{\lim}} - 1 \le 0$.

viii) Optimal Design Cost Estimates:

The total cost of steel in the RC beam is given as:

$$C_{ts} = \rho_s \left((A_s \times L^{'} + A_{sh}(b_r + h_r)(\frac{L}{s} + 1) \right) C_s$$

$$C_{ts} = \frac{0.212}{12^3} \left((2.08 + 0.92) \times (240 + 6 + 16) + 0.11 \times 2(6.0122 + 12.05)(\frac{240}{6} + 1) \right) \times 1900$$

$$= SR221.2$$

The total cost of concrete in the RC beam is given as:

$$C_{tcon} = C_{con} \left(\frac{h_o \times b_o \times L_a}{12^3} \right) = 6.75 \times \left(\frac{16 \times 8 \times (240 + 2 \times 8)}{12^3} \right) = SR128$$

The total cost of formwork in the RC beam is given as:

$$C_{tf} = C_f L_a \left(\frac{2h_o + b_o}{12^2} \right) = 3 \times (240 + 2 \times 8) \left(\frac{2 \times 16 + 8}{12^2} \right) = SR213.3$$

$$Total\ Cost = C_{tf} + C_{ts} + C_{tcon}$$

$$Total\ Cost = 221.2 + 120 + 213.3 = SR562.50$$

5.6.2 Case-Study on Optimal Design of a Axially-Loaded RC Square Column

The optimal design of an axially-loaded square column having 12 ft length and subjected to a live load of 440.92 kips and dead load of 202.46 kips is presented here based on the following given data:

Target service-life = 50 years, and service-life factor = 2

Aggregate from the Taif quarries.

Yield strength of steel = 60 ksi

Elastic modulus of steel = 29000 ksi

Chloride (NaCl) exposure concentration, C_{CHL} = 3% (Cs=1.8%) by cement weight

Chloride threshold value to initiate reinforcement corrosion, C_{th}= 0.4% by cement weight

Density of steel, ρ_s= 7.85 g/cm^3 (212 kg/ft^3)

Unit cost of concrete = SR 6.75/ft^3

Unit cost of steel = SR1.900 /kg

Unit cost of formwork = SR 3/ft^2

a) Methodology and Design Steps

Based on the design flow-chart shown in Figure 5.1, the steps for optimal design are as follows:

i) Mixture and Cover Thickness Optimization to Determine $f'_{c,\max}$, $E_{c,\max}$, $P_{r,\min}$:

The models for f'_c, E_c, P_r as given in Table 4.15 for *T*-aggregate concrete were used to determine the optimum values of cementitious materials content (Q_C), w/cm ratio ($R_{w/cm}$),

fine to total aggregate ratio ($R_{FA/TA}$), and cover thickness (T_{CV}) for given chloride concentration (C_{CHL}) of 3% NaCl. The optimum results from *Microsoft Excel Solver* are given in Table 4.17 as follows:

Q_C = 350kg/m^3 , $R_{w/cm}$ = 0.4, $R_{FA/TA}$ = 0.39, T_{CV} = 50 mm (2 in.)

$f'_{c,\max}$ = 24.84 MPa (3.602 ksi)

$E_{c,\max}$ = 23.89 GPa (3464 ksi)

$P_{r,\min}$ = 6.89 µm/year (0.00027555 in/year)

ii) Determination of Durability Parameters D_{app}, t_p, t_{corr} and C_r :

The diffusion coefficient, D_{app}, is first obtained by using equation Eq. 2.15 as follows:

$$D_{app} = [5.73R_{w/cm} - 0.006Q_C + 1.29]10^{-12}$$
$$= [5.73\times 0.42 - 0.006\times 350 + 1.29]10^{-12} = 1.5966\times 10^{-12}\,\text{m}^2/\text{s}$$

By using Eq. 2.16, the corrosion initiation time t_p is determined as:

$$t_p = \frac{1}{12D_{app}}\left[\frac{C_v}{1-\left(\frac{C_{th}}{C_s}\right)^{0.5}}\right]^2$$
$$= \frac{1}{12\times 1.5966\times 10^{-12}\times 3600\times 365\times 24}\left[\frac{50\times 0.001}{1-\left(\frac{0.4}{1.8}\right)^{0.5}}\right]^2$$

Therefore corrosion initiation time, t_p is $= 14.80\ years$

By using Eq. 2.17, the corrosion propagation time, t_{corr}, is determined as:

$$t_{corr} = Design\,life - t_p = 2\times 50 - 14.80$$

$$t_{corr} = 85.2 \text{ year}$$

By using Eq. 2.20, the curing coefficient, c_{cur}, is determined as:

$$c_{cur} = \frac{1}{0.85 + 0.17\log_{10}(d)}$$

$$= \frac{1}{0.85 + 0.17\log_{10}(28)} = 0.912$$

By using Eq. 2.19 for the rate of loss of structurally effective concrete, C_r, is determined as:

$$C_r = \frac{c_{env}.c_{ur}}{f_{ck}^{3.3}} = \frac{10000 \times 0.912}{24.84^{3.3}}$$
$$= 0.2264 \text{ mm/yr} \, (9.0793 \times 10^{-3} \text{ in/yr})$$

iii) Determination of Residual Cross-sectional Dimensions

The residual cross-section dimension of both concrete and steel are determined by first calculating the loss rate. For the concrete, the loss rate is then multiplied by the service-life time .The corrosion propagation time t_{corr} is used for the steel to obtain the residual or effective geometric dimensions such as: b', h', d', ϕ' and $\phi_{sh}^{'}$ as follows:

By using Eq. 2.21, loss of surface concrete Δc is determined as:

$$\Delta c = C_r t = 5.176 \times 10^{-3} \times 100 = 0.9079 in$$

By using Eq. 2.22, expression for residual width of the beam b' is determined as:

$$b^{'} = b_o - 2\Delta c = b_o - 2 \times 0.5176 = (b_o - 1.8159) \text{ in}$$

By using Eq. 2.26, loss diameter of rebar $\Delta\phi$ is determined as:

$$\Delta\phi = P_r.t_{corr} = 0.00027555 \times 85.2 = 0.02348 \text{ in}$$

By using Eq. 2.26, expression for residual diameter of main rebars ϕ' is determined as:

$$\phi^{'} = \phi_o - 2\Delta\phi = \phi_o - 2\times 0.02348 = (\phi_o - 0.0470)\text{ in}$$

Residual diameter of shear stirrups $\phi_{sh}^{'}$ is determined as:

$$\phi_{sh}^{'} = \phi_{sh} - 2\Delta\phi = \phi_{sh} - 2\times 0.02348 = (\phi_{sh} - 0.0470)\text{ in}$$

Taking the diameter of tension rebars as $\frac{11}{8}$in, the effective residual areas of one main bar ($A_{scac}^{'}$) is determined as:

$$A_{scac}^{'} = \frac{\pi}{4}\left[\frac{11}{8} - 0.0470\right]^2 = 1.3853\text{in}^2$$

iv) Design Load:

Assuming the load factors are: γ_L=1.6, γ_d=1.2 and live load 440.5 kips and dead load 202.5 kips, the ultimate design load is:

$$W_u = 1.2\times 202.46 + 1.6\times 440.492 = 948\,\text{kips}$$

v) Design for Axial Load:

Taking a starting value of width b_o = 15 in, $b^{'} = 15 - 1.8159 = 13.18\,in$

$$R_u = 0.87A_{sc}^{'} f_y + 0.67A_c^{'} f_c^{'}$$

$$R_u = 0.87A_{sc}^{'} f_y + 0.67(b^{'2} - A_{sc}^{'}) f_c^{'} = W_u$$

The required area of compression reinforcement area, A_{sc}' is based on Eqn. 5.31b:

$$A_{sc}^{'} = \frac{948000 - 0.67\times 3602\times 13.18^2}{0.87\times 60000 - 0.67\times 3602} = 10.62\,in^2 > 0.04\text{bh},$$

Hence increase the width, b_o = 17 in, $b^{'} = 17 - 1.8159 = 15.18\,in$

$$A_{sc}^{'} = \frac{W_u - 0.67 f_c^{'} b^{'2}}{0.87 \times f_y - 0.67 \times f_c^{'}}$$

$$A_{sc}^{'} = \frac{948000 - 0.67 \times 3602 \times 15.18^2}{0.87 \times 60000 - 0.67 \times 3602} = 7.87 in^2 < 0.04bh$$

Number of steel bars required $\#= \frac{A_{sc}^{'}}{A_{scac}^{'}} = \frac{7.87}{1.3853} = 5.68, \; say \; 6$

Actual area of steel provided to account for reinforcement corrosion is determined as:

$$A_{sc} = \frac{A_{sc}^{'}}{A_{scac}^{'}} \times \frac{\pi}{4}(\phi)^2 = 5.68 \times \frac{\pi}{4}\left(\frac{11}{8}\right)^2 = 8.43 in^2$$

In summary, provide 10 Numbers of 1 inch diameter bar (9.426 in^2), and provide ties of size 5/8 inch bar at @ 8 inches spacing for stirrup (A_{sh} = 0.3068 in^2).

vi) Optimal Design Cost Estimates:

$$C_{ts} = C_s \rho_s \left[A_{sc} L^{'} + 4A_{sh}(b_o - 2cv)(\frac{L}{s} + 1) \right]$$

$$C_{ts} = \frac{1.900 \times 212}{12^3} \left[9.426 \times 150 + 4 \times 0.3068(15 - 2 \times 2)(\frac{144}{8} + 1) \right] = SR389.37$$

$$C_{tcon} = \frac{b_o^{'2} \times H}{12^3} C_{con} = \frac{17^2 \times 144 \times 6.75}{1728} = SR \; 162.56$$

$$C_{tf} = \frac{4 \times b_o \times H \times C_f}{12^2} = \frac{4 \times 17 \times 15 * 3}{12^2} = SR204$$

$$\text{Total cost} = C_{ts} + C_{tcon} + C_{tf} = 389.37 + 162.56 + 180 = SR755.93$$

Therefore, for the design, the total cost SR 755.93

5.6.3 Automated Design Optimization Methodology:

To automate the solution of an optimal design for specified requirement in strength, durability and serviceability, a program is written on *Microsoft Excel* spreadsheet by using the *in-built* Solver. The Solver is based on the design steps implied in the flow-chart shown in Appendix V Fig A5.1 for the case of RC beam design, and Fig. 5A.2 for the case of RC column The Solver will pinpoint the optimal results corresponding to the minimum overall cost of the beam and column. Details of the design output, and samples print-out of the results are provided in Table A5.1 and Table A5.2 of Appendix V for the examples considered.

CHAPTER 6

CONCLUSIONS AND RECOMMENDATIONS

The main of this study aimed to develop the models for material parameters such as compressive strength, elastic modulus and corrosion penetration rate which are utilized in the development of an automated design methodology for the optimal design of reinforced concrete members in corrosive environments by using coarse aggregates from two different sources in Saudi Arabia (Dammam quarries representing the eastern and central regions and Taif quarries representing the western region). It is a combined research program that comprises both experimental and analytical studies. The key stages of the research study are:

1. The two types of aggregates were used to prepare and test un-reinforced and reinforced concrete specimens for generating data required for developing regression models for concrete compressive strength f'_c and elastic modulus of concrete E_c, and reinforcement corrosion penetration rate P_r .
2. The varying key design factors included cementitious materials content Q_C, water to cementitious materials ratio $R_{w/cm}$, fine to total aggregate ratio $R_{FA/TA}$, cover thickness T_{CV}, and level of simulated chloride exposure C_{CHL} by using NaCl aqueous solutions.
3. The models obtained were used to maximize compressive strength f'_c and elastic modulus E_c and minimize reinforcement corrosion penetration P_r by selecting

optimal levels of mixture parameters and cover thickness for a given level of chloride exposure.

4. An approach was proposed for carrying out the cost-effective design of beams and columns for specified strength and durability design requirements based on orders of design parameters obtained by utilizing the models developed in the present research.

The sequel includes particular conclusions derived from the research study and ends with recommendation for further research studies.

6.1 CONCLUSIONS

Based on the findings of the present research, the following conclusions may be drawn:

1. Compressive strength and elastic modulus of concrete cast are significantly affected by cementitious materials content Q_C, water cementitious material (w/cm) ratio $R_{w/cm}$, and fine to total aggregate ratio $R_{FA/TA}$.
2. Aggregates water absorption and abrasion losses are very important in determining the concrete strength rather than only the specific gravity (density). In fact aggregates with low water absorption, specific gravity, and abrasion loss value performed better in relation to strength and durability of concrete than aggregates that has higher specific gravity, water absorption and abrasion loss.
3. Chloride concentration, cover thickness and permeability of concrete matrix are major factors influence the corrosion penetration rate P_r which is capable of causing reinforcement corrosion.

4. Low fine-to-total aggregate ratio varied between 0.4 to 0.45 performs better in relation to strength and durability of reinforced concrete in corrosive environment compare to lower values.
5. Corrosion penetration rate of 5 μm/yr (0.5 μA/cm^2) could cause a significant damage to reinforced concrete at a shorter time due to tensile stress developed as a result of deposition of rust product on the rebar surface especially when the cover thickness is less than 37.5 mm.
6. Although the Taif (T-type) aggregates has a higher specific gravity and lower water absorption as compared to Dammam (H-types) aggregates, the *abrasion resistance* of Taif (T) aggregate was found to be lower than that of Dammam aggregate by about 25%.
7. The achievable maximum strength in the Dammam aggregate was 40 MPa at 0.38 w/cm ratio, a value of 31 MPa was achieved in the case of Taif aggregate concrete at 0.42 w/cm ratio.
8. The minimum achievable corrosion penetration rate P_r for Dammam aggregate concrete was 3.0 μm/yr, a value of 5.7 μm/yr was obtained with Taif aggregate concrete.
9. The maximum compressive strength $f_c^{'}$ and minimum corrosion penetration rate P_r for Taif aggregate was found to be respectively 35% lower and 47% higher than Dammam aggregate concrete. Hence Dammam aggregate performed better than Taif aggregate in both strength and reinforcement corrosion.
10. Based on the generated models, values of the cementitious materials content Q_C, water to cementitious materials ratio $R_{w/cm}$, and fine to total aggregate ratio $R_{FA/TA}$ that

gave highest strength and elastic modulus of concrete for both aggregate types were found to be 375 kg/m^3, 0.38, and 0.45, respectively for Dammam aggregate concrete. For Taif aggregates concrete, the same values were found to be 400 kg/m^3, 0.42, and 0.45 respectively.

11. Reinforcement corrosion penetration rate was found to be affected by all five factors (cementitious materials content Q_C, w/cm ratio $R_{w/cm}$, and fine to total aggregate ratio, $R_{FA/TA,}$ cover thickness T_{CV}, and level of chloride exposure C_{CHL}) for both T-type and H-type aggregates.

12. From the models obtained and at 3% chloride exposure C_{CHL}, values of cementitious materials content Q_C, w/cm ratio $R_{w/cm}$, and fine to total aggregate ratio $R_{FA/TA,}$ and cover thickness T_{CV}, that gave minimum corrosion penetration rate values P_r were found to be 400 kg/m^3, 0.38, 0.45 and 40 mm respectively for Dammam aggregate concrete. For Taif aggregates concrete, the same values were found to be, 400 kg/m^3, 0.43, 0.35 and 50 mm respectively.

9. For a given level of chloride exposure of 3%, the optimum values of cementitious materials content $Q_{C,}$ water to cementitious materials ratio $R_{w/cm}$, and fine to total aggregate ratio, $R_{FA/TA,}$ and cover thickness, T_{CV}, that give the optimum corrosion penetration rate values P_r and optimum compressive strength f_c' for Dammam aggregate concrete are found to be 400 kg/m^3, 0.38, 0.45 and 40 mm respectively. For Taif aggregates concrete, the same values were found to be, 350 kg/m^3, 0.42, 0.35 and 50 mm, respectively.

10. The developed models can be utilized for determining optimal values of mixture parameters and cover thickness at a given chloride exposure corresponding to a

maximum compressive strength f_c' and minimum reinforcement corrosion penetration rate, P_r.

11. The automated method outlined in this research work for optimal design of reinforcement concrete members may be used to obtain cost-effective and durable designs of RC beam and column.

12. The *Microsoft Excel* optimal design code achieved a 2% cost reduction for the case study considered in this research work of a simply supported beam with Dammam aggregate concrete, while 8% cost reduction was achieved for the axial column design with Taif aggregate.

6.2 RECOMMENDATIONS

As a further extension of this research work, it is recommended that further studies and utilization of the generated models be undertaken such that:

1. The specimens over which the research was conducted be utilized for further research study by carrying out the gravimetric measurement of corrosion rate of rebar in order to determine rebar loss of mass with time. From this, more refined corrosion rate model can be obtained.
2. The optimization developed can be greatly improved by Finite Element Analysis (FEA) where the values of moment and shear at every section of the beams can be obtained. This will further yield additional economy due to reduction in materials quantities. In addition, continuous beams and biaxial columns can be easily studied when the FEA model is used.
3. The models generated within this research work are based on two-aggregate from Taif (Western province) and Riyadh road quarries (Eastern province). The aggregate type (*namely*: *T*-type and *H*-type) are representative of most prevalent aggregates type used in Eastern and Western regions of Saudi Arabia. It is advisable to ensure that verification check (as regards the aggregate type) is conducted for the purpose of adequate utilization of the model for optimal design of RC structural members.

APPENDICES

Appendix I: Typical stress-strain curves of a specimen cast with H and T aggregates.

Appendix II: Procedure for Analysis of Variance (ANOVA).

Appendix III: Samples of ANOVA results obtained from MINITAB software.

Appendix IV: Details of Butler-Volmer Equation.

Appendix V: Automation design methodology.

i. Flow chart for RC beam;

ii. Flow chart for RC column

iii. Microsoft Excel output interface for optimal design of beam

iv. Microsoft Excel output interface optimal design of columns

Appendix I: Typical stress-strain curves of a specimen cast with H and T aggregates

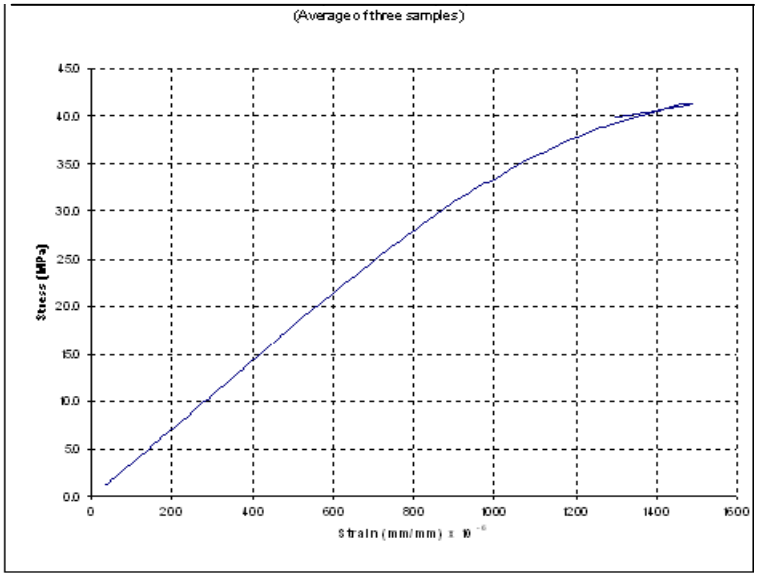

Figure A1.1: Typical stress-strain curve for *H*-test specimen

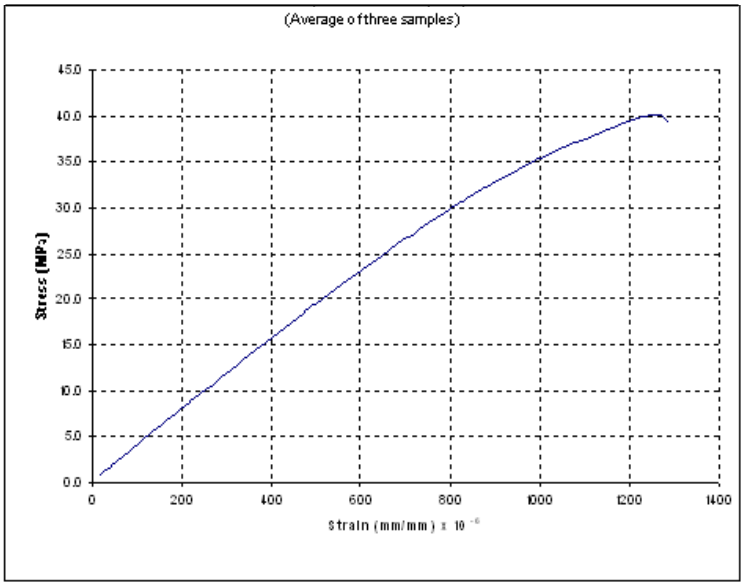

Figure A1.2: Typical stress-strain curve for *T*-test specimen

Appendix II: Procedure for Analysis of Variance (ANOVA)

Consider variable factors **A** (cementitious material content), **B** (w/cm ratio), and **C** (FA/TA ratio) and their three levels of variations, say levels **1**, **2**, and **3**. Sources of effects of these three factors would be as follows: **A**, **B**, **C**, **AB**, **BC**, **AC**, and **ABC**.

ANOVA involves calculation of the following **statistical parameters**:

- Overall mean ($\overline{Y}$)
- Correction factor (*CF*)
- Degree of freedom (*df*)
- Sum of squares (*SS*)
- Mean squares (*MS*)
- F-ratio

Overall mean ($\overline{Y}$)

$$\overline{Y} = \frac{\text{total sum of all observations}}{\text{total number of observations}}$$

Correction factor (*CF*)

$$CF = \frac{(\text{total sum of all observations})^2}{\text{total number of observations}}$$

Degree of freedom (*df*)

Degree of freedom is the number of observations that can be varied independently of each other.

df of a factor having *n* levels of variations = $n - 1$

Sum of squares (*SS*)

Total sum of squares (SS_T):

$$SS_T = \sum_{i=1}^{N} (Y_i - \overline{Y})^2$$

where

Y_i = i^{th} observation

$\overline{Y}$ = overall mean of the N observations

Sum of squares of individual factor A (SS_A):

$$SS_A = \frac{\left(\sum A1\right)^2 + \left(\sum A2\right)^2 + \left(\sum A3\right)^2 + ...}{\text{number of observations for each level}} - CF$$

Sum of squares of individual factor B (SS_B):

$$SS_B = \frac{\left(\sum B1\right)^2 + \left(\sum B2\right)^2 + \left(\sum B3\right)^2 + ...}{\text{number of observations for each level}} - CF$$

Sum of squares of individual factor C (SS_C):

$$SS_C = \frac{\left(\sum C1\right)^2 + \left(\sum C2\right)^2 + \left(\sum C3\right)^2 + ...}{\text{number of observations for each level}} - CF$$

Sum of squares of interactive factor AB (SS_{AB}):

$$SS_{AB} = \left[\frac{\begin{array}{l} \left(\sum A1B1\right)^2 + \left(\sum A1B2\right)^2 + \left(\sum A1B3\right)^2 + ... \\ + \left(\sum A2B1\right)^2 + \left(\sum A2B2\right)^2 + \left(\sum A2B3\right)^2 + ... \\ + \left(\sum A3B1\right)^2 + \left(\sum A3B2\right)^2 + \left(\sum A3B3\right)^2 + ... \end{array}}{\text{number of observations for each level}} \right] - SS_A - SS_B - CF$$

Sum of squares of interactive factor BC (SS_{BC}):

$$SS_{BC} = \left[\frac{\begin{array}{l} \left(\sum B1C1\right)^2 + \left(\sum B1C2\right)^2 + \left(\sum B1C3\right)^2 + ... \\ + \left(\sum B2C1\right)^2 + \left(\sum B2C2\right)^2 + \left(\sum B2C3\right)^2 + ... \\ + \left(\sum B3C1\right)^2 + \left(\sum B3C2\right)^2 + \left(\sum B3C3\right)^2 + ... \end{array}}{\text{number of observations for each level}} \right] - SS_B - SS_C - CF$$

Sum of squares of interactive factor AC (SS_{AC}):

$$SS_{AC} = \left[\frac{\begin{array}{l} \left(\sum A1C1\right)^2 + \left(\sum A1C2\right)^2 + \left(\sum A1C3\right)^2 + ... \\ + \left(\sum A2C1\right)^2 + \left(\sum A2C2\right)^2 + \left(\sum A2C3\right)^2 + ... \\ + \left(\sum A3C1\right)^2 + \left(\sum A3C2\right)^2 + \left(\sum A3C3\right)^2 + ... \end{array}}{\text{number of observations for each level}} \right] - SS_A - SS_C - CF$$

Sum of squares of interactive factor ABC (SS_{ABC}):

$$SS_{ABC} = \left[\frac{\begin{array}{l} \left(\sum A1B1C1\right)^2 + \left(\sum A1B1C2\right)^2 + \left(\sum A1B1C3\right)^2 + ... \\ + \left(\sum A1B2C1\right)^2 + \left(\sum A1B2C2\right)^2 + \left(\sum A1B2C3\right)^2 + ... \\ + \left(\sum A1B3C1\right)^2 + \left(\sum A1B3C2\right)^2 + \left(\sum A1B3C3\right)^2 + ... \\ \left(\sum A2B1C1\right)^2 + \left(\sum A2B1C2\right)^2 + \left(\sum A2B1C3\right)^2 + ... \\ + \left(\sum A2B2C1\right)^2 + \left(\sum A2B2C2\right)^2 + \left(\sum A2B2C3\right)^2 + ... \\ + \left(\sum A2B3C1\right)^2 + \left(\sum A2B3C2\right)^2 + \left(\sum A2B3C3\right)^2 + ... \\ \left(\sum A3B1C1\right)^2 + \left(\sum A3B1C2\right)^2 + \left(\sum A3B1C3\right)^2 + ... \\ + \left(\sum A3B2C1\right)^2 + \left(\sum A3B2C2\right)^2 + \left(\sum A3B2C3\right)^2 + ... \\ + \left(\sum A3B3C1\right)^2 + \left(\sum A3B3C2\right)^2 + \left(\sum A3B3C3\right)^2 + ... \end{array}}{\text{number of observations for each level}} \right] - \left[\begin{array}{l} SS_A - SS_B - SS_C - SS_{AB} \\ -SS_{BC} - SS_{AC} - CF \end{array} \right]$$

Sum of squares of residual error (SS_E):

$$SS_E = SS_T - \sum SS_A + SS_B + SS_C + SS_{AB} + SS_{BC} + SS_{AC} + SS_{ABC}$$

Mean squares (*MS*)

$$MS = \frac{SS}{df}$$

F-ratio

$$F - ratio = \frac{\text{MS of the source effect}}{\text{MS of the residual error}}$$

Hypothesis of Effectiveness of an Individual or Interactive Factor:

The hypothesis that an individual or an interactive factor has effect is accepted at a particular probability level when the *F-ratio* is found to be greater than the corresponding *F-value* obtained from the Fisher's distribution table.

Hypothesis: Effect of a source is significant if $\underline{P < 0.05}$ (i.e. at 95% confidence level)

Appendix III: Samples of ANOVA results obtained from *MINITAB* software.

Table A3: ANOVA Results for f'_c (response) versus A, B, C (predictors).

Factors	Type	Level	Scale values		
A	Fixed	3	0.875	0.938	1.000
B	Fixed	3	0.792	0.896	1.000
C	Fixed	3	0.778	0.889	1.000
Source	DF	Seq SS	Adj MS	F	P
A	2	39.672	19.380	1.990	0.199
B	2	464.501	232.250	23.260	0.000
C	2	135.281	67.640	6.770	0.019
A*B	4	23.686	5.921	0.590	0.678
A*C	4	4.993	1.248	0.120	0.969
B*C	4	22.437	5.609	0.560	0.697
Error	8	79.890	9.986		
Total	26	770.456			

Appendix IV: Details of Butler-Volmer Equation

During corrosion (oxidation), both anodic and cathodic rates couple together on the electrode surface at a specific current density known as I_{corr}. This is an electrochemical phenomenon which dictates that both reactions must occur at different sites on the metal/electrolytes interface. For a uniform process under steady-state conditions, the current densities at equilibrium are rated as $i_a = -i_c$ at E_{corr} with i_a being the anodic current density and i_c being the cathodic current density. It is important to point out that I_{corr} cannot be measured at E_{corr} since $i_a = -i_c$ and current will not flow through an external current-measuring device. When polarizing from corrosion potential with respect to anodic or cathodic current density, the over-potential expression given by Eqn. 1a and 1b.

$$\varepsilon_a = \beta_a \log(\frac{i_a}{i_{corr}}) \quad \ldots(1a)$$

$$\varepsilon_c = \beta_c \log(\frac{i_c}{i_{corr}}) \quad \ldots(1b)$$

$$\varepsilon_a = \Delta E = \left(E - E_{corr}\right) > 0 \text{ and } \varepsilon_c = \Delta E = \left(E - E_{corr}\right) < 0$$

$$i_a = i_{corr} \exp\left[\frac{2.303(E - E_{corr})}{\beta_a}\right] \quad \ldots(2)$$

$$i_c = i_{corr} \exp\left[\frac{2.303(E - E_{corr})}{\beta_c}\right] \quad \ldots(3)$$

$$i = i_a - i_c \quad \ldots(4)$$

substituting Eqs. 2 and 3 into 4

$$i = i_{corr} \exp\left\{\left[\frac{2.303(E - E_{corr})}{\beta_a}\right] - \exp\left[-\frac{2.303(E - E_{corr})}{\beta_a}\right]\right\} \quad \ldots(5)$$

Upon differentiating Eq. 5 with respect to *E*, the inverse polarization resistance R_p is obtained as in Eq. 6

$$\frac{1}{Rp} = \frac{di}{dE} = 2.303 i_{corr} \left\{ \beta^{-1} \exp\left[\frac{2.303(E - E_{corr})}{\beta_a} \right] - \beta^{-1} \exp\left[\frac{2.303(E - E_{corr})}{\beta_c} \right] \right\} \quad ...(6)$$

Further differentiating yields:

$$\frac{d^2 i}{dE^2} = 5.3038 i_{corr} \left\{ \beta^{-2} \exp\left[\frac{2.303(E - E_{corr})}{\beta_a} \right] - \beta^{-2} \exp\left[\frac{2.303(E - E_{corr})}{\beta_c} \right] \right\} \quad \ldots(7)$$

Let us set some conditions for Eq. 7, such that;

$$\frac{d^2 i}{dE^2} \Rightarrow \begin{cases} < 0 \ \ for\ E = E_{\max} > E_{corr} \\ = 0 \ \ for \text{ an inflection point} : E = E_{corr} \\ > 0 \ for\ E < E_{corr} \end{cases}$$

Evaluating Eq. 7 at inflection point, we get:

$$\left(\frac{d^2 i}{dE^2} \right)_{E=E_{corr}} = 5.3038 i_{corr} \left\{ \beta_a^{-2} - \beta_c^{-2} \right\} \quad \ldots(8)$$

Inflection point is achieved if and only if $\beta_a = \beta_c$,, evaluating Eq. 7 at $E = E_{corr}$

$$\left(\frac{di}{dE} \right)_{E=E_{corr}} = \frac{1}{R_p} = 2.303 i_{corr} \left(\frac{\beta_a + \beta_c}{\beta_a \beta_c} \right) \quad \ldots(9)$$

$$R_p = \left(\frac{di}{dE} \right)^{-1}_{E=E_{corr}} \ ; \ R_p = \left(\frac{\beta_a \beta_c}{2.303 i_{corr} (\beta_a + \beta_c)} \right)$$

$$R_p = \frac{B}{i_{corr}} \quad \ldots (10)$$

Eq.10 can be linearized as follows:

$$\log(R_p) = \log(B) - \log(i_{corr}) \quad \ldots(11)$$

where: β is as defined as Stern-Geary constant

I = current corresponding to an over-potential (ε)

$\varepsilon = E - E_{corr}$

E = polarized potential

E_{corr} = corrosion potential (i.e. open-circuit or corrosion potential)

I_{corr} = corrosion current corresponding to E_{corr}

β_a = anodic Tafel coefficient (< 1 V)

β_c = anodic Tafel coefficient (< 1V)

Appendix V: Automation design methodology

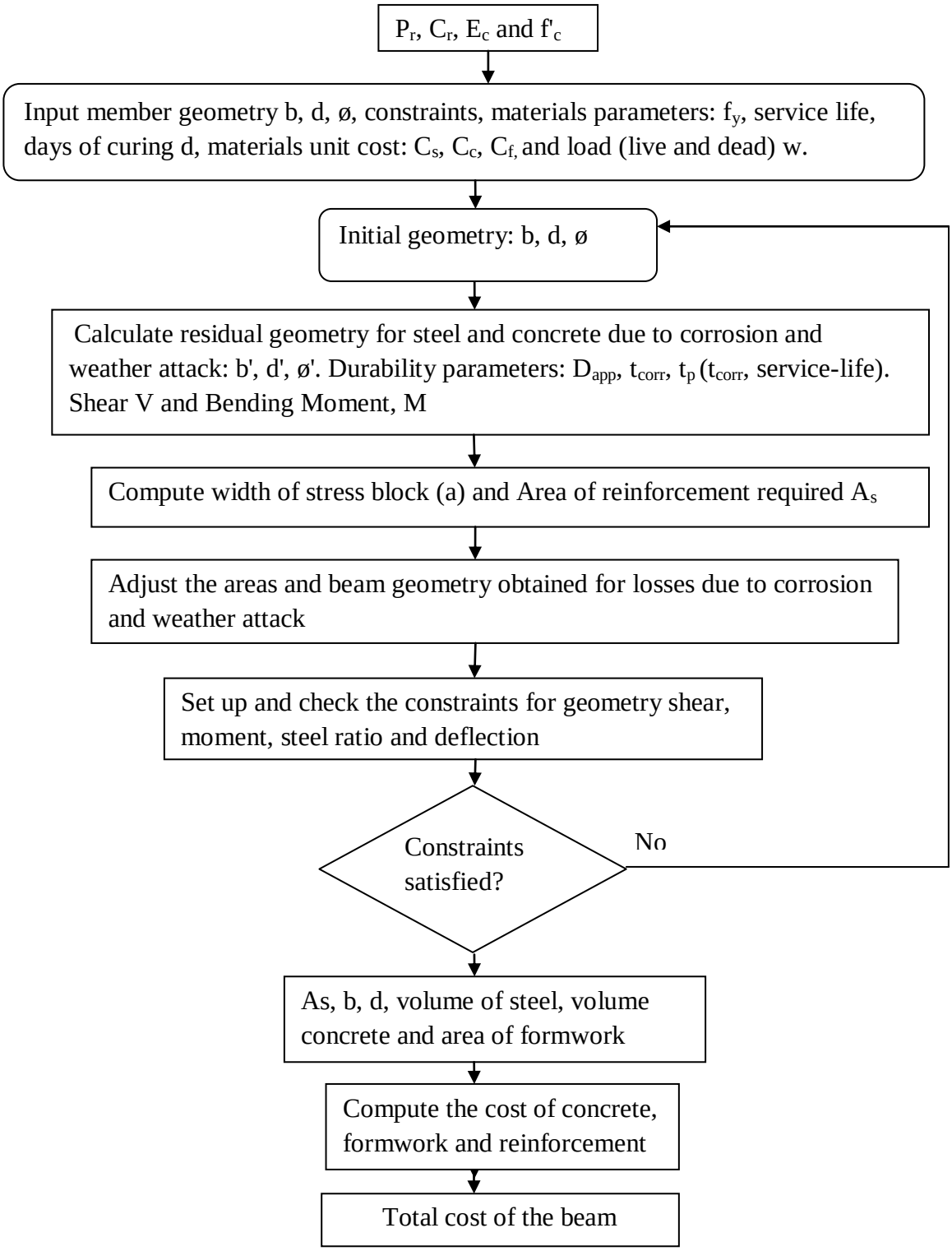

Figure A5.1: Flow-chart for automated design of RC beam.

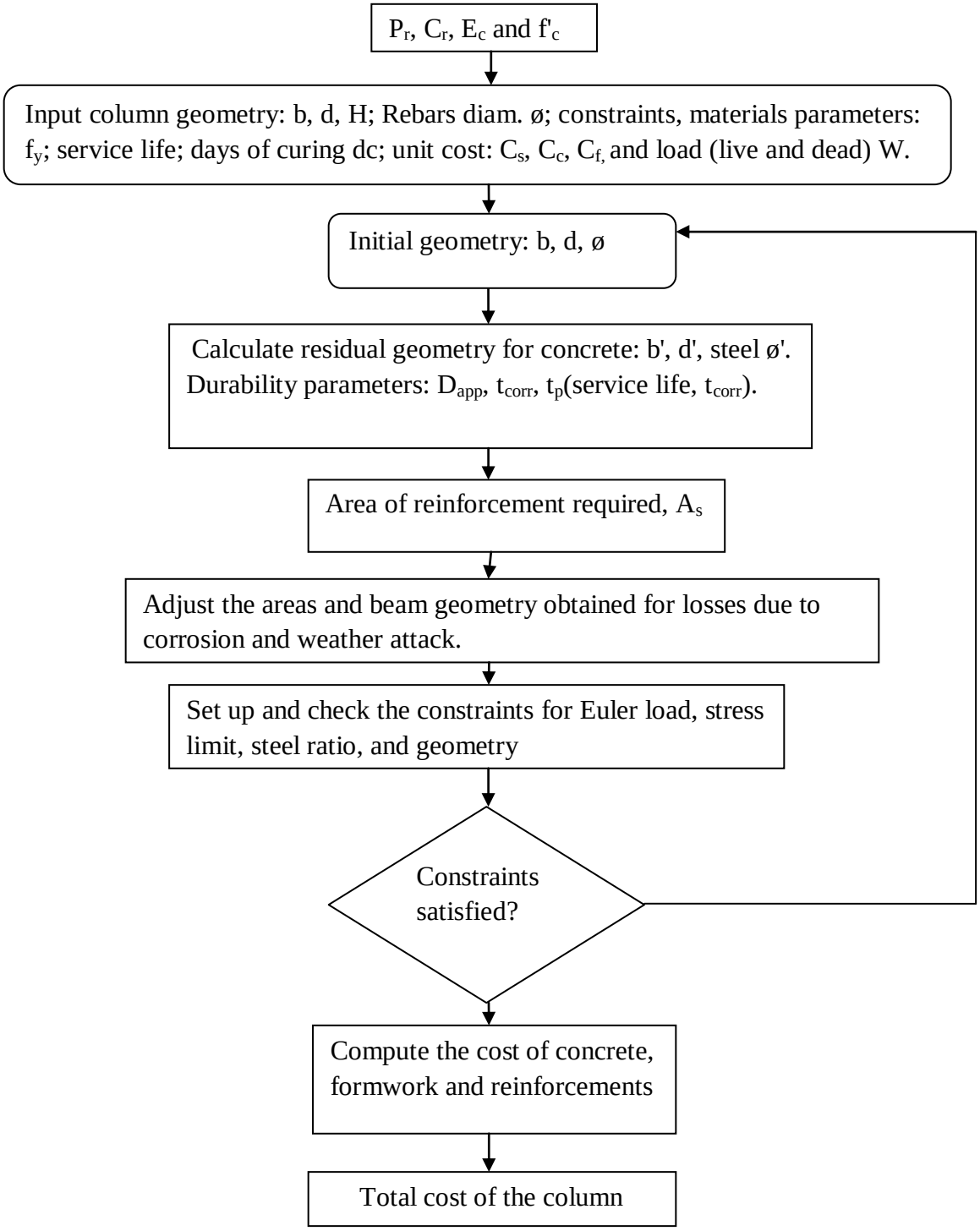

Figure A5.2: Flow-chart for automated design of RC column.

Table A5.1: Microsoft Excel interface for optimal beam design.

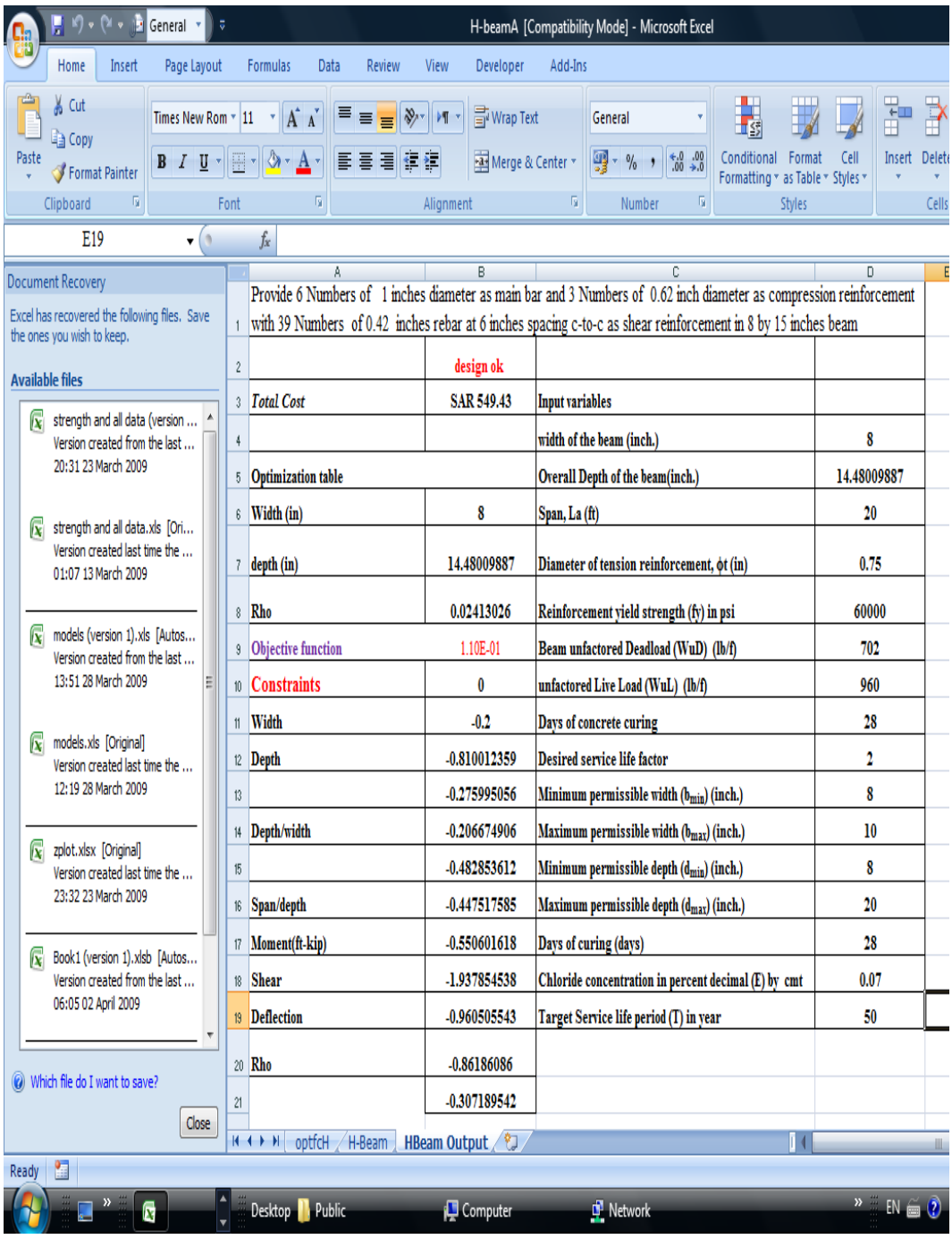

	A	B	C	D
1	Provide 6 Numbers of 1 inches diameter as main bar and 3 Numbers of 0.62 inch diameter as compression reinforcement with 39 Numbers of 0.42 inches rebar at 6 inches spacing c-to-c as shear reinforcement in 8 by 15 inches beam			
2		design ok		
3	*Total Cost*	SAR 549.43	Input variables	
4			width of the beam (inch.)	8
5	Optimization table		Overall Depth of the beam(inch.)	14.48009887
6	Width (in)	8	Span, La (ft)	20
7	depth (in)	14.48009887	Diameter of tension reinforcement, ϕt (in)	0.75
8	Rho	0.02413026	Reinforcement yield strength (fy) in psi	60000
9	Objective function	1.10E-01	Beam unfactored Deadload (WuD) (lb/f)	702
10	Constraints	0	unfactored Live Load (WuL) (lb/f)	960
11	Width	-0.2	Days of concrete curing	28
12	Depth	-0.810012359	Desired service life factor	2
13		-0.275995056	Minimum permissible width (b_{min}) (inch.)	8
14	Depth/width	-0.206674906	Maximum permissible width (b_{max}) (inch.)	10
15		-0.482853612	Minimum permissible depth (d_{min}) (inch.)	8
16	Span/depth	-0.447517585	Maximum permissible depth (d_{max}) (inch.)	20
17	Moment(ft-kip)	-0.550601618	Days of curing (days)	28
18	Shear	-1.937854538	Chloride concentration in percent decimal (E) by cmt	0.07
19	Deflection	-0.960505543	Target Service life period (T) in year	50
20	Rho	-0.86186086		
21		-0.307189542		

Table A5.2: Microsoft Excel interface for optimal axial column design.

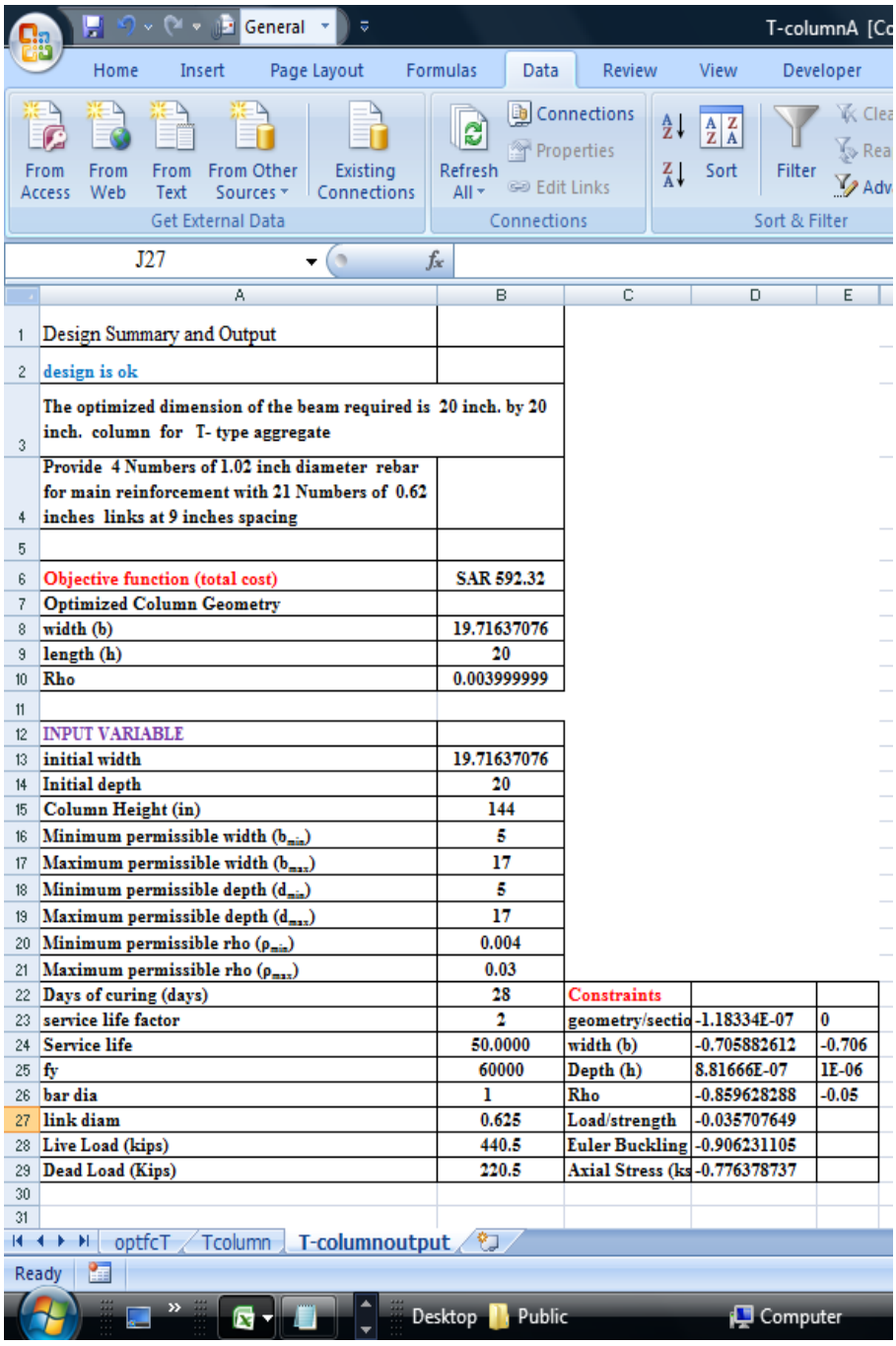

	A	B	C	D	E
1	Design Summary and Output				
2	design is ok				
3	The optimized dimension of the beam required is 20 inch. by 20 inch. column for T- type aggregate				
4	Provide 4 Numbers of 1.02 inch diameter rebar for main reinforcement with 21 Numbers of 0.62 inches links at 9 inches spacing				
5					
6	Objective function (total cost)	SAR 592.32			
7	Optimized Column Geometry				
8	width (b)	19.71637076			
9	length (h)	20			
10	Rho	0.003999999			
11					
12	INPUT VARIABLE				
13	initial width	19.71637076			
14	Initial depth	20			
15	Column Height (in)	144			
16	Minimum permissible width (b_{min})	5			
17	Maximum permissible width (b_{max})	17			
18	Minimum permissible depth (d_{min})	5			
19	Maximum permissible depth (d_{max})	17			
20	Minimum permissible rho (ρ_{min})	0.004			
21	Maximum permissible rho (ρ_{max})	0.03			
22	Days of curing (days)	28	Constraints		
23	service life factor	2	geometry/sectio	-1.18334E-07	0
24	Service life	50.0000	width (b)	-0.705882612	-0.706
25	fy	60000	Depth (h)	8.81666E-07	1E-06
26	bar dia	1	Rho	-0.859628288	-0.05
27	link diam	0.625	Load/strength	-0.035707649	
28	Live Load (kips)	440.5	Euler Buckling	-0.906231105	
29	Dead Load (Kips)	220.5	Axial Stress (ks	-0.776378737	
30					
31					

REFERENCES

[1] Tremper, B., Beaton, J.L; and Stratfull, R.F., *Causes and Repair of Deterioration to a California Bridge due to Corrosion of Reinforcing Steel in a Marine Environment II*: Fundamental factors Causing Corrosion, Bulletin No. 182 Highway Research Board, Washington, D.C., 1958, pp.18-41.

[2] Bentur, A.; Diamond, S.; and Berke, N. S., *Steel Corrosion in Concrete: Fundamentals and Civil Engineering* Practice, E & FN Spon, London, UK, 1997, p. 201.

[3] Bhide, S. *Material Usage and Condition of Existing Bridges in the U.S. SR342*, Portland Cement Association, Skokie, Ill, 1999, p. 28.

[4] AS 3600; *Concrete Structures Code*. Sydney: Standard Association of Australia; 1994

[5] Dimitri, V.V; Mark, G. S. : *Life Cycle Cost Analysis of RC Structures in Marine Environments*, Elsevier Ltd, www.elsevier.com/locate/strusafe, 2003.

[6] MEC , *As solid as concrete*, Middle East Construction, April/May 1987, pp. 20-21.

[7] Schutt, W.R., *Cathodic Protection of New HigH-Rise Buildings In Abu Dhabi*, Concrete International, May, 1992, pp. 45-46.

[8] ACI 222R-01, *Protection of Metals in Concrete Against Corrosion*, America Concrete Institute, 2001, pp2-4.

[9] Morinaga, S., *Prediction of Service Lives of RC Buildings Based on the Corrosion Rate of Reinforcing Steel*, Proceedings of Building Materials and Components, Brighton, UK, 7-9 November 1990, pp. 5-16.

[10] Cabrera, J.G., *Deterioration of Concrete Due to Reinforcement Steel Corrosion*, Cement & Concrete Composites, 18, 1996, pp. 47-59.

[11] Bazant, Z.P., *Physical Model for Steel Corrosion in Concrete Sea Structures-Application*, ASCE Journal of Structural Division, Vol. 105, 1979, pp. 1155-1166.

[12] Wang, X.M. and Zhao, H.Y., *The Residual Service-life Prediction of R.C. Structures*, *Durability of Building Materials and Components 6*. Edited by Nagataki S *et al.*, E & FN Spon., pp. 1107-1114, 1993.

[13] Bertolini, L; Bernhard E.; Pedeferri, P.; and Polder, R., *Corrosion of steel in concrete*, Wiley –VCH Verlag GmbH & Co.KGA, Germany, 2004.

[14] Gjrov, O.F., *Durability of Concrete Containing Condensed Silica Fume*, ACI SP-79, Detroit, Vol. 2, 1983, pp. 695-708.

[15] Shakhmenko, G. and Birsh, J., *Concrete Mix Optimization*, Riga technical University, Department of Building Materials, Azenes str. 16, LV 1658, 1998.

[16] Goltermann, P., Johansen, V., and Palbol, L. (1997), *Packing of Aggregates: An Alternative Tool to Determine the Optimal Aggregate Mix*, ACI Materials Journal, VOL 94, No. 5, Sep.-Oct., pp. 435-443.

[17] Kasperkiewicz, J., *Optimization of Concrete Mix Using a Spreadsheet Package*, ACI Materials Journal, Vol. 91, No. 6, Nov.-Dec. 1994, pp. 551-559.

[18] Garstecki, A., Glema, A., and Scigallo, J., *Optimal Design of RC Beams and Frames*, Computer Assisted Mechanics and Engineering Sciences, 3, 1996, pp. 223-231.

[19] Coello, C.C., Hernandez, F.S., and Farrera, F.A., *Optimal Design of RC Beams Using Genetic Algorithms*, Expert Systems with Applications, Vol. 12, No. 1, 1997, pp. 101-108.

[20] Alghamdi, S.A., and Leiva, J.P., *Optimal Shape Design of Twin-Cell Steel Box Girder Structures with Frequency Constraints*, Proc., 4th World Congress of Structural and Multi-disciplinary Optimization, (Org.: ISSMO & DUT), Department of Civil Engineering, Dalian University of Technology, Dalian, China, June 4-8, 2001.

[21] Azmy, A.M. and Eid, M.H., *Cost-Optimum Design of RC Beams based on Strength, Ductility, and Serviceability Requirements and Practical Considerations*, Journal of Engineering and Applied Science, Vol. 46, No. 3, June. 1999a, pp. 435-452.

[22] Dole, R.M., Ronghe, G.N., and Gupta, L.M., *Optimum Design of RC Beams Using Polynomial Optimization Technique*, Advances in Structural Engineering, Vol. 3, No. 1, 2000, pp. 67-79.

[23] Zielinsky, Z.A., Long, W., and Troitsky, M.S., *Designing RC ShorT-Tied Columns Using the Optimization Technique*, ACI Structural Journal, Vol. 92, No. 5, Sep.-Oct. 1995, pp. 619-626.

[24] Sarja, A. and Vesikari, E., *Durability design of concrete structures*, Report of RILEM Technical Committee, E & FN Spon, 1996.

[25] Anoop, M.B., Rao, K.B., and Appa Rao, T.V.S.R., *A Methodology for Durability-Based Service-life Design of RC Flexural Members*, Magazine of Concrete Research, Vol. 55, No. 3, June 2003, pp. 289-303.

[26] Soudki, K.A; Salakawy, E.F and Elkum, N.B, *Full Factorial Optimization of Concrete Mix Design for Hot Climate*, Journal of Mat. in Civil Engineering, Nov/ Dec.2001.

[27] Waseem, M. Optimization of Concrete Mix Design Using a Statistical Approach. Masters Thesis, KFUPM, 1982.

[28] Maruyama. I; Noguchi, T. and Manabu K., *Optimization of the Concrete Mix-proportions Centered on Fresh Properties through the Genetic Algorithm* .www.degas.nuac.nagoya-u.ac.jp/ippei/paper_e/2002 accessed 3/11/2008.

[29] Kuntjoro, W; Mahmud, J., *Optimization of Structural Configuration using Mathematical Programming*, STG Report, Bureau of Research and Consultancy, Universiti Teknologi, MARA, Malaysia 2004.

[30] Morris, A.J (1982); *Foundations of Structural Optimization*: A Unified Approach. John Wiley & Sons, 1st ed., UK, 1982.

[31] Reddy, R.R., Gupta, A., and Singh, R.P., *Expert System for Optimum Design of Concrete Structures*, Journal of Computing in Civil Engineering, Vol. 7, No. 2, 1993, pp. 146-161.

[32] Azmy, A.M. and Eid, M.H., *Cost-Optimum Design for Shear RC Beams*, ACI Structural Journal, Vol. 96, No. 1, Jan.-Feb. 1999b, pp. 122-126.

[33] Balaguru, P.N., *Optimum Design of Singly Reinforced Rectangular Sections*, Journal of Civil Engineering Design, Vol. 2, No. 2, 1980a, pp. 149-169.

[34] Balaguru, P.N., Cos*T-Optimum Design of Doubly RC Beams*, Building and Environment, Vol. 15, No. 4, 1980b, pp. 219-222.

[35] Barros, M.H.F.M., Martins, R.A.F., and Barros, A.F.M., *Cost Optimization of Singly and Doubly RC Beams with EC2-2001*, Structural and Multidisciplinary Optimization, Vol. 30, No. 3, September, 2005, pp. 236-242.

[36] Min, S. and Kikuchi, N., *Optimal Reinforcement Design of Structures under the Buckling Load Using the Homogenization Design Method*, Structural Engineering and Mechanics, Vol. 5, No. 5, 1997, pp. 565-576.

[37] Arup, H., *The Mechanism of the Protection of Steel by Concrete, in Corrosion of Reinforcement in Concrete Construction*, Ellis Horwood Ltd., Chichester, 1983, pp.151-157.

[38] Pedefferi, P., *Cathodic Protection and Cathodic Prevention*, Construction and Building Materials, 10, 391-402, 1996.

[39] Alonso C., Castellote, M. and Andrade, C. , *Dependence of Chloride Threshold with the Electrical Potential of Reinforcement*, Proc 2nd International RILEM Workshop on Testing and Modelling the Chloride Ingress into Concrete, C. Andrade, J. Kropp (Eds.) PRO 19, RILEM Publication 415-425, 2000.

[40] Polder, R.B. , *Cathodic Protection of Reinforced Concrete Structures in the Netherlands*-Experience and Developments in Corrosion of Reinforcement in Concrete-Monitoring, Prevention and Rehabilitation, Papers from Eurocorr'97, J. Mietz, B Elsener, R. B Polder (Eds), *The European Federation of Corrosion Publication number 25*, The Institute of Materials, London, 1998, 172-184.

[41] Schuten G. And Leggedoor, J. and Polder, R.B., *Cathodic Protection of Concrete Ground- floor Elements with Mixed- in Chloride*, Papers from Eurocorr '99, J. Mietz, R. B Polder (Eds),B. Elsener,.The European Federation of Corrosion Publication number 31, The Institute of Materials, London, 2000, pp.85-92.

[42] COST 521, *Determination of Chloride Threshold in Concrete*, C. Andrade, in Corrosion of Steel in RC structures. Final report, ed. R. Cigna, C. Andrade, U. Nurnberger, R. Polder, R. Weydert, E Seitz, European Community EUR 20599, Luxembourg 2003, pp. 100-108.

[43] Glass, G.K.; Buenfield, N.R , *The Inhibitive Effects of Electrochemical Treatment Applied to Steel in Concrete*, Corrosion Science, Vol. 42, 2000, pp. 923-927.

[44] Glass, G.K.; Buenfield, N.R , *The Presentation of Chloride Threshold Level for Corrosion of Steel in Concrete*, Corrosion Science, Vol. 39, 1997, pp. 1001-1013.

[45] Page C.L, *Advances in Understanding and Techniques for Controlling Reinforcement Corrosion*, 15th International Corrosion Congress, Granada, 22-27 September, 2002.

[46] Hausmann, D.A, *Steel Corrosion in Concrete, How Does It Occur?* Material Protection, Vol 11, 1967, pp.19-23.

[47] Page, C.L., Short, N.R., and Holden, W.R., *The Influence of Different Cements on Chloride-Induced Corrosion of Reinforcing Steel*, Cement and Concrete Research. Vol. 16, No. 1, 1986, pp. 79-86.

[48] Frederiksen, J.M (Ed.), *Chloride Penetration into Concrete. State of the Art. Transport Processes, Corrosion Initiation, Test* Methods and Prediction Models, The Road Directorate, Report No. 53, Copenhagen, 1996.

[49] Khatri, R,P. and Sirivivantnanon, V., *Characteristic Service-life for Concrete Exposed to Marine Environment*, Cement and Concrete Research, Vol. 34. 2004, pp. 745-752.

[50] Clemeña, G. G. (1992), *Benefits of Measuring Half-Cell Potentials and Rebar Corrosion Rates in Condition Surveys of Concrete Bridge Decks*. Virginia Transportation Research Council, Report Number VTRC 92-R16.

[51] Ramniceanu, A., *Investigation of parameters governing the corrosion protection efficacy of fusion bonded epoxy coatings*, Ph.D Dissertation submitted to the faculty of the Department of Civil and Environmental Engineering, Virginia Polytechnic Institute and State University.

[52] Nagi, M. A. and Whiting, David A., *Electrical Resistivity of Concrete—A Literature Review.* R&D Serial No. 2457, Portland Cement Association, Skokie, Illinois, USA, . 2003, 57 pages.

[53] Gowers, K. R. and Millard, S.G., *Measurement of Concrete Resistivity for Assessment of Corrosion Severity of Steel Using Wenner Technique*. ACI Materials Journal, vol. 96, n. 5, September – October 1996, p. 536 – 541.

[54] Feliu, S., *Techniques to Assess the Corrosion Activity of Steel Reinforced Concrete Structures.* ASTM STP 1276; 1996.

[55] Broomfield, J. P., *Corrosion of Steel in Concrete*. 1st Edition, Chapman & Hall, New York.,1997.

[56] Elsener, B.; Böhni, H. and Wojtas, H. *Inspection and Monitoring of RC Structures - Electrochemical Methods to Detect Corrosion*. Insight on Non–destructive Testing and Condition Monitoring, vol. 36, n. 7, July 1994, p. 502 – 506.

[57] Clear, K.C., *Measuring Rate of Corrosion of Steel in Field Concrete Structures*, Transportation Research Record 1211, 1989, pp. 28-37.

[58] Macdonald, D.D., Urquidi-Macdonald, M. ,Rocha-Filho ,R.C. and El-Tantawy, Y., *Determination of the Polarization Resistance of Rebar in RC*, Corrosion, Vol.47, No.5, May 1991, pp. 330-335.

[59] Clear, K.C., *Measuring Rate of Corrosion of Steel in Field Concrete Structures*, Transportation Research Record 1211, 1989, pp. 28-37.

[60] Rodriguez, J., Ortega, L.M. García, A.M., Johansson, L. Petterson, K. *On-site Corrosion Rate Measurements in Concrete Structures Using A Device Developed under the Eureka Project EU-401* Int. Conference on Concrete Across Borders, Odense, Denmark, vol. I, pp. 215-226.

[61] Andrade, C. and Gonzalez, J.A., *Quantitative measurements of corrosion rate of reinforcing steels embedded in concrete using polarization resistance measurements*, Werkst. Korros., 29, 515 (1978).

[62] Saetta, A.V., *Deterioration of RC Structures Due to Chemical-Physical Phenomena: Model-Based Simulation*, Journal of Materials in Civil Engineering, ASCE, Vol. 17, No. 3, June, 2005, pp. 313-319.

[63] Thompson, N.G. and Lankard, D.R., *Improved Concretes for Corrosion Resistance* (Report No. FHWA-RD-96-207), Federal Highway Administration, Washington, DC, 1997, p 176.

[64] Virmani, Y.P. and Clemena, G.G., *Corrosion Protection of Concrete Bridges* (Report No. FHWA-RD-98-088), Federal Highway Administration, Washington, DC, 72 pp. 16. ACI (1996). *Corrosion of Metals in* Concrete, Report No. ACI 222R-96, American Concrete Institute, Detroit, MI, 30 pp. 1-30.

[65] Shameem, M., Maslehuddin, M., Saricimen, H., and Al-Mana, A.I., *Extending the Life of RC Structures in the Arabian Gulf Environment, Proceedings of Conference on Structural Faults and Repair*, London, July 1995.

[66] Jaegermann, C., *Effect of Water-cementitious Material Ratio and Curing on Chloride Penetration into Concrete Exposed to Mediterranean Sea Climate*, ACI Materials Journal, 87(4), 1990, pp. 333-339.

[67] Ho, D.W.S., and Lewis, R.K., *Carbonation of Concrete and Its Prediction*, Cement and Concrete Research, 17, 1987, pp. 489-504.

[68] Al-Amoudi, O.S.B., Maslehuddin, M., and Rasheeduzzafar, *Permeability of Concrete: Influential Factors*, Proceedings of 4th International Conference on Deterioration and Repair of RC in the Arabian Gulf, Bahrain,10-13, October, 1993, pp. 717-733.

[69] Federal Highway Administration, *Material and Method for Corrosion Control of reinforced and Prestressed concrete Structures in New Construction*, US Department of Transportation. Pub. No. 00-081, 6300 Georgetown Pike, Mclean VA 22101-2296, 2001 pp.1-29.

[70] Clear, K. C., *Time-to-Corrosion for Reinforcing Steel in Concrete Slabs: Performance after 830 Daily Salt Applications*, FHWA-RD-76-70, Federal Highway Administration, Washington D.C., Apr., 1976, p. 64.

[71] Goto, S. and Roy, D.M., *The Effect of W/C Ratio and Curing Temperature on the Permeability of Hardened Cement Paste*, Cement and Concrete Research, 1981, p. 575.

[72] Al-Saadoun, S.S., Rasheeduzzafar, and Al-Gahtani, A.S., *Mix Design Considerations for Durable Concrete in the Arabian Gulf Environment*, The Arabian Journal for Science and Engineering, 17(1), 1992, pp. 17-33.

[73] Al-Amoudi, O.S.B., *Studies on the Evaluation of Permeability and Corrosion Resisting Characteristics of Portland Pozzolan Concretes*, M.S. Thesis, King Fahd University of Petroleum and Minerals, Dhahran, 1985.

[74] ACI 201.2R *Guide to Durable Concrete Chemical Admixtures for Concrete*., Farmington Hills, Mich., 2002.

[75] ACI 211.1 *Standard Practice for Selecting Proportions for Normal, Heavyweight, and Mass Concrete*. Farmington Hills, Mich., 2001.

[76] Ahmad. S. and Bhattacharjee, B. (1995), *A Simple Arrangement and Procedure for In-situ Measurement of Corrosion Rate of Rebar Embedded in Concrete*, Corrosion Science, Vol. 37, No. 5, pp.781-791.

[77] Al-Tayyib, A.J. and Khan. M.S. (I988), *Corrosion Rate Measurement of Reinforcing Steel in Concrete by Electrochemical Techniques*. ACI Materials J., May-June, pp. 172-177.

[78] Metha, P.K, *Effect of Cement Composition on Corrosion of Reinforcing Steel in Concrete,* Chloride Corrosion of steel in Concrete , STP 629, ASTM, West Conshohocken, Pa., 1977, pp. 12-19.

[79] Mehta, P.K., Durability *of Concrete in Marine Environment: a review, Performance of Concrete in Marine Environment*, ACI Publication, SP-65, 1986, P.1.

[80] Maslehuddin, M., *Influence of the Arabian Gulf Environment on Corrosion of Reinforcing Steel*, Ph.D. Dissertation, Aston University, England, 1994.

[81] Hussain, S.E., *Mechanisms of High Durability Performance of Plain and Blended Cements*, Ph.D. Thesis, King Fahd University of Petroleum and Minerals, Dhahran, 1991.

[82] Page, C. L., N. R. Short and A. El-Tarras, *Diffusion of Chloride Ions in Hardened Cement Pastes*, Cement and Concrete Research, Vol. 11, No. 3, 1981, pp. 295-406.

[83] Page, C. L., N. R. Short and W. R. Holden, *The Influence of Different Cements on Chloride-Induced Corrosion of Reinforcing Steel*, Cement and Concrete Research, Vol. 16, No. 1, 1986, pp. 79-86.

[84] Al-Amoudi, O.S.B, Abduljauwad, S.N., Rasheeduzaffar, and Maslehuddin, M., *Effect of Chloride and Sulfate Contamination in Soils on Corrosion of Steel and Concrete*, Transportation Research Record, No. 1345, 1992, pp. 67-73.

[85] Rasheeduzaffar, Dakhil, F.H. and Bader, M.A., *Toward Solving the Concrete Deterioration Problem in the Arabian Gulf Region*, The Arabian Journal for Science and Engineering, Vol. 11, No.2, 1986, pp. 129-146.

[86] ACI 116.00R, *Chemical Admixtures for Concrete*, American Concrete Institute, Farmington Hills, Mich., 2000.

[87] ACI 212.3R, *Chemical Admixtures for Concrete*, American Concrete Institute, Farmington Hills, Mich., 2003.

[88] ACI Education Bulletin E4-03, *Chemical Admixture for Concrete*, prepared under supervision of ACI Committee E-701 Material for Construction.

[89] Maslehuddin, M., Saricimen, H., and Al-Mana, A.I., *Effect of Fly-ash Addition on the Corrosion Resisting Characteristics of Concrete*, ACI Materials Journal, January-February 1987, pp. 42-50.

[90] Ozyildirim, C., *Laboratory Investigation of Concrete Containing Silica Fume for Use in Overlays*, ACI Materials Journal, V. 84, No.1, Jan.-Feb 1987, pp. 3-7.

[91] Kumar, A., Komarneni, S. and Roy, D.M., *Diffusion of K^+ and Cl^- through Sealing Materials*, Cement and Concrete Research, Vol. 17, No. 1, 1987, pp. 153-160.

[92] ACI Education Bulletin E1-99, *Aggregate for Concrete*, Developed for Committee E-701, Material for Concrete Construction, American Concrete Institute, Farmington Hills, Mich., 1999, p.2.

[93] ASTM C33-03, *Standard Specification for Concrete Aggregate*, ASTM International West Conshohocken, PA, www.astm.org. 2004.

[94] Mehta, P.K. and Monteiro, P.J.M., *Concrete: Structure, Properties, and Materials*, 2nd Edition, Prentice-Hall, Inc., New Jersey, 1993.

[95] Cordon, W.A., and Gillespie, A., *Variables in Concrete Aggregates and Portland Cement Which Influence the Strength of Concrete*, ACI Journal Proceedings, V. 60, 1963, p. 1029.

[96] U.S. Bureau of Reclamation, *Concrete Manual*, Denver, 37, 1975.

[97] Maslehuddin, M., *Optimization of Concrete Mix Design for Durability in the Eastern Province of Saudi Arabia*, M.S. Thesis, King Fahd University of Petroleum and Minerals, Dhahran, 1981.

[98] ACI Committee 201, *Guide to Durable Concrete (ACI 201.2R-77) (Reapproved 1982),* American Concrete Institute, Farmington Hills, Mich., 1977, pp.1- 37.

[99] Beeby, A.W., *Corrosion of Reinforcing Steel in Concrete and its Relation to Cracking*, The Structural Engineer, 56A (3), 1978, pp. 77-81.

[100] Schiessl, P., *Admissible Crack Width in RC Structures, Contribution II, 3-17*, International Colloquium on the Behavior in Service of Concrete Structures, 1975.

[101] Malhotra (ed.), V. M., *American Concrete Institute*, Farmington Hills, Mich., 1980, pp. 21-38.

[102] McDonald, D, *Design Options for Corrosion Protection*, Concrete 95-Toward Better Concrete Structures, Concrete Institute of Australia, 1995, pp. 75-83.

[103] ACI 318: Building *Code Requirement for Structural Concrete,* American Concrete Institute, 38800 Country Club Drive, Farmington Hills, MI 48331, USA, 2005.

[104] American Association of State Highway Transport Officials (ASHTO)-1993, *Standard Specification for Highway Bridges, 16th Edition,* American Association of State Highway and Transportation Officials, Washington, DC, 1993,760pp.

[105] ACI 301- *Specifications for Structural Concrete*, American Concrete Institute, Farmington Hills, Mich.

[106] ACI 304R *Guide for Measuring, Mixing, Transporting and Placing Concrete*, American Concrete Institute, Farmington Hills, Mich.

[107] ASTM C33-03, *Standard Specification for Ready-Mixed Concrete,* ASTM International West Conshohocken, PA, www.astm.org. 2004.

[108] Kaplan, M. F., *Effect of Incomplete Consolidation on Compressive and Flexural Strength, Ultrasonic Pulse Velocity, and Dynamic Modulus of Elasticity of Concrete*, ACI JOURNAL, Proceedings V. 56, No. 9, Mar. 1960, pp. 853-867.

[109] Whiting, D., and Kuhlmann, L., *Curing and Chloride Permeability*, Concrete International, V. 9, No. 4, Apr., 1987,pp. 18-21.

[110] ASTM C 192 *Practice for Making and Curing Concrete Test Specimens in the Laboratory,* ASTM International West Conshohocken, PA, www.astm.org. 2004.

[111] AASHTO T 277 *Standard Method of Test for Rapid Determination of the Chloride Permeability of Concrete*, American Association of Highway and Transport Officials, 444 N. Capitol St. NW, Suite 249 Washington, DC 2001.

[112] Clear, K. C., and Hay, R. E., *Time-to-Corrosion of Reinforcing Steel in Concrete Slabs: Effect of Mix Design and Construction Parameters*, *Report* No. FHWARD-73-32, 1973, pp. 103.

[113] ACI 308R *Guide to Curing Concrete,* American Concrete Institute, Farmington Hills, Mich., 48333-9094.

[114] Saricimen, H., Maslehuddin, M., Shameem, M., Khan, M.S., and Al-Tayyib, A.J., *Effect of Curing on the Permeability of Plain and Pozzolanic Concrete*, Proceedings of 4th International Conference on Fly-ash, Silica Fume, Slag, and Natural Pozzolans in Concrete, Turkey, May 3 to 8, 1992.

[115] Powers, T. C., Copeland, L. E.; and Mann, H. M., *Capillary Continuity or Discontinuity in Cement Pastes,* Journal of the PCA Research and Development Laboratories, V. 1, No. 2, 1959, pp. 38-48.

[116] Mangat, P.S. and Mally, B.T., *Prediction of Long Term Chloride Concentration in Concrete,* Materials and Structures Journal, 27(1994), pp. 338–346.

[117] Collepardi, M., Marcialis, A., and Turriziani, R., *Penetration of Chloride Ions into Cement Pastes and Concretes*, Journal of the American Ceramic Society, 55(10)(1972), pp 534–535.

[118] Tutti, K., *Corrosion of Steel in Concrete*. Report No. Fo. 4, Swedish Cement and Concrete Research Institute, Stockholm, 1982.

[119] Siemes T. and Edvardsen, C., *Duracrete*: *Service-life Design for Concrete Structure*, Eighth International Conference on Durability of Building Materials and Components, Vancouver, Canada, 1999, pp. 1343–1356.

[120] Isgor, O.B. and Razaqpur, A.G., *Modelling Steel Corrosion in Concrete Structures,* Materials and Structures Journal, 39(2006), pp. 291–302.

[121] Marchand, J., *Modelling the Behavior of Unsaturated Cement Systems Exposed to Aggressive Chemical Environments*, Materials and Structures Journal, 34(2001), pp. 195–200.

[122] Browne, R., *Design Prediction of the Life for RC in a Marine and other Chloride Environment*, Durability of Building Materials. Vol 1, No 2, 1982, pp.113-125.

[123] Bohni, H., *Corrosion in RC Structures*, Woodhead Publishing Limited, Cambridge, England, 2005.

[124] Crank, J. *The Mathematics of Diffusion*, 2nd edn. London: Oxford University Press, 1975.

[125] Al-Kutti, W.A., *Compliance Criteria for Quality Concrete*, MS Thesis submitted to King Fahd University of Petroleum & Minerals, Dhahran, Saudi Arabia, May 2005.

[126] Ahmad, S. and Bhattacharjee, B., *Empirical Modelling of Indicators of Chloride-Induced Rebar Corrosion*, Journal of Structural Engineering, Vol. 27, No. 3, October, pp. 195-207, 2000.

[127] Pihlajavaara, S.E., *Contributions for the Development of the Estimation of Long-term Performance and Service-life of Concrete*. Helsinki University of Technology, Faculty of Civil Engineering and Surveying, Espoo, Report 3, pp. 1-26, Articles 49 pp., 1994.

[128] Vesikari, E., *Service-life Design of Concrete Structures*, Association of Finnish Civil Engineers RIL, Helsinki. RIL 183-4.9. 120 pp., 1995.

[129] Ijsseling F.P., *Application of electrochemical methods of corrosion rate determination to system involving corrosion product layers*, British Corrosion Journal, 21(2), pp. 95-101, 1986.

[130] Sarja, A. and Vesikari, E., *Durability Design of Concrete Structures*, Report of RILEM Technical Committee, E & FN Spon, 1996.

[131] Alghamdi S. A. and Shamsad, A., *Multi-criteria Optimal Design Methodology for Durable RC Members in Corrosive Environments–An Experimental Investigation*; Proceedings; Vol II, Int. Conf. on Durability of Concrete Structures; Hangzhou, China, Nov. 26-27, 2008; pp. 851-860.

[132] ASTM C128 - 07a *Standard Test Method for Density, Relative Density (Specific Gravity), and Absorption of Fine Aggregate* ASTM, West Conshohocken PA.

[133] Alghamdi, S.A. and Ahmad S., *Multi-criteria Optimal Designs of R/C Beams and Columns - Experimental and Analytical Studies*, Prog. Reports I-V; KACST Project AT-23-21, 2005.

[134] *PowerCORR User's Manual*. Corrosion Measurement Software, Princeton Applied Research, USA, 2001.

[135] ASTM C617 - 98(2003) *Standard Practice for Capping Cylindrical Concrete* Specimens ASTM, West Conshohocken PA, www.astm.org.

[136] ASTM C31, C39, C617, C1077, C1231, *Annual Book of ASTM Standards*, vol.04.02, ASTM, West Conshohocken PA, www.astm.org.

[137] Ahmad, S., and Bhattacharjee, B., *A Simple Arrangement and Procedure for In-situ Measurement of Corrosion Rate of Rebar Embedded in Concrete*, Corrosion Science, Vol. 37, No. 5, 1995, pp.781-791.

[138] Perez, N., *Electrochemistry and Corrosion Science*, Published by Springer, 2004, pp 90-105.

[139] Stern, M., and Geary, A. L., *Electrochemical Polarization: I. Theoretical Analysis of the Shape of Polarization Curves*, Journal of the Electrochemical Society, V. 104, No. 1, 1957, pp. 56-63.

[140] Berkeley, K.G.C, *Cathodic Protection of Reinforcement Steel in Concrete*, Butterworths, 1990.

[141] Dimitri V. Val, *Deterioration of Strength of RC Beams due to Corrosion and Its Influence on Beam Reliability*, Journal of Structural Engineering, Vol. 133, No. 9, September 1, 2007.

[142] Osyczka, A., *Multicriterion Optimization in Engineering with Fortran Programs*, Ellis Horwood Limited, Market Cross House, PO19 1B, England, 1984.

[143] *MINITAB Statistical Package Release 13 for Windows 95 and 98*. *Minitab* Inc., 2000. www.minitab.com .

[144] MacGregor, J. G., *Reinforced Concrete: Mechanics and Design*, 3rd Ed., Prentice-Hall, Upper Saddle River, N.J., 1997.

Curriculum Vitae

Name: Moruf Olalekan **Yusuf**

Place and Country of Birth: Ibadan, Nigeria

Nationality: Nigerian

Academic Background:

-National Diploma in Civil Engineering from the Federal Polytechnic, Ilaro with **Upper Credit** grade (4.45/5.0).

-Received Bachelor Degree from University of Ibadan in Civil Engineering with **Distinction** grade (6.3/7.0) in 2005.

Work Experiences:

-Worked as Civil Engineer with Zainab Construction Ltd, Nigeria from March 2005 to Jan 2006.

-Worked at Federal Polytechnic, Ede as Assistant Lecturer from Jan 2006 to Feb. 2007

-Joined KFUPM as Research Assistant and Masters Student in Civil Engineering (Structures and Materials) in Feb. 2007 with the completion of the program with 3.31/4.0 and submission of MS thesis in Aug. 2009.

E mail: yusmor2002@yahoo.co.uk,
moruf@kfupm.edu.sa